Integration of EEG-FMRI in an Auditory Oddball Paradigm Using Joint Independent Component Analysis

Jain Mangalathu Arumana
Marquette University

INTEGRATION OF EEG-FMRI IN AN AUDITORY ODDBALL PARADIGM USING
JOINT INDEPENDENT COMPONENT ANALYSIS

by

Jain Mangalathu Arumana, B.Sc., M.Sc.

A dissertation submitted to the Faculty of the Graduate School,
Marquette University,
in Partial Fulfillment of the Requirements for
the Degree of Doctor Philosophy

Milwaukee, Wisconsin

August 2012

ABSTRACT
INTEGRATION OF EEG-FMRI IN AN AUDITORY ODDBALL PARADIGM USING
JOINT INDEPENDENT COMPONENT ANALYSIS

Jain Mangalathu Arumana, B.Sc., M.Sc.

Marquette University, 2012

The integration of event-related potential (ERP) and functional magnetic resonance imaging (fMRI) can contribute to characterizing neural networks with high temporal and spatial resolution. The overall objective of this dissertation is to determine the sensitivity and limitations of joint independent component analysis (jICA) within-subject for integration of ERP and fMRI data collected simultaneously in a parametric auditory oddball paradigm. The main experimental finding in this work is that jICA revealed significantly stronger and more extensive activity in brain regions associated with the auditory P300 ERP than a P300 linear regression analysis, both at the group level and within-subject. The results suggest that, with the incorporation of spatial and temporal information from both imaging modalities, jICA is more sensitive to neural sources commonly observed with ERP and fMRI compared to a linear regression analysis. Furthermore, computational simulations suggest that jICA can extract linear and nonlinear relationships between ERP and fMRI signals, as well as uncoupled sources (i.e., sources with a signal in only one imaging modality). These features of jICA can be important for assessing disease states in which the relationship between the ERP and fMRI signals is unknown, as well as pathological conditions causing neurovascular uncoupling, such as stroke.

ACKNOWDLEDGEMENTS

Jain Mangalathu Arumana, B.Sc., M.Sc.

I would like to thank my two advisors, Dr. Scott Beardsley and Dr. Einat Liebenthal for their constant support, patience and guidance. I appreciate the time educating me on writing manuscripts, conducting research and presenting at conferences. I appreciate the time both of them took to meet with me on a regular basis and discussing research ideas.

I would also like to thank all of my colleagues at the Medical College of Wisconsin who have assisted me as a graduate student in the lab. I would like to especially thank Anjali Desai who helped me in multiple studies with EEG preparation and great feedback on fMRI analysis. I would like to thank Dr. Merav Sabri for the introduction to EEG analysis. I would also like to thank Dr. Tom Prieto and Tim Thelaner for the constant help in troubleshooting the EEG system. I would also like to thank the late Jim Verduin who introduced me and gave me insight into presentation programming. I would also like to thank Julie Peay, Tina Kostenko, Dr. Li Yiu and Dr. Vinai Roopchansingh in the biophysics department who helped me with MR scans and the protocol development.

I would also like to recognize my colleagues at Marquette University, Megan, Prajakta, Tushar, Chintan, Sampada and David. All of them were always happy to help,

participate in my studies and gave great feedback in our research meetings. A special thanks goes to David who helped me a lot with the computing cluster at Marquette.

I greatly appreciate all of the volunteers who participated in my EEG-fMRI experiments, which are by far not the most comfortable studies. Without them, this work would have not been possible.

Lastly, I would like to acknowledge the constant support and love of my family, my parents Theresiamma and John and my sister Sally during the time of my graduate studies. Most importantly thanks to my husband Winston for his constant support and love while I worked on my dissertation.

TABLE OF CONTENTS

LIST OF TABLES

LIST OF FIGURES

CHAPTER 1

INTRODUCTION AND BACKGROUND

1.1   INTRODUCTION

There is much interest in how the brain executes complex sensory and cognitive processes such as language perception and production, memory, multisensory integration and learning. Characterizing the cortical networks involved in these processes could improve our understanding of brain function and dysfunction, help model neural processes, and even help diagnose or rehabilitate patients with neurologic deficits. A major challenge in understanding such networks in the human brain involves the noninvasive characterization of neural activity with both high spatial and high temporal resolution. The integration of electroencephalography (EEG), reflecting the temporal dynamics of large-scale neural activity, with spatially well-defined fMRI activity (Bonmassar et al., 2001; Dale and Halgren, 2001; Liebenthal et al., 2003), can help to determine the spatio-temporal dynamics of neural activity in the brain.

A variety of model-based (Dale and Halgren, 2001; Debener et al., 2005; Eichele et al., 2005; Benar et al., 2007; Philiastides and Sajda, 2007; Laufs et al., 2008; Goldman et al., 2009; Ou et al., 2009; Rosa et al., 2011) and data-driven methods (Martinez-Montes et al., 2004; Calhoun et al., 2006; Correa et al., 2008; Brookings et al., 2009; Brown et al., 2010; Lei et al., 2010; Luessi et al., 2010) have been developed to integrate EEG and fMRI. Model-based approaches, such as linear regression, are robust. However, at the same time, model-based approaches are limited due to the inherent assumption that EEG and fMRI vary consistently across time and space (for example, linearly). In contrast, data-driven techniques, such as joint independent component analysis (jICA), are not limited to linear relationships and may therefore provide a more comprehensive description of neural activity, especially in cases when the underlying relationship between EEG and fMRI is unknown.
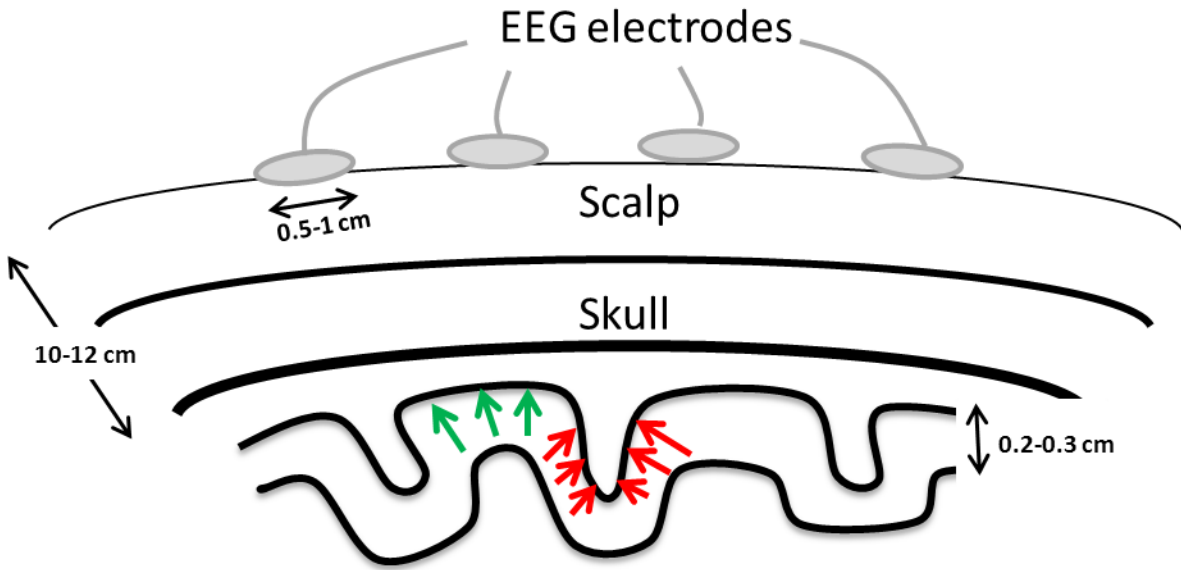
ERPs describe the measured electrical potential to the occurrence of a temporally well-defined event, such as a stimulus, whose response is usually obtained by averaging across many trials. To date, jICA has been tested for integration of single channel ERP and fMRI group data, and the results have suggested that the method is sensitive for extracting activation commonly observed in both neuroimaging modalities (Calhoun et al., 2006; Moosmann et al., 2008; Calhoun et al., 2009; Mijovic et al., 2012). This dissertation aimed to evaluate experimentally the performance of jICA for integration of ERP and fMRI data within-subject, including all spatio-temporal information from both imaging modalities to increase the sensitivity of the method. A comprehensive computational analysis of jICA was then performed by varying several experimental factors to determine their importance and the limitations of the method for extracting common activation between ERP and fMRI.

The following sections provide an overview of the types of signals measured with ERP and fMRI. The advantages associated with integrating ERP and fMRI in an event-related experimental paradigm will be reviewed and the relationship between neural activity and the hemodynamic response will be outlined. Finally, the current status of model-based and data-driven approaches to integrate ERP and fMRI will be reviewed, and current understanding of the neural networks associated with the auditory oddball paradigm, used here as a model experimental system within which to characterize jICA, will be discussed.

1.2 Electroencephalography and ERPs

Electroencephalography (EEG) is a noninvasive measurement of electrical activity in the brain (Berger, 1929). EEG is recorded at the scalp as the voltage difference between a 'live' electrode and a reference electrode (most commonly the central parietal electrode, CPz). EEG

mainly reflects the postsynaptic activity of neurons, rather than the spiking output of neurons (Logothetis et al., 2001). More specifically, the magnitude of measurable electric potential at the scalp is believed to be dependent on the summation of excitatory and inhibitory postsynaptic potentials, which arise from the apical dendrites of tens of thousands or millions of pyramidal cells that are spatially aligned in the outer layer of the cerebral cortex. The contribution of action potentials to the recorded EEG signal is believed to be rather small due to their brief temporal duration, resulting in less temporal overlap than post-synaptic potentials (Nunez and Srinivasan, 2005). When neurons are activated, excitatory and/or inhibitory synapses produce local current sinks and sources. The mass activity of aligned pyramidal neurons leads to volume currents that can be modeled as a dipole, consisting of a source-sink combination (Nunez and Srinivasan, 2005). Pyramidal neurons along the wall of a sulcus will tend to result in tangential dipoles relative to the surface electrodes, whereas neurons located on a gyrus will produce radial dipoles (Nunez and Srinivasan, 2005), see Figure 1-1.

Figure 1-1: Tangential and radial dipoles
Illustration of the scalp, skull and cortex. The cortex shows the gyri and sulci structures and the tangential dipoles (red arrows and radial dipoles (gree arrows) measured with the EEG electrodes on the scalp. Reproduced from (Nunez and Srinivasan, 2005)

Radial and tangential dipoles both contribute to the measured EEG signal, although it is thought that radial dipoles contribute more than tangential dipoles to EEG scalp recordings. Radial dipoles are thought to be produced by synchronous sources in many gyri that have dipole axes perpendicular to the skull/scalp, unlike tangential dipoles which result in dipoles oriented parallel to the skull/scalp (Nunez and Srinivasan, 2005). Indeed, a simulation study showed that tangential dipoles of the same strength and depth of radial dipole generally made smaller contribution to scalp potentials (Nunez and Srinivasan, 2005). In addition, tangential dipoles are located more often in deeper locations. However, despite the fact that EEG is mostly sensitive to aligned cortical structures, reports have shown that EEG is also able to detect activity in some strongly folded and deep structures, e.g. in hippocampus and amygdala (Lantz et al., 2001; Michel et al., 2004). The measured surface potential depends on the distribution of current

sources and sinks across the cortex. The neural current caused by the postsynaptic potentials, is also known as the primary current or the current of interest. EEG measures the potential field setup by scalp reaching currents, which are secondary currents in the surrounding medium. The skull causes attenuation and dispersion of the measured ionic currents. These volume currents occur due to effects of the electric field on extra-cellular charge carriers (Plonsey, 1969). The physics of an electrical dipole indicates that the potential produced in the surrounding medium falls off with the square of the distance. Physiologically, that would suggest that the deeper the source, the smaller the recorded EEG signal. In the case of a dipole layer such as the cortical surface, the fall-off with distance from a dipole layer is much slower compared to a single dipole. In addition, the head and skull are inhomogeneous, which can cause decreases in scalp potentials from sources close to the cortex surface, and increases in scalp potentials from deeper sources, due to the current line compression on the head (Nunez and Srinivasan, 2005). Therefore EEG is not only able to depict local sources, but also deeper sources. The lateral surface of the superior temporal cortex will be the focus of this dissertation.

Event-related potentials (ERPs) describe the measured electrical potential to the occurrence of temporally well-defined events or stimuli. ERP signals are typically very small and embedded in a background of spontaneous electrical activity (Sanei and Chambers, 2007). Therefore, most commonly, trials are averaged over repeated instances of the same event to increase the signal-to-noise ratio (SNR) and obtain an ERP response. Generally, ERP waveforms are characterized by three main features: amplitude, latency and scalp distribution. ERP signals are labeled according to the direction of their amplitude and their latency. For example, the N100 denotes a negative ERP response occurring at ~100ms, whereas the P300 describes a positive ERP response occurring at ~300ms (Sanei and Chambers, 2007). It is believed that earlier components

in the ERP generally reflect sensory processing, whereas later components are associated with cognitive processes.

In order to identify the loci of neural activation observed with ERPs, source localization techniques are applied. Source localization is not trivial because an infinite number of different source configurations can produce the same scalp potential, a problem known as the inverse problem(Nunez and Srinivasan, 2005). The model of the underlying system consists of a head and a source model. The head model describes the volume conductor (brain, scalp, skull), and the source model describes the current distribution produced by large sets of neurons. There are two main types of source models: dipole and distributed models. Dipole models apply best to over-determined systems, with fewer neural sources than recording electrodes. Distributed models are better representations for under-determined systems, with more sources than electrodes. In this dissertation, distributed modeling was used for source reconstruction because multiple sources contribute to the P300 ERP component of interest in this study.

1.3 Functional MRI

Magnetic resonance imaging (MRI) was invented in 1973 by Paul Lauterbur (Lauterbur, 1973) and applied to cognitive neuroscience in the mid-1980s. In the past decade, functional MRI has become widely used to study the normal human brain, degenerative brain diseases like Alzheimer's (Prvulovic et al., 2011; Sperling, 2011) and Parkinson's (Ibarretxe-Bilbao et al., 2011), learning disabilities such as dyslexia (Shaywitz et al., 2006), and for presurgical mapping, for example in epilepsy patients (Swanson et al., 2007).

The blood-oxygen level dependent (BOLD) contrast, on which fMRI is based, is most often used to detect hemodynamic changes in the brain, typically associated with neural activity (Belliveau et al., 1990; Ogawa et al., 1990). The process of neuronal firing requires energy in the form of ATP. During periods of increased activity, the energy reserves become depleted within active neurons, and a hemodynamic response is triggered in the brain to ensure rapid delivery of new ATP. This process facilitates the generation of energy required by active neurons and leads to a surplus of oxyhemoglobin. Hemoglobin, which is diamagnetic when oxygenated and paramagnetic when deoxygenated, can be detected with the MR scanner such that a local increase in deoxyhemoglobin causes a local decrease in the BOLD signal. Higher BOLD signal intensities arise from increases in the concentration of oxygenated hemoglobin. The local ratio of oxyhemoglobin to deoxyhemoglobin causes a change in the BOLD contrast measured with fMRI. BOLD, like ERPs, has been shown to be more strongly correlated with local field potentials, reflecting mostly the synaptic input to a neural circuit. However, multi-unit activity, reflecting mostly the spiking output from a neural circuit also contributes to the BOLD signal (Logothetis et al., 2001).

FMRI is widely used in neuroimaging due to its high spatial resolution, on the order of 1-2 mm in humans (Huettel et al., 2009). However, the specificity of the fMRI signal is dependent on the MR acquisition parameters and MR hardware used. For example, gradient-echo sequences are sensitive to large vessels (in addition to small vessels), which may reflect neural activity from a more remote brain area. However, this problem is minimal at higher field strengths (3T or higher). In contrast, spin-echo sequences represent mostly capillary signals, reflecting activity from nearby brain areas (Ullsperger and Debener, 2010). Nevertheless, gradient-echo sequences are widely used because they enable faster whole brain fMRI acquisition compared to spin-echo

sequences. In addition, the availability of scanners with higher field strengths, has essentially eliminated the problem of sensitivity of the BOLD signal to large vessels.

FMRI has low temporal resolution due to the sluggish nature of the hemodynamic response. Thus, fMRI does not typically reflect quick neuronal changes, even if images can be obtained rapidly (Faro, 2006). Brief synchronous neural activity (<hundreds of milliseconds) may not elicit a measurable hemodynamic response with BOLD, making fMRI more sensitive to prolonged activation (>hundreds of milliseconds) in the brain. Another case when an fMRI response may not be elicited is when a cortical patch generates an EEG signal by increasing synchronicity in a small patch of cortex without changing the metabolic consumption (Babiloni and Cincotti, 2004). The hemodynamic response following neural activation is observed at one to two seconds latency and reaches its peak from four to eight seconds following neural activation (Faro, 2006).

1.4   Relationship between neural activity and hemodynamic changes

Neural activity in the brain causes local hemodynamic changes to support the increased metabolic demands of active neurons. In active neurons, the generation of action potentials and synaptic transmission at the dendrites introduce excess K^+ and H^+ into the extracellular matrix, causing dilation of arterioles (Kuschinsky et al., 1972; Nguyen et al., 2000). In addition, a sudden increase in the demand for energy during synaptic activity can result in a relative lack of O_2 and glucose, causing an increase in blood flow and blood volume (Attwell and Iadecola, 2002). The increase in intracellular Ca^{++} during neural activity activates the Ca-dependent enzyme neuronal nitric oxide synthase (nNOS), which produces the vasodilator nitric oxide (NO). There is ample evidence that NO also contributes to the increase in cerebral blow flow (CBF) produced by functional activity (Northington et al., 1992; Akgoren et al., 1994; Iadecola et al., 1995; Lindauer et al., 1999; Buerk et al., 2003).

Linear and nonlinear relationships between neural activity and the hemodynamic response have been found in humans (Logothetis et al., 2001; Zhang et al., 2008a; Liu et al., 2010) and in animal models (Mathiesen et al., 1998; Ngai et al., 1999; Ances et al., 2000; Heeger et al., 2000; Rees et al., 2000; Logothetis et al., 2001; Hewson-Stoate et al., 2005). At a macroscopic level, changes in neural activity can produce linear or nonlinear changes in the hemodynamic response. For example, it was shown that if the inter-stimulus interval is very short (0.25-4s), the BOLD response is often non-linear due to non-linearity in the vascular response (Liu et al., 2010). For longer intervals, a strong linear relationship between neural activity and hemodynamic response may be observed (Liu et al., 2010).

1.5 Temporal dynamics of information processing in brain networks

The brain can be described as an incredibly complex set of networks of functionally and structurally interconnected regions that continuously share information. A brain network can be described in terms of the temporal evolution of information flow between brain regions. While the information flow reflects the activity of millions of neurons over short timescales (tens to hundreds of ms), the neural activity results in a slow and sluggish hemodynamic response in the brain (Boynton et al., 1996). For example, one study showed that in the understanding of intention, two functionally separable cortical networks are recruited (Grafton, 2009). A frontal-parietal network, "action-observation network", which performs sensorimotor integration and a second "social" network, involving the insula, prefrontal cortex, amygdala and precuneate cortex. There has been much interest in exactly how, when, and where in the brain these networks share information. In this work, specifically we are trying to identify the spatio-temporal relationship of brain networks associated with the auditory oddball paradigm using fMRI and ERP.

1.6 Simultaneous fMRI and ERP

Unimodal neuroimaging is limited by lack of spatial or temporal specificity, and/or invasiveness. Numerous analysis techniques have been developed to combine fMRI and ERP data to generate high temporally and spatially resolved images, see Rosa et al. for a review (Rosa et al., 2011). Compared to other integrated neuroimaging approaches, such as combining magnetoencephalography (MEG) with near infrared spectroscopy (NIRS) (Mackert et al., 2008) or with intracortical recordings (Weber et al., 2008), the advantages of combined acquisition of fMRI and ERP include the ability to (1) acquire data from both modalities simultaneously, (2) collect data non-invasively (compared to intracortical recordings), (3) achieve high 3D spatial resolution via fMRI (compared to the lower resolution of NIRS) and high temporal resolution via ERP (Nunez and Srinivasan, 2005). (4) Furthermore, unlike MEG or NIRS, both fMRI and ERP are readily available in most clinical settings. Compared to MEG, ERP has the added advantage of being more sensitive to deep neural sources (Nunez and Srinivasan, 2005). On the other hand, magnetic fields are less prone to smearing by non-conductive elements (the skull) than electrical fields, resulting in somewhat higher spatial resolution of superficial sources with MEG compared to ERP.

Simultaneous fMRI/ERP can be enhanced by using clustered image acquisition. In this method, image acquisition is clustered at relatively long intervals (7 sec and above), such that artifacts in the ERP related to fMRI acquisition are limited to ERP epochs with no events of interest (Liebenthal et al., 2003). The effect of acoustic scanner noise during sound presentation

is also minimized, an important feature for auditory tasks (Yang et al., 2000), such as those used in the studies detailed here.

1.7   Model-based and data-driven techniques for the integration of fMRI and ERP

Approaches to integration of fMRI and ERPs can broadly be divided into model-based and data-driven techniques. A variety of model-based methods have been developed to integrate ERP and fMRI data, see Huster et al. and Rosa et al. for a review (Rosa et al., 2011; Huster et al., 2012). Linear regression is a well-known and robust method for multimodal integration, but it may neglect nonlinear relationships and therefore not fully capture brain activity. In the simplest formulation, the peak amplitude of an ERP component in an ERP time-series is used as a regressor in the fMRI data analysis, within the framework of the general linear model (Horovitz et al., 2002; Liebenthal et al., 2003). The ERP source analysis can also be informed by spatial constraints extracted from the fMRI maps (Babiloni et al., 2000; Dale and Halgren, 2001; Vanni et al., 2004; Esposito et al., 2009).

A variety of studies have reported data-driven approaches for ERP-fMRI data fusion using a trial by trial design in individual data, for example using a multiway partial least squares analysis to correlate between fMRI time courses and spectral components of the ERP (Martinez-Montes et al., 2004). Another proposed method to integrate ERP and fMRI uses a multi-set canonical correlation analysis, which maximizes correlated variations across trials between ERP and fMRI (Correa et al., 2010). ERP and fMRI can also be combined by extracting fMRI ICA components that are then used to compute cross-modal correlations with single-trial ERP

amplitudes (Huster et al., 2011). Bayesian frameworks have been developed to integrate ERP and fMRI (Daunizeau et al., 2007) and also MEG and fMRI (Plis et al., 2010).

Recently, data-driven approaches such as joint independent component analysis (jICA), have been implemented to integrate ERP and fMRI data by searching for co-varying signals across subjects (Calhoun et al., 2009; Mijovic et al., 2012). The advantage of ICA, and data-driven approaches in general, lies in their ability to estimate the underlying processes when detailed *á priori* models are not available (Calhoun et al., 2006). A distinction of the jICA approach is the use of a common mixing matrix for the ERP and fMRI data. Compared to other approaches using a separate mixing matrix (Correa et al., 2008; Brown et al., 2010), jICA may be particularly sensitive to linked activation between ERP and fMRI (Calhoun et al., 2006; Mangalathu-Arumana et al., 2012), but not limited to correlated sources, such as the P300 linear regression model. JICA, unlike other data-driven techniques, assumes a common modulation profile across task conditions. This is a reasonable assumption, especially in parametric paradigms, where neural activity is systematically modulated across experimental levels.

Some data-driven techniques limit the analysis to just a few (1-4) electrodes of interest (Eichele et al., 2005; Calhoun et al., 2006; Correa et al., 2010). JICA has been applied to experimental ERP and fMRI data to spatially and temporally resolve brain areas active during auditory and visual oddball detection, albeit using data from a single EEG electrode across a group of subjects (Calhoun et al., 2006; Mijovic et al., 2012). Computational simulations have suggested that jICA may be applicable to within-subject analysis, using spatial and temporal information from multi-channel ERP and spatial information from fMRI (Moosmann et al., 2008). JICA of multi-channel ERP data for within-subject analysis has also recently been demonstrated experimentally (Mangalathu-Arumana et al., 2012). In this work, the full array of

ERP multichannel data was used in the context of a parametric paradigm to enhance the sensitivity of the technique to co-varying ERP and fMRI signals.

1.8   Auditory oddball paradigm

The oddball paradigm was chosen in this dissertation, since it is well documented, proven to be clinically useful (Polich and Corey-Bloom, 2005), and yields relatively robust and large responses. Auditory stimuli have been selected for this investigation because auditory processing is essential for speech perception, one of the main functions of the brain that can be impaired following stroke. The auditory oddball paradigm consists of a sequence of frequent standard sounds and infrequent target or deviant sounds. Attentive deviance detection, typically studied with an oddball paradigm, elicits most notably a positive ERP component at an approximate latency of 300 ms (termed the P300). Simultaneous fMRI/ERP has been used to determine the major brain areas involved in attentive auditory deviance detection (Menon et al., 1997; Opitz et al., 1999; Mulert et al., 2004). Amplitude and latency measures of the P300 have proven to be clinically useful indices in a number of diseases, such as Alzheimer's (Polich and Corey-Bloom, 2005), dementia (Kraiuhin et al., 1986; Sara et al., 1988), and schizophrenia (Louza and Maurer, 1989; Louza et al., 1992). Intracortical recordings from epileptic patients indicate that the P300 elicited during an auditory oddball paradigm receives contributions from temporal lobe structures (Halgren et al., 1980; McCarthy et al., 1989). Scalp recordings from patients with lesions in the temporo-parietal lobe suggest that the integrity of the temporo-parietal junction is critical for the generation of the auditory P300 (Knight, 1984; Verleger et al., 1994). FMRI activation and ERP source reconstruction results from our study suggest that the major

generators of the auditory P300 are distributed in areas of the temporo-parietal junction and parietal cortex (Liebenthal et al., 2003; Mangalathu-Arumana et al., 2012).

1.9   Aims and Significance of Research

The goal of the proposed work is to develop an optimal paradigm and tailored analysis methods to fuse fMRI and ERP, with high temporal and spatial resolution. To achieve this goal, the research addresses three specific aims:

Specific Aim 1:   Develop an optimal parametric paradigm for determining the spatial and temporal dynamics of activity measured with ERP and fMRI in a wide neural network in healthy human subjects. An auditory P300 ERP oddball paradigm will be used in the context of a parametric manipulation to extract neural signals that vary with experimental condition (deviant level). The parametric paradigm has the virtue of increasing the variability of the measured signal, and thereby the sensitivity of the analysis method to detecting ERP and fMRI changes that are systematically related to the varied parameter.

Specific Aim 2: Evaluate joint independent component analysis (jICA) for the fusion of fMRI and ERP signals in individual data, incorporating the full spatial and temporal information from both imaging modalities. The jICA approach will be compared to a multiple regression analysis using the P300 peak amplitude in a general linear model. Spatio-temporal jICA will be applied to localize neural sources related to the P300 within-subject. The full multi-channel array of EEG electrodes will be used, to enhance the sensitivity of jICA for extracting neural sources measured with fMRI and ERP.

Specific Aim 3: Characterize the separation of neural sources with jICA as a function of the experimental design and the coupling relationship between fMRI and ERP sources. Investigate the effect of various parameters of the experimental design on the jICA results, by simulating fMRI and ERP measurements of neural sources. A computational model will be implemented on a distributed computing cluster such that hundreds of simulations can be performed to test jICA in a wide range of conditions. The computational model will simulate fMRI and ERP measurements to known sources of neural activity to test the reliability of the jICA method for localizing neural activity as a function of several factors including, the SNR of ERP and fMRI measurements, the number of experimental samples, and the nature of the relationship between ERP and fMRI signals.

This work is based on the data-driven technique termed jICA, first developed by Calhoun and colleagues (Calhoun et al., 2006) to integrate ERP and fMRI data across subjects. In jICA, a joint coefficient matrix between ERP and fMRI is incorporated to extract linked activations across task conditions. A distinct advantage of jICA is that it is not limited to linear relationships between ERP and fMRI, such as generalized linear models, but is also sensitive to nonlinear relationships. To date, jICA has been used to integrate fMRI with ERP across subjects, using just one EEG recording electrode (Calhoun et al., 2006). A specific novelty in the present work (Aim 2) is that jICA is applied to individual datasets, using spatial and temporal information from all EEG electrodes and all fMRI trials, in order to increase the sensitivity of the method to detection of neural sources observed in ERP and fMRI. Developing a method for individual data analysis is critical for clinical assessment of pathological conditions, where patient-specific diagnosis is needed. The inclusion of all spatio-temporal information from the ERP and spatial information

from the fMRI is expected increase the detection of neural sources with ERP and fMRI, not only at the group level, but also at the single subject level.

Computational simulations will be used in Aim 3 to test the reliability of jICA for detection of neural sources measured with ERP and fMRI under different experimental conditions. Specifically, the SNR of neuroimaging data, number of experimental conditions, and type of relationship between ERP and fMRI signals will be investigated. A comprehensive sensitivity analysis of jICA, using a theoretical model to simulate sources throughout the brain, has not been published before and is a necessary pre-requisite before systematic and wide-spread use of jICA to fuse neuroimaging modalities can occur.

The ultimate goal of the proposed work is to establish a reliable method to assess neural activity recorded with ERP and fMRI. The methods developed here could have a significant impact for future studies of brain networks involving sensory-motor, language and memory processing in healthy brains, and eventually in patients with altered or dysfunctional brains. For example, in some diseases such as Alzheimer's the increase in CBF following activation is attenuated, leading to local alterations of the normal relationship between neural activity and hemodynamic responses in the brain. The methodology proposed here to integrate fMRI and ERP is an important step toward establishing its clinical relevance, and toward enhancing the study of functional processing in the brain with high spatial and temporal resolution

CHAPTER 2

Within-subject joint independent component analysis of simultaneous fMRI / ERP in an auditory oddball paradigm

2.1 INTRODUCTION

The following chapter addresses Aims 1 and 2 of the dissertation and is largely based on a paper published recently in the journal *Neuroimage* (Mangalathu-Arumana et al., 2012). The advent of neuroimaging has led to major advances in understanding how the brain processes complex sensory information such as speech, and controls cognitive functions such as memory and learning. Characterizing the cortical networks involved in these processes has improved our understanding of brain function, our ability to model neural processes, and our ability to diagnose and rehabilitate patients with neurologic deficits. Non-invasive neuroimaging techniques, such as fMRI, electroencephalography (EEG) and magnetoencephalography (MEG) are at the heart of current research in Cognitive Neuroscience. Major efforts have been directed toward optimizing the methods to temporally and spatially resolve neural activity. FMRI can be acquired in a single-slice with a temporal resolution of 100 ms, and recent developments hold the promise for sub-second temporal resolution for whole brain acquisitions (Feinberg et al., 2010; Lee et al., 2010). Source reconstruction of EEG, and especially MEG, data can under ideal conditions resolve neural activity within one centimeter with high temporal resolution. Nevertheless, the slow nature of the hemodynamic response recorded in fMRI, and the inverse problem in EEG and MEG source reconstruction, pose inherent limitations for these techniques. Therefore, an attractive alternative to unimodal neuroimaging is to fuse non-invasive imaging methodologies that together offer high spatial and high temporal resolution (Dale and Halgren, 2001). A recent development in this respect has been the integration of event-related potentials (ERPs) and functional magnetic resonance imaging

(fMRI) recorded simultaneously in large-scale networks to capitalize on the high temporal resolution of ERPs and the spatially well-defined fMRI response (Bonmassar et al., 2001; Liebenthal et al., 2003).

Despite the consensus that fMRI and ERPs both reflect essentially the same type of neural activity (synaptic potentials), it is important to note that there are significant differences between the measures, which may cause discrepancies in the estimation of neural sources. In particular, brief synchronous neural activity may be captured with EEG but not with imaging of the slow BOLD response. In contrast, neural activity in a limited brain region may be visible with fMRI, but located too deep or oriented such that it does not elicit a significant ERP response (Nunez and Silberstein, 2000).

A variety of model-based methods have been developed to integrate ERP and fMRI data. Linear regression provides a well-known and robust method for multimodal integration, but it may not fully capture the richness of human brain activity. In the simplest formulation, the peak amplitude of an ERP component in an EEG time-series is used as a regressor in the fMRI data analysis, within the framework of the general linear model (Horovitz et al., 2002; Liebenthal et al., 2003). The ERP source analysis can also be informed by spatial constraints extracted from the fMRI maps (Dale and Halgren, 2001; Vanni et al., 2004; Esposito et al., 2009).

Recently, data-driven approaches such as joint independent component analysis (jICA) have been implemented to integrate ERP and fMRI data, by searching for co-varying signals across subjects (Calhoun et al., 2009; Mijovic et al., 2012). The advantage of ICA, and data-driven approaches in general, lies in their ability to estimate the underlying processes when detailed *á priori* models are not available (Calhoun et al.,

2006). JICA can recover both linear and non-linear relationships across experimental conditions and between imaging modalities. Another advantage of jICA is that it permits incorporation of multiple sources of spatial and temporal information, thereby potentially enhancing the sensitivity of the method to co-varying signals. This approach has been applied to experimental ERP and fMRI data to spatially and temporally resolve brain areas active during auditory and visual oddball detection, albeit using data from a single EEG electrode across a group of subjects (Calhoun et al., 2006; Mijovic et al., 2012). Computational simulations have suggested that jICA may be applicable to within-subject analysis, using spatial and temporal information from multi-channel ERP and spatial information from fMRI (Moosmann et al., 2008). But the potential benefits of incorporating multichannel ERP data, and its application to experimental results, have not been systematically tested.

In this study, we examined the sensitivity of jICA and the value of incorporating the full spatial and temporal array of fMRI and ERP data for resolving neural activity at a single subject level using a parametric auditory oddball paradigm (Specific Aims 1 & 2). The oddball paradigm was selected because it yields extensive and robust responses in brain regions associated with sensory processing, categorization, response selection, and motor planning and execution. The P300 ERP response associated with the oddball paradigm reflects neural processes related to target detection (Ritter and Vaughan, 1969; Coles et al., 1988; Picton, 1992; Polich, 2007), and the neural generators of this response have been studied with electrophysiological methods (Smith et al., 1990; Basile et al., 1997; Menon et al., 1997; Halgren et al., 1998; Mecklinger et al., 1998) and fMRI (Linden et al., 1999; Kiehl et al., 2005; Friedman et al., 2009). Another advantage of the

oddball paradigm is that it lends itself well to a parametric design. In particular, the P300 peak amplitude decreases with the increase in target detection difficulty, as indicated by decreased performance accuracy and/or increased reaction time (Polich, 2007)). In the present study, task difficulty was manipulated and a general linear model analysis of the fMRI data based on the ERP P300 peak amplitude was used as a reference (Aim1) to compare with jICA of single subject and group data (Aim2).

2.2   METHODS

2.2.1   Participants

Twenty-four healthy, right-handed volunteers, ages 18-40 years, participated in the study. Participants provided written and informed consent according to the Institutional Review Boards of the Medical College of Wisconsin and Marquette University, and were compensated for their participation in the study. Participants with no history of neurological disease and normal hearing as assessed by audiometry at 1-4 kHz were enrolled in the study. Prior to scanning, psychometric curves were obtained for each subject based on their ability to discriminate differences in frequency (ranging from 2-40 Hz) about a 1000 Hz tone. A minimum discrimination accuracy of 95% at 40 Hz difference was required for inclusion in the study, and all participants passed this criterion. Data from four participants were subsequently excluded, two due to excessive motion during scanning, and two due to noisy EEG. The criterion for excessive motion was a rejection of more than 5% of the total number of trials due to motion greater than 5% of the total number of voxels in the dataset relative to a base functional magnetic resonance image (see image analysis below). The criterion for noisy EEG was defined as a mean baseline variance across electrodes that exceeded 10 µV.

A group size of twenty-four subjects and 40 images per experimental condition was chosen based on simulations showing that a sample size of approximately twenty

subjects is necessary to achieve 80% power at $\alpha=0.002$ (two-tailed) (Desmond and Glover, 2002). Kiehl showed that a high reproducibility of the hemodynamic response in a target detection task can be obtained with a group of 20 subjects (Kiehl and Liddle, 2003). However, there are no relevant papers regarding how many trials are needed at an individual data analysis in an auditory oddball paradigm.
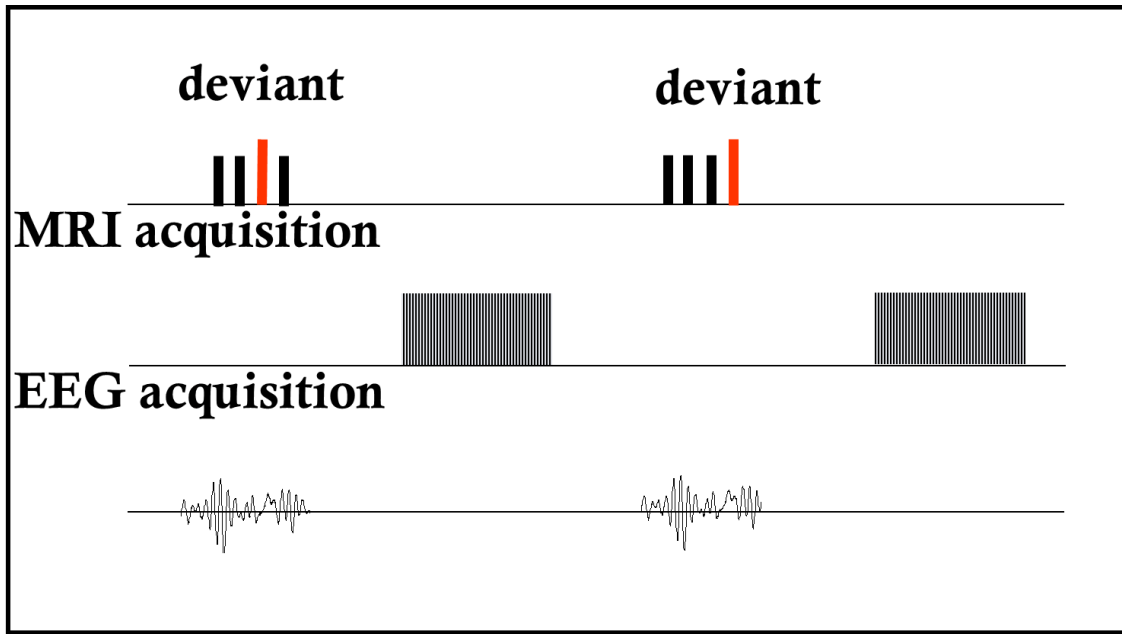
In simultaneous fMRI-ERP acquisition, the SNR of ERPs is often degraded due the MRI environment noise. Generally, it is recommended to collect two or three times more trials than the number collected outside of the MRI scanner (Kruggel et al., 2001). In this study, based on pilot testing in five subjects with data collected inside and outside the scanner, a total number of one-hundred and forty four trials was determined to be sufficient to extract ERPs in the MRI scanner of comparable quality to those acquired outside of the scanner. Artifacts in the ERP and fMRI measurements caused by subject movement were reduced through use of a memory foam pillow to restrict head movement during scanning. The pillow also provide added comfort by helping to minimize the pressure of the EEG electrodes. Since subject motion has been found to increase with experiment duration, especially after 45-60 min (Lemieux et al., 2001), the ERP-fMRI study was divided into two sessions, each 40 minutes long. This reduced the discomfort of the subject, but still provided sufficient SNR in each modality.

2.2.2   Experimental Design

A tone auditory oddball paradigm was employed, composed of three repetitive standard 1000 Hz tones and one rare deviant target tone presented binaurally, which was

higher or lower in frequency compared to the standard tone (2 - 40Hz) is shown in Figure 2-1. This frequency range was chosen due to the sensitivity of the human auditory system in this frequency range. The task consisted of pressing one of two buttons to indicate whether a deviant tone was of a higher or lower frequency than the repetitive standard tones (and to guess if they could not detect the deviant). The tones were of 100 ms duration with rise/fall times of 5ms, and were presented at 800 ms stimulus onset asynchrony (SOA). This SOA time allowed for the neural activity to return to baseline before the next stimulus was applied. The frequency deviant was inserted in position 3 or 4 in the sequence in order to reduce subject's expectation of the deviant tone and also sustain attention to the task. Subject would participate in a total of three sessions. Session one was a behavioral study, where each subject was tested on sixteen levels of deviant frequency differences (2-40Hz lower or higher compared to standard tone=100Hz). Each participant's psychometric curve was determined, using a least-square error Weilbull fit to determine five levels of difficulty corresponding to 50%, 65%, 75%, 85% and 95% accuracy for testing during the simultaneous fMRI-ERP session. Session two and three subjects would participate in an FMRI-ERP experiment. The deviant tone was chosen from one of ten possible frequencies, five lower and five higher than the standard tone frequency, corresponding to five levels of task difficulty. One hundred and forty four trials were presented at each of the five levels, for a total of 720 trials, broken into twelve separate runs, acquired in two recording sessions on separate days. The onset of each auditory sequence was jittered relative to the time of image acquisition, such that the deviant tone was always presented 4000 ms before the middle of the next image acquisition block, and the image acquisition coincided with the estimated peak of the

BOLD response (Hall et al., 1999). Auditory stimuli were delivered using a pneumatic, MRI-compatible headphone system (Avotec, Inc., Stuart, FL), and the sequence of stimulus presentation was controlled with the Presentation software (Neurobehavioral Systems Inc., San Pablo, CA).

Figure 2-1: Auditory oddball paradigm
Auditory oddball paradigm consisting of three standard tones and one deviant tone. FMRI was acquired in a clustered manner, and EEG was acquired continuously. However, ERPs were analyzed only around the deviant tone during the silent interval, where MRI gradients were off.

2.2.3 fMRI Acquisition

The study was conducted on a GE 3T Signa Excite scanner (GE Health Care, Milwaukee, WI). Functional MR images consisted of T_2^*-weighted, gradient-echo, echo planar images acquired using a clustered volume acquisition (Belin et al., 1999; Edmister et al., 1999; Liebenthal et al., 2003) (TE=25ms; flip angle=77°; TR=7s; slices=33), with a five second silent interval. Axially-oriented contiguous slices (3x3x3.5mm voxels)

covering the entire brain were acquired (image acquisition=2.0s). High-resolution anatomical images of the entire brain were also acquired using a 3D spoiled gradient-echo (SPGR) sequence (0.9x0.9x1mm voxels).

Clustered image acquisition offers several advantages: (1) the silent interval allows the subject to listen to the auditory sequences without acoustic masking by the MR gradients; (2) The clustered acquisition helps avoid gradient artifacts in the EEG periods of interest. Since in this study we are specifically interested in the ERPs around the deviant tone, which are presented during the time when MR gradients are switched off; (3) clustered image acquisition provides maximal separation between the hemodynamic response to the acoustic noise of the scanner (of no interest) and the hemodynamic response to the sound stimuli (which are the objective of the study) (Liebenthal et al., 2003). One of the major disadvantages with the clustered acquisition is that only one image is collected per trial and therefore the temporal course of the hemodynamic response cannot be assessed, also there is a strong assumption that the collection is at the peak of the hemodynamic response function, which could be missed, since only one data point is acquired for each trial.

2.2.4   EEG Acquisition

EEG was recorded continuously using an MRI-compatible MagLink system consisting of a 64-channel MagLink cap (62 monopolar electrodes, and 2 bipolar leads for ECG and VEOG), SynAmps 2 amplifiers, and a Scan 4.4 Workstation (Compumedics
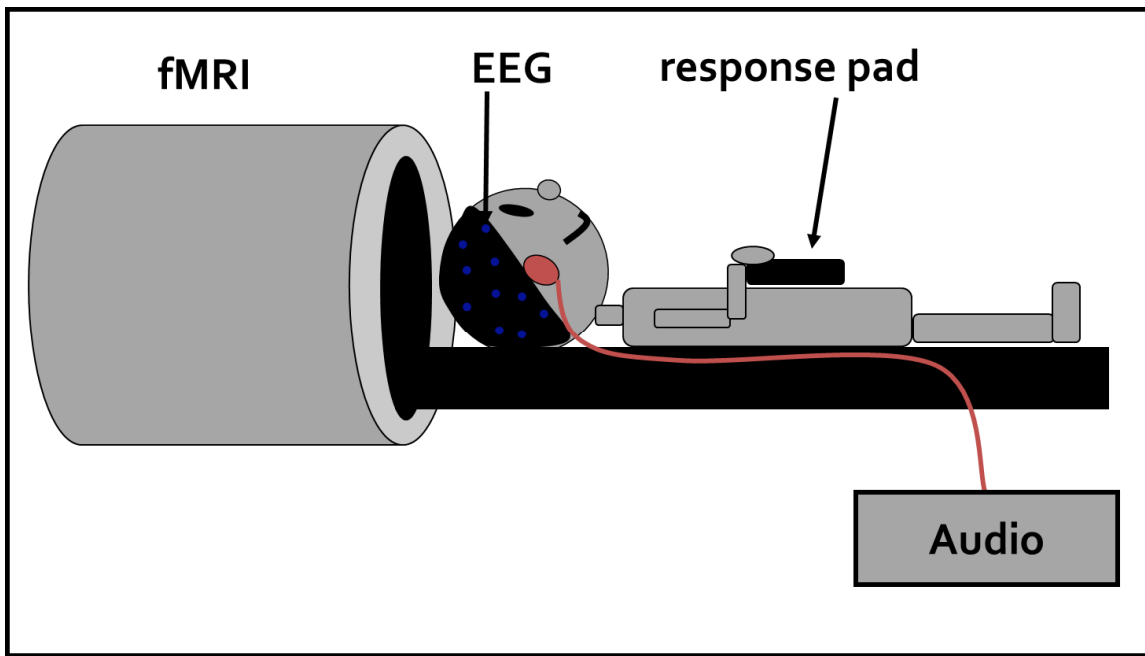
Neuroscan, Inc., TX). An experimental setup of the subject in the MRI scanner wearing a

EEG cap is shown in

Figure 2-2. Maglink is a passive, carbon-fiber system. The Synamps' 2 amplifiers were

used with wide bandwidth DC recording to allow fast recovery after large gradient

artifacts and ensure that the amplifier did not saturate. The Maglink cap is an elastic

electrode cap with three types of head sizes (small, medium, large). Sintered Ag/Ag-Cl

electrodes were positioned according to the extended International 10-20 system (Jasper,

1958), with a hard-wired reference located at CPz. EEG was recorded at 500Hz, and

subsequently band-limited from 0-100Hz for analysis.

Subjects were asked to wash their hair right before the experiment and to not use

any hair products (gel and hair spray) that could coat the scalp and reduce the SNR of

EEG recordings. Prior to cap-positioning, subjects were asked to brush their hair for

about 5 minutes to remove dead skin cells from the scalp and reduce interface

impedances between the scalp and the electrodes. An appropriate cap size (small,

medium, large) was chosen for each subject, as determined manually by locating three

main electrodes (FZ, CZ, PZ) on the head (middle fronto-central, middle central, middle

parietal). Electrode gel was injected into each electrode to reduce the impedance (to < 5

$– 10$ kΩ) between the scalp and the electrodes. The amount of electrode gel used in each

electrode was limited to prevent bridging between adjacent electrodes and ensure

collection of unique information. In addition to the electrodes on the cap,

electrocardiogram (ECG) and electrooculogram (EOG) bipolar electrodes, and two

monopolar mastoid electrodes were used. Before positioning these loose electrodes, the

chest area, mastoids (left and right) and eye area (above and below left eye) were cleaned

with alcohol and exfoliated. Gel was injected into the electrodes and the electrodes were taped onto the skin.

The heart beat causes a ballistocardogram artifact, which can subsequently be removed by computing a template ECG waveform from the ECG electrodes and subtracting it from the EEG data. EOG electrodes are typically used for removing eye blink artifacts. However in this study, subjects were instructed to not blink during the auditory sequences and therefore the occurrence of blinks during EEG periods of interest was minimal. Trials in which the EEG signal exceeded amplitudes of 200µV were rejected. Since eye blink artifacts are larger than 200 µV, this procedure removed any remaining trials contaminated with eye blink artifacts, and specific eye blink artifact removal was not necessary.

Figure 2-2: Experimental setup of subject
Experimental setup of subject in the MRI scanner, with EEG acquisition using an elastic EEG cap. The response pad was positioned under the right hand for responses to the deviant tone. Auditory tones were delivered through headphones.

2.2.5   FMRI linear regression analysis

Functional MR image analysis was performed using the AFNI software package (Cox, 1996). The raw fMRI data 2D image slices were converted into 3D datasets using the to3D function (AFNI). For each subject the functional images were volumetrically registered to a base image (image 3 in run 1) (3dvolreg function in AFNI), which was acquired close in time to the anatomical images and after the BOLD signal had stabilized. Volume registration was performed to account for head movements during scanning and also to ensure that each voxel always corresponded to the same location in the brain for all trials. In addition, motion parameters were also saved with this analysis for later use in the general linear model. Images with excessive motion were rejected, the criterion for excessive motion was a rejection of more than 5% of the total number of trials due to motion greater than 5% of the total number of voxels in the dataset relative to a base functional magnetic resonance image, which was determined using the 3dToutcount function (AFNI). Multiple linear regression analysis was then performed to extract BOLD activity associated with the P300 (3dDeconvolve, AFNI function). The 3dDeconvolve program can be used for multiple linear regression analysis, where an input stimulus and the measured fMRI time series are used to estimate the hemodynamic response at each voxel.

In this study, a clustered image acquisition was used and therefore, only one image was collected for each trial. A reference function coding the peak amplitude of the trial-averaged P300 ERP component in each task level was used as an individual regressor to

estimate the hemodynamic response at each voxel. Translation and rotation motion parameters estimated during registration were used as noise covariates in the regression. Anatomical images were transformed into Talairach-Tournoux coordinates (Tournoux, 1988) to spatially normalize data between subjects (@auto_tlrc, AFNI function). The functional images were transformed into Talaraich-Tournoux coordinates using the aligned anatomical images as a template volume (@auto_tlrc, AFNI function). The individual functional maps were then smoothed with a 6mm full width half maximum gaussian filter, and the group results were computed using a random effects voxel-wise t-test against zero (3dttest, AFNI function). The output dataset was thresholded voxel-wise at $p<0.05$, and clusters larger than 882 µl were removed to obtain a map-wise threshold of $\alpha<0.05$, as indicated by Monte-Carlo simulation using alphasim (Cox, 1996). The application of the cluster analysis corrects for multiple comparison by computing the statistical power of cluster formation by chance. A total of 2000 images with a sample mask consisting of the same voxel size as the functional image (64x64x33) were randomly simulated. In order to account for voxel correlation, these images were also blurred with a 6mm gaussian kernel.

2.2.6 EEG preprocessing

EEG analysis was performed using the Scan 4.4 Edit module (Compumedics Neuroscan Inc., TX). Channels showing a variance > 20 µV during the baseline period (-200 to -50 ms) were removed from further analysis. The average number of channels excluded per subject was seven. EEG data were first filtered using a 0.1 – 30 Hz zero-

phase bandpass FIR filter with a 48 dB/octave roll-off. Signals were then corrected to remove the ballistocardiogarm artifact (BA) introduced by the MR environment. ERPs were computed using an epoch time from -200 ms to 800 ms relative to deviant onset. Epochs were baseline corrected to compensate for drifts that occurred during EEG acquisition due to DC mode acquisition. Epochs in which the signal exceeded ±200 µV were deemed to contain artifacts and were discarded. The average number of accepted trials per subject and per condition was 86%. All ERP data were re-referenced to the mastoid electrodes, which is commonly done to visualize the P300 data. In the group analyses, the grand average ERP waveform in each condition was computed by averaging the ERPs across subjects.

2.2.7   Joint Independent Component Analysis (JICA)

The full spatial and temporal array of fMRI and ERP data was integrated here, in a within-subject variation of the group jICA approach described by Calhoun et al. (Calhoun et al., 2006; Calhoun et al., 2010; Edwards et al., 2011). ICA is a data-driven technique used to separate signal mixtures measured from multiple sources. It assumes that the mixture of signals results from distinct sources whose activity is statistically independent. JICA, a variant developed in the context of neuroimaging data, assumes a common mixing matrix between ERP and fMRI sources and making it sensitive to joint activity across neuroimaging modalities. In the formulation developed here, the infomax algorithm (Bell and Sejnowski, 1995), is used to maximize the output entropy of sources

with nonlinear outputs, thereby maximizing the statistical independence of the extracted signals. Entropy is a measure of uncertainty or unpredictability and described as follows:
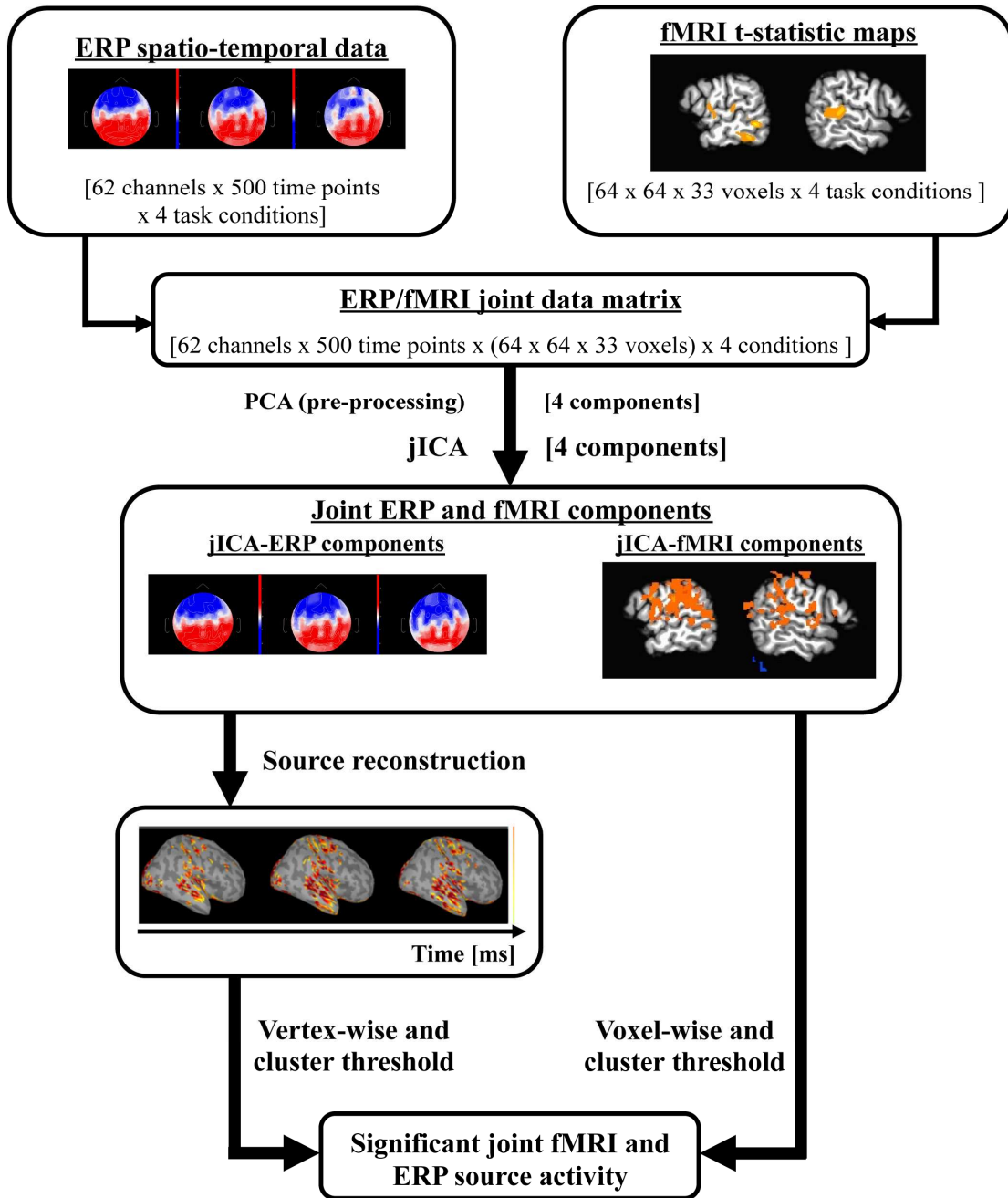
$$H(y) = -\int p(y)\log(p(y)dy \qquad [1]$$

where y represents a random vector with density p(y). High entropy reflects that the variable is random or independent. If **x** is a matrix of measured fMRI and ERP signals across task conditions, reflecting mixtures of the same underlying neural sources, an individual source, y_i, can be extracted

$$y_i = \varphi_i\left(\boldsymbol{b}_i^T \boldsymbol{x}\right) + n \qquad [2]$$

by determining the weight vector, b_i, that maximizes the system entropy with respect to a Gaussian probability density function where ϕ_i is a nonlinear scalar function, and n is additive gaussian noise (Hyvarinen, 2001b).

For jICA within-subject, the unblurred t –statistic fMRI maps were restructured into a NxM matrix where each row corresponded to the flattened image volume (M voxels) obtained for a single experimental condition relative to task level 1(task difficulty level, N=4). The ERP data was restructured into an NxP matrix with each row containing the flattened spatiotemporal sequence of data across electrodes for a single task condition (Figure 2-3).

Figure 2-3: Experimental setup of jICA
Schematic of within-subject jICA across task levels. The ERP data is first concatenated across time points, electrodes and conditions. In the case of the fMRI, voxels are concatenated across conditions. ERP and fMRI datasets are concatenated into a single joint data matrix. PCA is applied as a pre-processing step to whiten the data and jICA was applied to the whitened joint data matrix. Source localization of the jICA-ERP components was used to reconstruct the spatial distribution of source activity across the cortical surface. JICA-fMRI components were voxel-wise and cluster thresholded and jICA-ERP components were vertex-wise and cluster thresholded to identify components with significant joint fMRI and ERP source activity.

The fMRI and ERP data sets were then concatenated to create a joint-Nx(M+P) matrix encompassing the full data set obtained across experimental conditions and imaging modalities. The signals associated with each modality were normalized to their standard deviation, in order to equalize variations across modalities. Principal Component Analysis (PCA) was applied to the normalized joint-matrix to whiten the signal, but the dimension of the dataset was not reduced. Principal component analysis finds projections onto an orthonormal set of basis that span the input and maximizes the data variance across each subsequent projection. Specifically, PCA extracts signals, or principal components, that have an orthogonal basis to each other. The first eigenvector and its weight, which is the first PCA component, give the direction of the maximum variance in the data. PCA basically restructures the correlated variables in a dataset into uncorrelated components by identifying directions in the dataset with maximum variance. Often PCA is used to reduce a large number of measured variables, by discarding principal components with the lowest variance. Whitening reduces the number of parameter estimated with jICA, instead of estimating n^2 parameters in the original mixing matrix A, only need to estimate an orthogonal mixing matrix. Therefore PCA reduces the complexity of the JICA computation. JICA was performed on the PCA extracted components. The jICA model for the ERP and fMRI data was defined as follows:
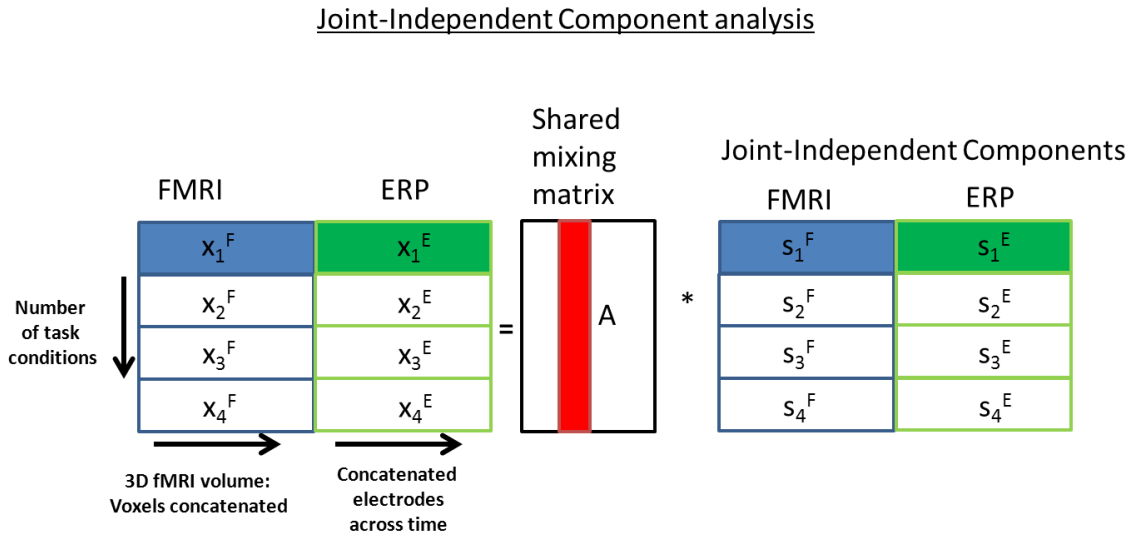
fMRI: $\qquad\qquad\qquad\qquad \mathbf{x^F=As^F}$ $\qquad\qquad\qquad\qquad$ [3]

ERP: $\qquad\qquad\qquad\qquad \mathbf{x^E=As^E}$ $\qquad\qquad\qquad\qquad$ [4]

where $\mathbf{x}^F = [\, x_1^F \; x_2^F \; x_3^F \; x_4^F \,]^T$ and $\mathbf{x}^E = [\, x_1^E \; x_2^E \; x_3^E \; x_4^E \,]^T$ describe the data recorded with fMRI and ERP respectively across four task conditions (Task condition=Levels 2 – 5, Baseline=Level 1), and the common mixing matrix, $\mathbf{A}$, implicitly assumes that the recordings reflect a common mixture of the underlying neural sources in the brain. Since

jICA is applied on the PCA components, $\mathbf{A} = \begin{bmatrix} a_{11} & a_{12} & a_{13} & a_{14} \\ a_{21} & a_{22} & a_{23} & a_{24} \\ a_{31} & a_{32} & a_{33} & a_{34} \\ a_{41} & a_{42} & a_{43} & a_{44} \end{bmatrix}$ describes the mixing

of sources across PCA components. The fMRI and ERP sources, denoted as $\mathbf{s}^F$ and $\mathbf{s}^E$ respectively and referred to as "ICA components", represent the common underlying neural source which varies across task conditions as shown in Figure 2-4. In order to extract the source or ICA component, weight matrix $\mathbf{W} = \mathbf{A}^{-1}$ must be estimated. ICA weights $\mathbf{W}$ were estimated using the infomax algorithm (Bell and Sejnowski, 1995) to minimize mutual information across components.

Joint-Independent Component analysis

Figure 2-4: Illustration of Joint-Independent Component Analysis
JICA assumes a shared mixing matrix (**A**) for the two imaging modalities, fMRI and ERP. The recordings of each modality are denoted by **x**. The 3D fMRI volume, $\mathbf{x}^F$, is concatenated into one row for each task condition. Similarly ERP signals were concatenated across electrodes and time, $\mathbf{x}^E$, for each task condition.

The resulting jICA components consisted of a spatial jICA-fMRI map and a spatiotemporal jICA-ERP map. The jICA-fMRI map was thresholded at $p<0.05$ (voxelwise, as determined from the distribution of all jICA-fMRI components). A corrected map-wise threshold of $\alpha<0.05$ was applied, relative to chance distribution computed by randomizing the jICA-fMRI voxel values of all four components. JICA components whose fMRI signal survived this threshold, and their corresponding jICA-ERP components, were selected for further analysis. With this thresholding scheme, a single jICA-fMRI component survived in each subject.

In the group analysis, the jICA-fMRI map was created by computing the t-value of the mean of twenty components that survived significance against zero. The t-test map was thresholded voxelwise at $p<0.05$ and a corrected map-wise threshold of $\alpha<0.05$ was

applied. The jICA group map consisted of the mean of the twenty jICA-ERP components that survived significance.

In a subsequent analysis, jICA was also applied to a single EEG electrode (Pz) and the entire fMRI data set, to compare against the full spatiotemporal jICA in which all sixty-two EEG channels were used. This analysis was performed to investigate the sensitivity of jICA when more spatiotemporal information is included. The statistical analyses of the jICA components in this were the same as those described above.

2.2.8 Source Reconstruction

Source reconstruction of the individual ERP data and jICA-ERP components was performed using the weighted minimum norm estimate (wMNE) to solve the inverse problem (Brainstorm 3.0, Matlab 2010b). Minimum-norm estimates favor superficial-based currents, this tendency can be alleviated with wMNE, which weights deeper sources. For each subject, the head was modeled in BrainVISA (v. 4.1.1) using the individual high-resolution T1-weighted MR images, and a 3-shell sphere Berg approximation representing the brain, scalp and skull, with conductivities of 0.33, 0.0042 and 0.33, respectively. The cortical surface was parsed and represented as a high-density mesh of vertices, and subsequently down-sampled to 15,000 vertices (in Matlab). Sample electric dipoles were positioned at each vertex, with their directions constrained to be perpendicular to the cortical surface. Electrode positions were determined manually based on the EEG gel artifact observed in the MR images. Source reconstruction of the

grand average ERP and jICA-ERP waveforms was also computed, using the template Colin brain available in Brainstorm.

Current source density estimates were z-score normalized relative to the baseline (-200 to -50 ms prior to deviant onset). Each source map was thresholded vertex-wise at $p<0.05$ relative to the post-stimulus distribution of all vertices across time, and a cluster-threshold (five vertices connected) was applied.

2.2.9 Region of Interest analysis

The source density profiles of the ERP and jICA-ERP data in several regions of interest (ROI) were examined in order to characterize the temporal dynamics of task-related neural sources. ROIs were determined functionally from the fMRI P300 linear regression group maps, and constrained using anatomical definitions from the TT_N27 atlas in Afni. Four ROIs were selected, in the right and left posterior superior temporal gyrus (STG) and in the right and left supramarginal gyrus (SMG). These regions were selected for analysis, because they are commonly activated in the auditory oddball paradigm (Polich, 2007), including in the present study.
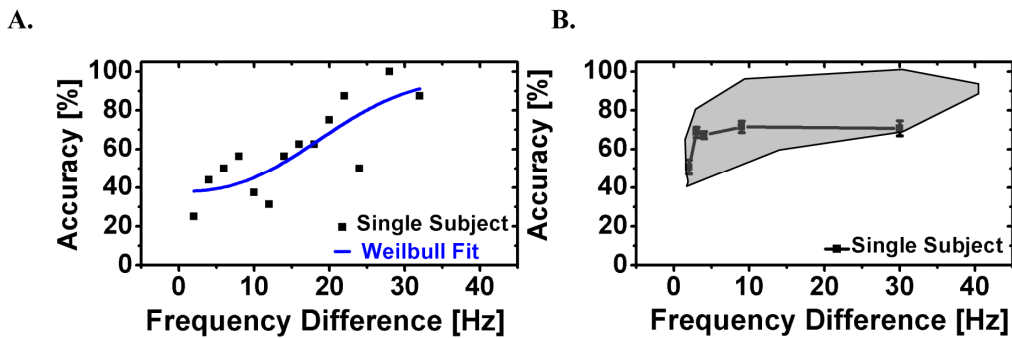
The Colin brain surface model was created using the Colin brain from Brainstorm, reconstructed in Freesurfer (v 5.0). ROIs were projected onto the Colin surface model, which samples the voxel in the gray matter along the direction of the surface normal using nearest neighbor interpolation, and discontinuities in region boundaries were smoothed using a two-vertex region growing algorithm, followed by a two-vertex region reduction to maintain the approximate surface area of the original ROI. For each ROI, the

signal-to-noise ratio (SNR), and the number of vertices that survived a vertex-wise significance threshold of $p<0.05$ relative to the distribution of all vertices across the post-stimulus time interval (0-800 ms), were computed. SNR was computed over time, as the difference between the mean current density across ROI vertices with significant activity ($p<0.05$) in the post-stimulus period and the mean current density across the cortical surface in the baseline period, divided by the variance of the baseline source activity. Vertices in the baseline period were selected randomly with the constraint that the overall number of vertices matched that of the activated vertices within the ROI. Subsequently, the area under the SNR curve was computed for the N100 window at 50-200 ms and for the P300 window at 350-700 ms.

2.3 RESULTS

2.3.1 Behavioral Results

The psychometric curve for tone discrimination in a typical subject (4138) is shown in Figure 2-5 A. In this subject, accuracy varied from 22 to 100 % for frequency differences of 2 and 40 Hz, respectively, and generally increased with frequency difference. A least-square Weilbull fit was used to determine the five task levels for the scanner study, corresponding to prescan accuracies of 50, 65, 75, 85 and 95%. The tone discrimination performance of subject 4138 during the fMRI/ERP study, and the range of performance across the group of twenty participants, are shown in Figure 2-5 B. The results confirm that with increasing frequency difference, performance accuracy increased.
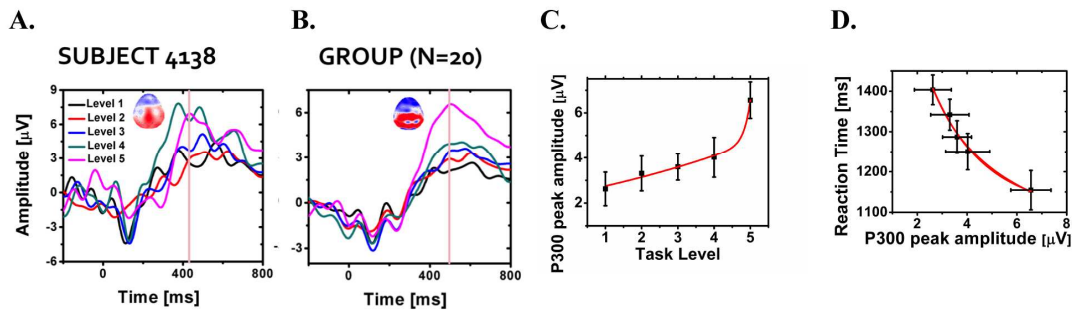
Figure 2-5: Behavioral Results
(A) Prescan tone discrimination performance on the oddball task and least-square error Weibull fit to the psychometric curve for subject 4138. (B) Tone discrimination accuracy (±1 S.E.) for subject 4138 in the fMRI/ERP session at five deviant levels corresponding to 50, 65, 75, 85 and 95% prescan accuracy (black line). The grayed region shows the range in performance accuracy across 20 subjects.

2.3.2 ERP Waveforms

Subject 4138 (A) and grand average (B) ERP waveforms at electrode Pz, at the five task-difficulty levels, are shown in Figure 2-6. The insets show the scalp topography of the ERP component at the peak of the response to the level five frequency difference (420 ms for subject 4138 and 430 ms for the grand average). For both the single subject and the grand average, the increase in amplitude with task difficulty of the component peaking around 430 ms, and its parietal topography, are consistent with the P300 (Polich, 2007). Across subjects, P300 peak amplitude increased with deviant levels (Figure 2-6 C), while reaction time decreased with P300 peak amplitude (Figure 2-6 D). It is noteworthy that the P300 peak response was more accurately modeled as nonlinear (2-parameter exponential) versus linear relative to task level (r^2 = 0.98 and 0.75, respectively), and reaction time (r^2 = 0.96 and 0.86, respectively).
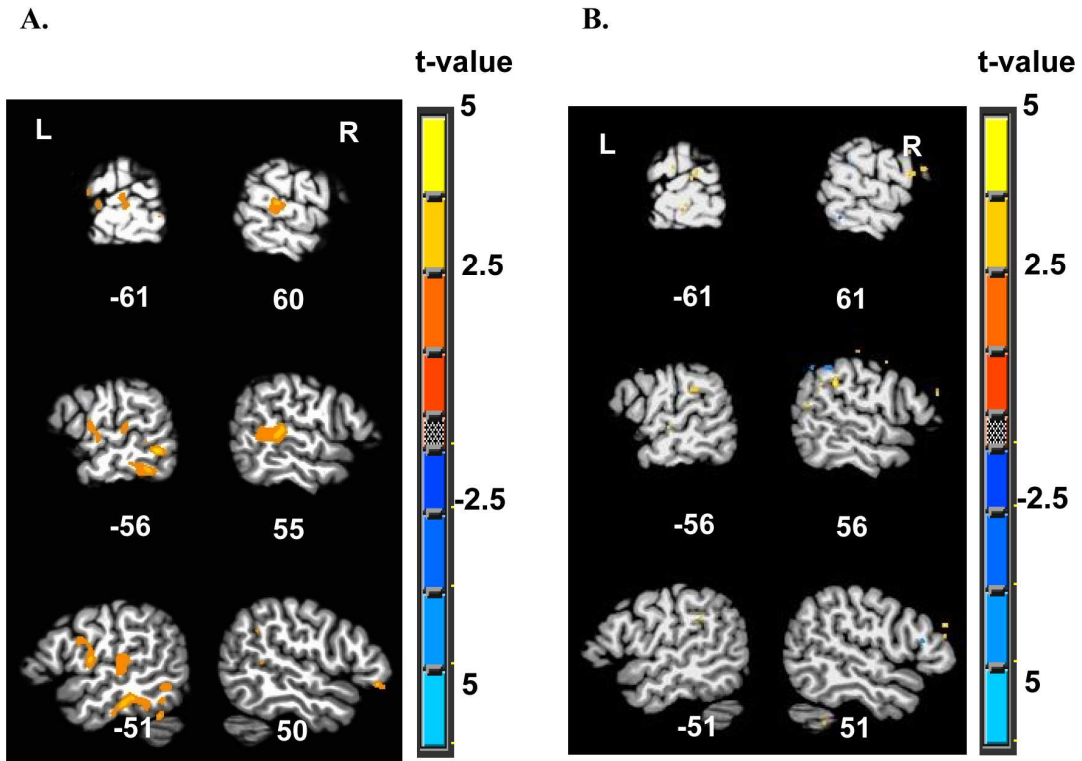
Figure 2-6: ERP Results
ERP responses at electrode Pz to five deviant frequency levels corresponding to 50-95% prescan performance accuracy for (A) subject 4138 and (B) the group. (C) Group mean P300 peak amplitude at electrode Pz as a function of task level and (D) task reaction time as a function of P300 peak amplitude. Plots in C and D are fit with a two-parameter exponential curve (red trace). Error bars denote standard error across subjects.

2.3.3 FMRI Linear Regression Maps

The group fMRI linear regression map, obtained using the individual level-wise P300 peak amplitudes for within-subject analysis, is shown in Figure 2-7 A. The primary areas activated in this map were the right middle and posterior portions of the superior temporal gyrus (STG), the left middle STG, the left inferior temporal gyrus (ITG), and the left inferior frontal gyrus (IFG). Results for the P300 linear regression in subject 4138 are shown in Figure 2-7 B. This map showed small regions of positive activation in the middle and posterior STG and supramarginal gyrus (SMG), bilaterally. Supplementary Table 5-1 and

Table 5-2 in the Appendix lists the peak coordinates and extent of all significant clusters of activation found in the fMRI regression maps for the group of twenty subjects and for subject 4138, respectively. The size range of significant clusters in the linear regression analysis was 1103-22,704 μl in the group map (with two large clusters corresponding to activity in the left inferior parietal lobule, and right superior parietal lobule) and 1-379 μl for subject 4138.
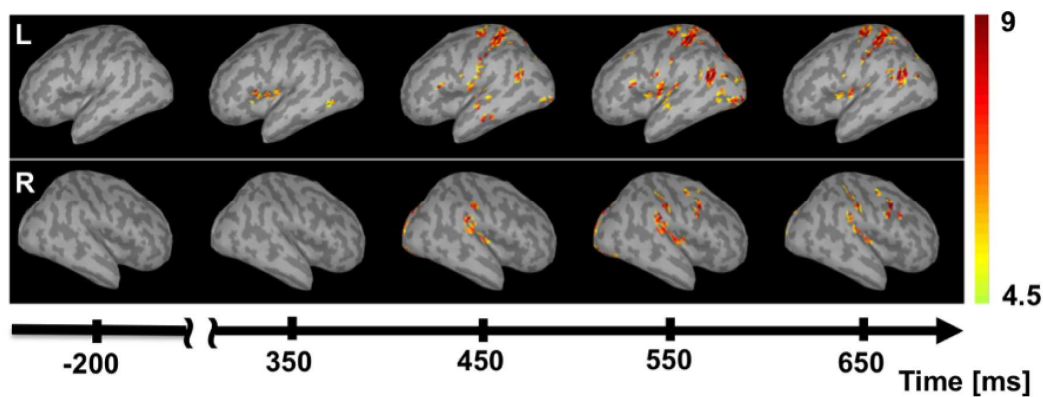
Figure 2-7: FMRI Results
FMRI activity using the P300 peak amplitude as a regressor (A) in a group of 20 subjects ($\alpha<0.05$, corrected for multiple comparisons), and (B) in subject 4138 ($p<0.05$, uncorrected), overlaid on a template brain in Talairach space (TT_N27 Colin brain). Slice numbers, indicating the distance (in mm) in the sagittal plane from the origin in the anterior commissure are shown. L-left; R-right.

2.3.4 Source Reconstruction of the P300 ERP component

Source reconstructions of the group P300 ERP response for task level 5 are shown in Figure 2-8. Task level 5 was selected for the source reconstruction because the P300 amplitude is largest at this level. Source reconstruction of the group activity revealed sources in the time window of the P300, in the left pre- and post- central gyri (PreCG and PostCG, respectively), left IFG, left posterior STG, and left occipital cortex. On the right,

sources were observed in the superior temporal plane and gyrus (STP/STG), in the supramarginal gyrus (SMG) and in the middle frontal gyrus (MFG). The single subject source reconstructions (not shown) were generally noisy, with sources observed in multiple brain regions and at additional time points outside the N100 and P300 time windows. This result is likely related to the low SNR of the ERPs in a single subject (SNR≈2) compared to the grand average ERPs (SNR≈5).

Figure 2-8: Group ERP source reconstruction
Source reconstruction for the grand average (N=20) level 5 ERP in the baseline period prior to deviant onset (-200 to 0 ms), and at 100 ms intervals during the P300 response (350 to 650 ms), in the left (L) and in the right (R) hemispheres. Source magnitude is expressed as a z-score relative to the magnitude during the baseline period.
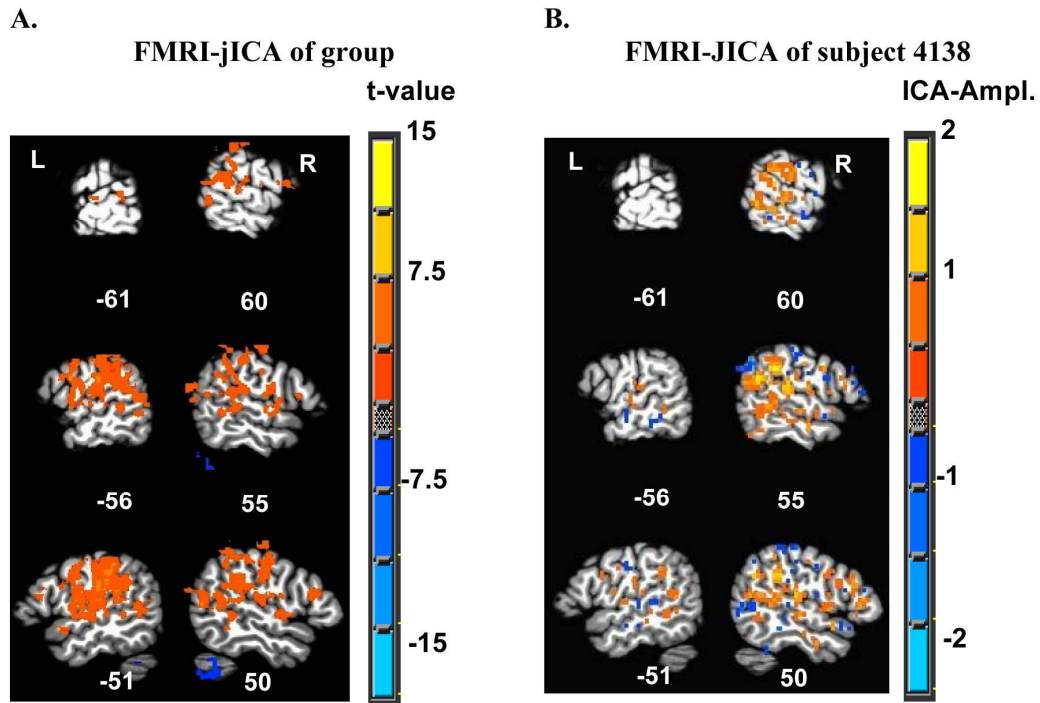
2.3.5 jICA fMRI maps

JICA was applied on the ERP and fMRI data across task levels. Only one jICA fMRI-ERP component in each subject survived the significance threshold, and therefore a total of twenty components were used in the group analysis. The group fMRI jICA map (Figure 2-9 A) revealed activity in the middle and posterior STG and in the SMG, bilaterally, as well as in the PreCG, PostCG and IFG, predominantly on the left. Clusters

in this analysis ranged 412-25,055 µl (with one large cluster corresponding to activity in the left postcentral gyrus). This pattern of activity was similar to that observed in the group P300 linear regression map (Figure 2-7 A) in the superior temporal and frontal cortex. However, the activity returned by jICA was stronger (approximately 50% increase in t- value in the right middle and posterior STG and SMG, and in the left PreCG and PostCG)) and more extensive, as evident from comparison of cluster sizes between the two maps (see

Table 5-3 in the appendix). Other important differences were that activity in the PreCG and PostCG, consistent with that observed in the P300 source reconstruction maps (Figure 2-8 and Figure 2-11), was observed only in the fMRI jICA maps. In contrast, activity in the right ITG was observed only in the P300 regression maps.

The fMRI jICA maps for subject 4138 (Figure 2-9) showed strong activity in the middle and posterior STG and in the SMG, predominantly on the right, as well as in PreCG, PostCG and IFG, bilaterally (clusters ranged 189-2142 µl shown in

Table 5-4 in the appendix). The single subject jICA map was very similar to that of the group in that the same network of regions was activated. However, the pattern of lateralization of the individual and group maps was somewhat different. The differences in lateralization may reflect individual differences, which result in more bilateral activity at the group level. The single subject jICA results were far more robust than those for the single subject P300 linear regression, as evidenced by the strong similarity of the individual jICA (but not P300 regression) map to the group maps.
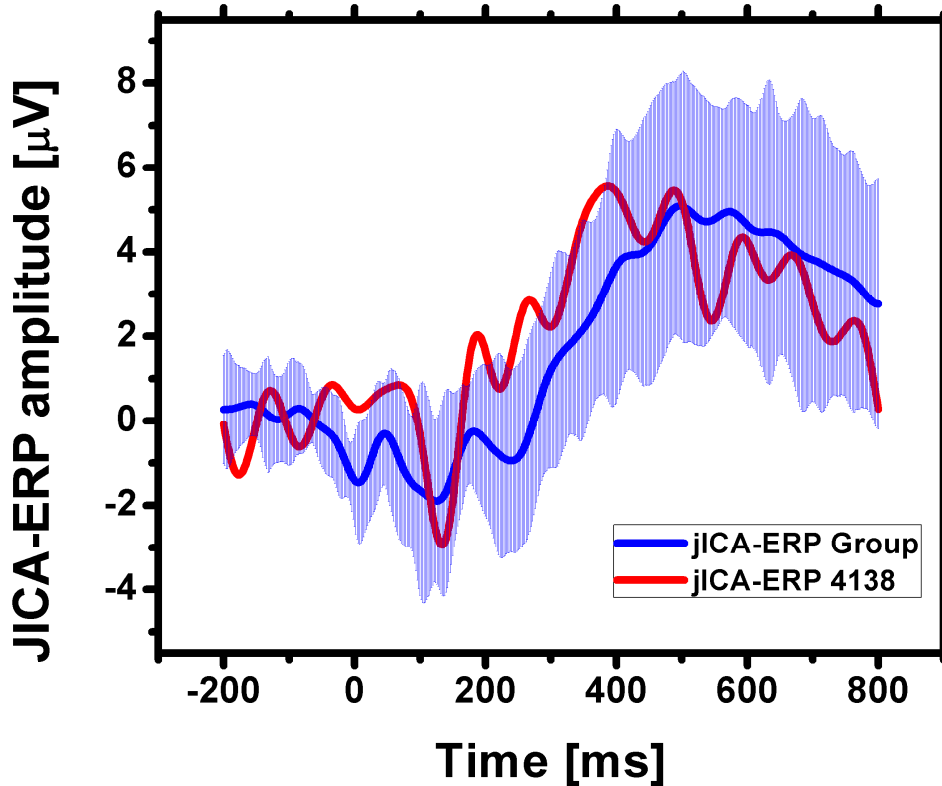
Figure 2-9: JICA-fMRI maps
FMRI jICA for (A) the group of twenty subjects (t-test of twenty components against zero), and for (B) subject 4138 (both at $\alpha < 0.05$, corrected for multiple comparisons), overlaid on the TT_N27 Colin brain. Slice numbers are indicated.

2.3.6 ERP jICA

The ERP jICA waveforms at electrode Pz for the group of twenty subjects (blue) and for subject 4138 (red) are shown in Figure 2-10. The group and single subject waveforms overlap closely, with a marked increase in amplitude during the P300 time window (as observed in the group and individual ERP waveforms shown in Figure 2-6). There is also a negative phase peaking around 140 ms and corresponding to the N100 time window. The peak amplitudes in the negative and positive phases of the ERP are larger, and the negativity is more distinct, in the single subject jICA results. These

differences may be due to smoothing in the group maps that reflects inter-individual differences in the latency of N100 and P300.
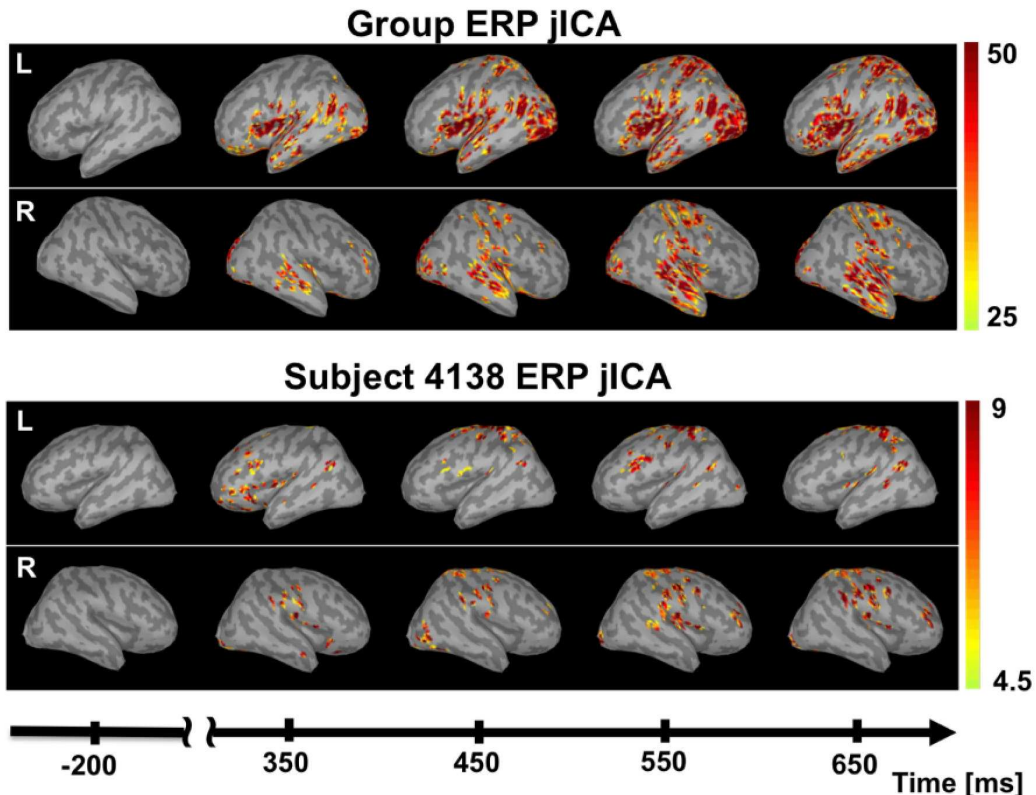
Figure 2-10: JICA-ERP temporal profile
JICA-ERP at electrode Pz for the group of twenty subjects (mean shown in dark blue and standard deviation shown in light blue) and subject 4138 (red).

2.3.7   Source Reconstruction of the ERP jICA

Source reconstructions of the ERP jICA data, for the group of subjects and for subject 4138, are shown in Figure 2-11. Source magnitudes are reported as a z-score computed relative to the baseline interval (-200 to-50 ms). The group source reconstruction (top panel) showed significant P300 related activity in the STG, and SMG,

bilaterally, and in the occipital cortex, IFG, and PreCG and PostCG, predominantly on the left, similar to the group ERP source reconstructions and group fMRI jICA map. In subject 4138 (bottom panel), activity was observed in the same network of regions, albeit with smaller z-scores, likely due to the lower SNR observed at the individual level.
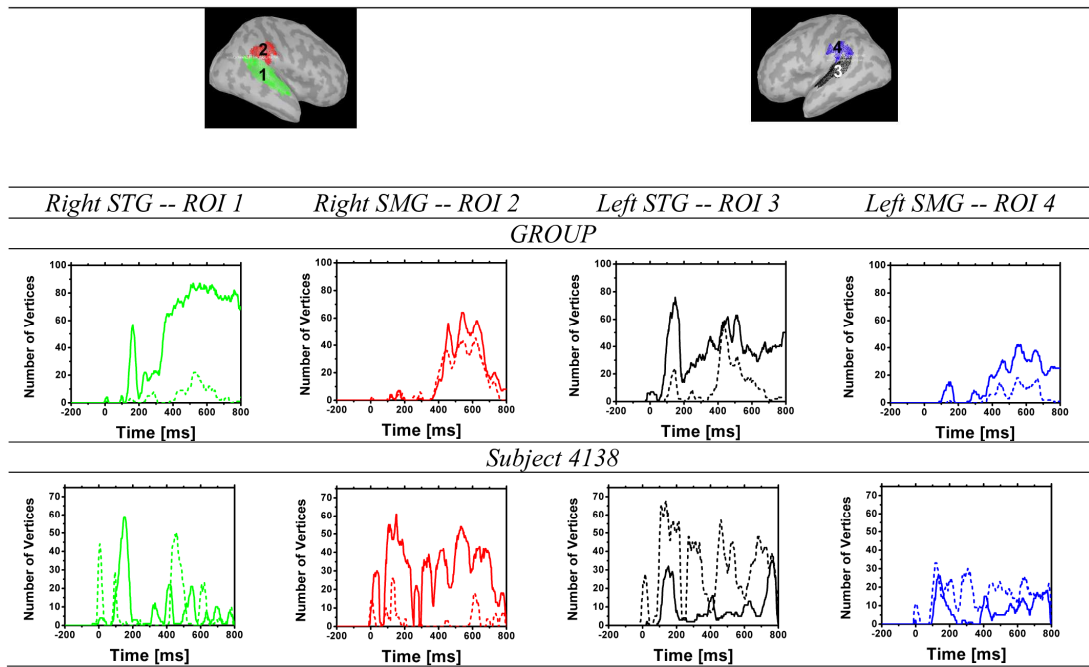
Figure 2-11: JICA-ERP source reconstruction
Time series of the ERP jICA source reconstruction in the baseline interval (-200 to 0 ms), and at 100 ms intervals during the P300 response (350 to 650 ms), for the group (top) and for subject 4138 (bottom), in the right (R) and left (L) hemispheres. Source magnitude is expressed as a z-score relative to the magnitude during the baseline period.

2.3.8   Region of interest analysis

Figure 2-12 shows the mean time course of statistically significant vertices (p<0.05) in four task-relevant ROIs (left and right STG and SMG), for sources reconstructed from jICA (solid line) and task level 5 (dashed line) activity in the group (top panel) and subject 4138 (bottom panel).

Figure 2-12: Number of active vertices for ERP JICA-ERP source activity within ROIs
Number of vertices within each ROI with significant ERP activity (p<0.05), for jICA exctracted across task levels (solid line), and for level 5 (dotted line), as a function of time relative to deviant onset at 0 ms. Results are shown separately for the group (top) and for subject 4138 (bottom)in the left and right SMG (red and blue, respectively) and the left and right STG (green and black, respectively).

This measure roughly reflects the extent of activation within each ROI as a function of time. At the group level (top panel), the jICA sources contained a larger

number of statistically significant vertices compared to the Level 5 sources in all ROIs, particularly during the N100 (STG ROIs) and P300 (all ROIs) time windows. In subject 4138 data, the number of significant vertices was generally smaller in the jICA relative to level 5 sources (except in the right SMG). However, the temporal profiles of the jICA sources in the individual data were better defined in that they showed increases relative to the baseline specifically during the time windows of the N100 and P300.

Figure 2-13 shows the time course of the SNR in the same four ROIs, for the group data (top panel) and for subject 4138 (bottom panel). In the group data, the jICA compared to the task level 5 results showed a 20% increase in the area under the SNR curve from 350 to 700 ms in the right STG, and a 70% increase in the right SMG. In subject 4138, the jICA results showed a 300% increase in SNR area from 350 to 700ms in the right SMG. Detailed SNR area results are also shown in Table 2-1 for the N100 peak from 50-200 ms, and the P300 peak from 350 to 700 ms at the four ROIs, for subject 4138 and the group.
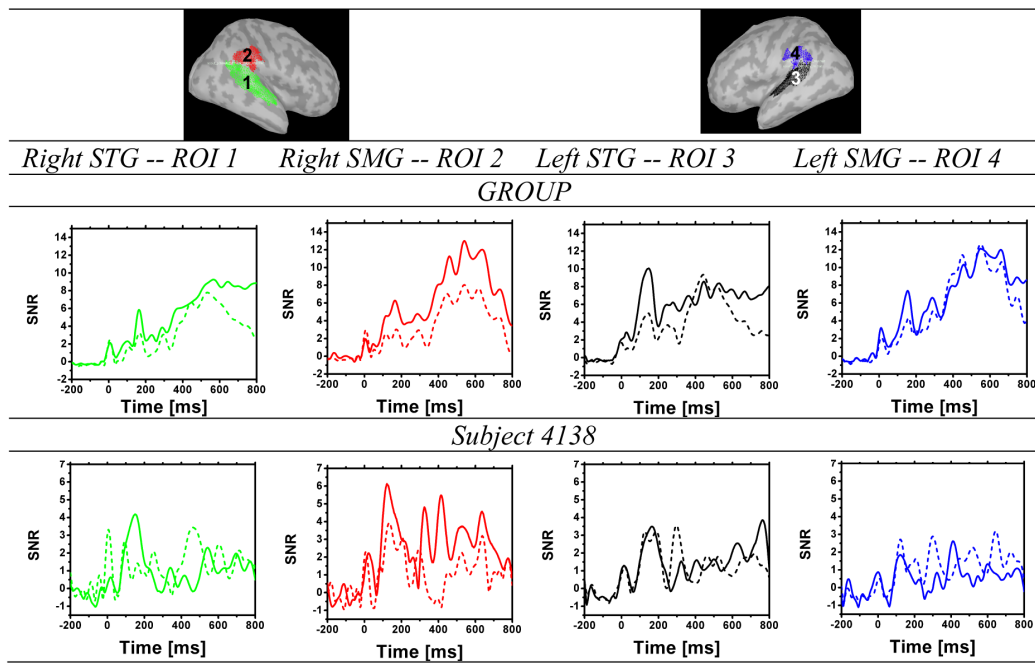
	STG R		SMG R		STG L		SMG L	
Group	*N100*	*P300*	*N100*	*P300*	*N100*	*P300*	*N100*	*P300*
Level 5	225	2071	268	2097	464	2216	366	3458
jICA	430	2725	592	3485	982	2549	594	3477
Subject 4138								
Level 5	164	615	328	365	305	410	172	528
jICA	377	339	543	1146	307	520	117	309

Table 2-1: Area under curve for the N100 and P300 component
Area under the curve (representing SNR) of the level 5 and jICA N100 and P300 components, in the four ROIs, for the group and for subject 4138. The N100 interval was selected from 50-200 ms and the P300 interval from 350-700 ms.

The single subject temporal profiles were generally consistent with those of the group and those reported in the literature for auditory oddball detection, revealing a

progression of neural activity from STG to SMG associated with the N100 and P300 responses. Differences in the activation pattern between the single subject and group data may reflect individual variations in the location and lateralization of temporoparietal activity related to auditory oddball detection, and/or deviations in the positioning of ROIs and source localization relative to individual

neuroanatomy.

Figure 2-13: SNR for ERP and ERP-jICA source activity within ROIs
SNR is shown for the group (top) and for subject 4138 (bottom) ERP jICA extracted across task levels (solid line) and ERP activity in level 5 (dotted line),as a function of time relative to deviant onset at 0 ms, in the left and right SMG (red and blue, respectively)and the left and right STG (green and black, respectively).
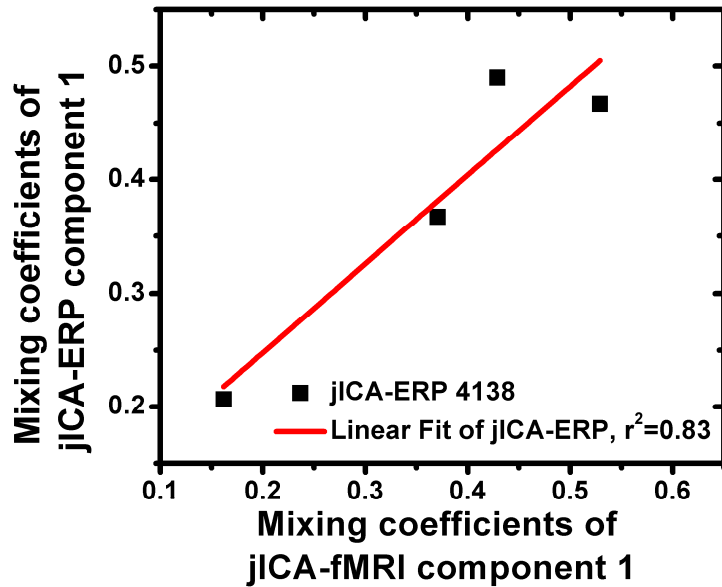
2.3.9 Relationship between ERP and fMRI joint components

JICA can also be used to extract the underlying relationship between ERP and fMRI activity using the mixing coefficients of the linked jICA ERP and fMRI components. The mixing coefficient matrix "A" (see 2.2.7), describes the mixing of the underlying sources across samples. That is, the coefficients describe how ERP and fMRI signals vary across samples, and thereby the relationship between ERP and fMRI. In general, ICA extracts the unmixing coefficients "W", which can be used to retrieve the mixing coefficients "A" by computing the pseudo-inverse of the unmixing coefficients ($A = W^{-1}$). Since jICA was applied on whitened and normalized data, the data first need to be unwhitened and unnormalized

$$A_{rE}(MxP) = (D(MxP) \times A(MxP) \cdot N_E(MxP) \tag{5}$$

$$A_{rF}(MxP) = (D(MxP) \times A(MxP)) \cdot N_F(MxP) \tag{6}$$

where D is the pseudo-inverse of the original whitening matrix, N_E and N_F are the pseudo-inverses of the normalization matrices applied to the ERP and fMRI data respectively, and A_r describes the reconstructed coefficients for the ERP "A_{rE}" and fMRI "A_{rF}" sources respectively and M and P equal 4. Figure 2-14 shows the mixing coefficients of the joint ERP and fMRI components plotted against one another. Results show that jICA extracted a nearly linear relationship between ERP and fMRI (r^2=0.83).
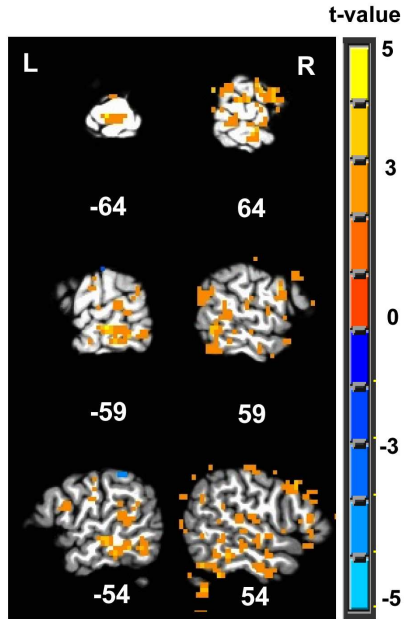
Figure 2-14: Relationship between ERP and fMRI joint components
The mixing coefficients of the jICA-ERP components are plotted against the mixing coefficients of the jICA-fMRI components.

2.3.10 Multi-Channel versus Single-Channel ERP jICA

In order to investigate whether the sensitivity of jICA for extracting common fMRI and ERP sources is increased when multiple ERP channels are included, jICA was compared between two data sets. One set with all sixty-two ERP channels and the entire fMRI volume (described above), and the other with only one ERP channel (Pz) and the entire fMRI volume. A voxelwise t-test showing the differences between the resulting fMRI jICA maps is shown in Figure 2-15. The difference map shows that jICA with the full array of spatiotemporal information yielded significantly more activity in regions specifically associated with the P300, including the STG, bilaterally, and the right SMG. With the exception of activity immediately below the Pz electrode, there were no areas

that showed stronger activity for the single ERP channel analysis. The results suggest that there is an advantage to using the full array of ERP electrodes in jICA.

Figure 2-15: Multi-channel ERP JICA vs. single-ERP channel jICA
T-test between the jICA fMRI group maps obtained using the full spatiotemporal sequence of multi-channel ERP activity, and using a single electrode, Pz.

2.4   DISCUSSION

The integration of neural activity recorded simultaneously with ERP and fMRI can highlight the temporal dynamics of different brain regions. In particular, the integration of ERP and fMRI within-subject could be useful for the diagnosis of neuropathology. This paper examined the potential advantages of using jICA to fully integrate parametric fMRI and ERP P300 data within-subject, relative to using the P300 ERP peak amplitude as a regressor in a general linear model. The jICA approach depicts linear and non-linear covariations between the ERP and fMRI signals, and therefore has the potential to be more sensitive and comprehensive than the general linear regression model. In addition, the full array of ERP electrodes and ERP data points was used here in the jICA approach, as opposed to the single electrode and point in time (peak activity) used (here and typically) in the linear regression analysis, thereby potentially allowing for more sensitive characterization of neural activity.

The group and single subject jICA results revealed activity in the superior temporal and supramarginal cortex, predominantly on the right. These areas have been associated with auditory processing and auditory oddball detection in previous work (Linden et al., 1999; Linden, 2005), and also in the P300 linear regression performed in the present work. Activity was also observed in the precentral and postcentral gyri, predominantly on the left, likely reflecting right-hand motor planning and motor control. This interpretation is consistent with the strong relationship between mean motor response time and mean P300 peak amplitude observed here (Figure 2-6), and with

previous work suggesting involvement of this region in motor response during an oddball task (Linden et al., 1999; Strobel et al., 2008).

The source reconstruction of the jICA group data revealed activity during the P300 time window in the superior temporal and supramarginal gyri, bilaterally, and in the occipital, inferior frontal, and pre- and post- central gyri, predominantly on the left. These maps are generally consistent with previous reports of the P300 neural sources (Halgren et al., 1980; Linden, 2005). The jICA source reconstruction maps were also largely consistent with the source reconstruction maps of the group ERP data, and the group fMRI maps, reconfirming the strength of the jICA approach for spatially and temporally resolving task related neural activity (Calhoun et al., 2006; Moosmann et al., 2008). However, activity in the left occipital cortex was observed only in the ERP source reconstructions, but not in the fMRI maps. Activation of the occipital cortex has been reported in previous Loreta source reconstructions of the auditory P3b ERP component, although the significance of this finding remains uncertain (Anderer et al., 1998; Volpe et al., 2007).

A primary difference between the fMRI P300 linear regression and jICA maps was that only the jICA maps showed activity in the precentral and postcentral gyri. This result may be related to the fact that mean response times did not vary linearly with the mean P300 peak amplitude (Figure 2-6), and were therefore not well modeled in the P300 linear regression. Another difference between the fMRI maps was that the main areas associated with the P300, namely the right superior temporal and supramarginal gyri, were activated more strongly and extensively with the jICA approach. This difference may again be related to the fact that the P300 ERP peak amplitude did not vary perfectly

linearly with task level (Figure 2-6), such that co-variations between the ERP and fMRI data were better modeled with the jICA approach.

A general drawback of the general linear model (GLM) is that assumptions about the co-linearity of the ERP and fMRI data may not always hold, for example at low levels of sensory stimulation (Logothetis et al., 2001), or in pathological conditions such as stroke, Alzheimer's or Parkinson's disease (Polich and Pitzer, 1999; Polich and Corey-Bloom, 2005; Girouard and Iadecola, 2006). In such cases, jICA could be particularly advantageous for ERP and fMRI data fusion because the method is applicable to both linear and nonlinear relationships.

In this work, the full array of spatial and temporal information from the ERPs was incorporated into the jICA approach. In contrast, the P300 linear regression used information from only one electrode at the time point of the P300 peak amplitude. The superior sensitivity of the jICA relative to the GLM may be largely related to these factors. The importance of including additional ERP channels is supported by the comparison of the single and multi-channel ERP jICA. Our comparison showed that with one electrode, the sensitivity of jICA to P300 related activity in the right superior temporal and supramarginal gyri was significantly reduced. Taken together, the results suggest that incorporating more spatiotemporal information is useful for fusing ERP with fMRI. The benefits from incorporating more temporal information from the ERP waveform will be investigated in computational modeling studies aimed at further optimization of jICA for ERP-fMRI data fusion.

Perhaps the most significant finding of this study is that the approach proposed here, using jICA to fully integrate fMRI and ERP data in the context of a parametric

paradigm, lends itself well to within-subject analysis. The single subject fMRI jICA data, and source reconstruction of the ERP jICA component, were both consistent with the group jICA maps. In contrast, the individual fMRI P300 regression maps and ERP source reconstructions were generally too noisy to evaluate, demonstrating an advantage of the jICA approach particularly for individual data analysis. This finding is particularly important because analysis of individual patient data is necessary for implementation of multimodal neuroimaging as a clinically relevant diagnostic tool.

CHAPTER 3

Theoretical evaluation of Joint-Independent Component Analysis for the integration of multi-channel ERP and fMRI data

3.1   Introduction

Combining functional magnetic resonance imaging (fMRI) and event-related potential (ERP) responses has become a popular approach for studying neural activation with high temporal and spatial resolution (Dale and Halgren, 2001; Horovitz et al., 2002; Liebenthal et al., 2003; Liebenthal et al., 2010; Dubois et al., 2012; O'Connell et al., 2012). A number of methods for integrating the information between the two modalities, that capitalize on the respective strengths of each, have been proposed. Linear, model-based approaches have been used successfully to characterize joint activity (see (Rosa et al., 2011; Huster et al., 2012) for a review), at the expense of assuming a direct linear relationship between ERP and fMRI measures. However, linear models can be too rigid to capture the richness of human brain activation. Recently, data-driven approaches such as joint independent component analysis (jICA) have been implemented to integrate ERP and fMRI data, by searching for co-varying signals across a group of subjects (Calhoun et al., 2009; Mangalathu-Arumana et al., 2012; Mijovic et al., 2012). An advantage of ICA, and data-driven approaches in general, lies in their ability to identify statistical relationships between signals when detailed *á priori* models are not available (Calhoun et al., 2006). Another advantage of jICA that makes it well-suited for individual data analysis is the separation of noise and signal into separate components (known as denoising). Although linear approaches denoise datasets as well, it has been shown that noisy fMRI datasets may follow non-gaussian distributions (Zarahn et al., 1997), to which ICA methods are particularly sensitive. The benefits of jICA for individual data
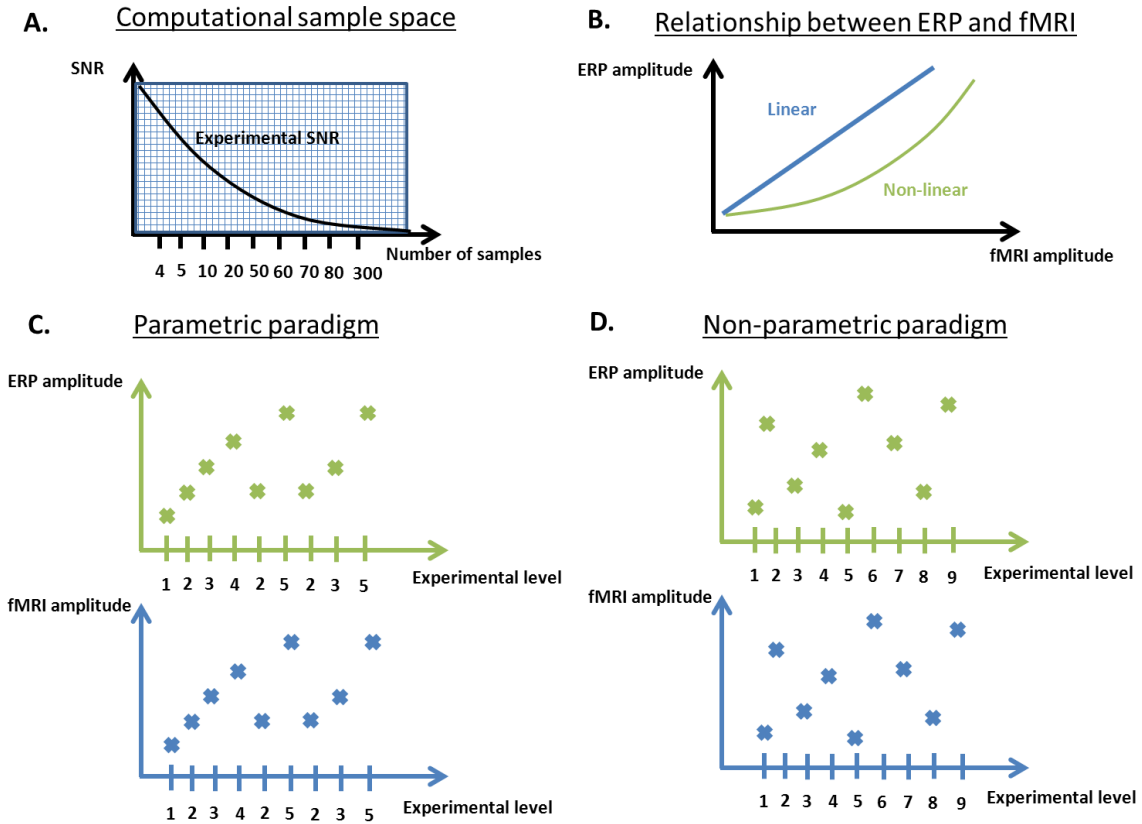
analysis can further be enhanced by using spatial and temporal information from multi-channel ERPs (Mangalathu-Arumana et al., 2012).

In a previous study, using a parametric design with four experimental levels in each subject, a single jICA-fMRI component was found to carry all the significant neural activity associated with the perceptual task (Mangalathu-Arumana et al., 2012). This result was hypothesized to be related to the relatively low variability in the dataset (small number of experimental levels), hindering the separation of neural sources into different components. The segregation of sources into separate components is desirable for characterization of their spatiotemporal dynamics. Thus, increasing data variability by using a trial-by-trial design or an increased number of experimental levels could improve source segregation with jICA. On the other hand, single-trials have lower signal-to-noise ratio (SNR), which could lower the sensitivity of jICA.

Stimulus-induced changes in neural activity can produce linear or nonlinear changes in the hemodynamic response, depending on the brain area activated and the rate and intensity of stimulation. With short inter-stimulus intervals (0.25-4s), the fMRI response can be non-linearly related to the neural response, whereas at longer intervals a strong linear relationship is typically observed (Rees et al., 1997; Mechelli et al., 2000; Birn and Bandettini, 2005; Liu et al., 2010). Similarly, a brief period of synchronous neural activity, resulting in increased firing coherence among a small percentage of neurons, may be captured with ERPs without significantly changing local metabolic consumption, resulting in little, if any, change in the much slower BOLD response (Babiloni and Cincotti, 2004). Conversely, neural activity of limited extent may be visible with fMRI, but located too deep or oriented such that it does not elicit a

significant ERP response (Nunez and Silberstein, 2000). Aside from normative instances of neurovascular uncoupling, pathological conditions can also lead to highly non-linear (essentially uncoupled) relationships between neural activity and the hemodynamic response (Girouard and Iadecola, 2006). The performance of jICA with linearly varying neural and hemodynamic signals is relatively well established (Calhoun et al., 2006; Mangalathu-Arumana et al., 2012), but the application of the technique to non-linear relationships has not been systematically examined.

The current study uses computer simulations to characterize the sensitivity of jICA for extracting known neural sources in individual data, as a function of imaging SNR, number of experimental samples and the relationship between ERP and fMRI signals (linear, nonlinear, and uncoupled sources). The ability of jICA to localize neural sources measured with fMRI and ERPs under these conditions was examined in the context of both a parametric and a nonparametric experimental paradigm. An illustration summarizing the different parameters simulated is shown in Figure 3-1.

Figure 3-1: Illustration of experimental design and relationship between ERP and fMRI signals.
Illustration of the parameter space tested, SNR vs number samples (A) for linear and nonlinear relationship between ERP and fMRI (B), and for parametric (C) and nonparametric (D) experimental designs. In a parametric paradigm, response amplitude varies systematically with experimental level. In a non-parametric paradigm, there is no systematic relationship between response amplitude and experimental level.

Through the simulations, we show that jICA is able to extract linear, nonlinear, as well as uncoupled relationships, with the degree of segregation between sources dependent on the SNR, number of samples and the experimental design used.

3.2   Methods

3.2.1   Overview of Computational Model
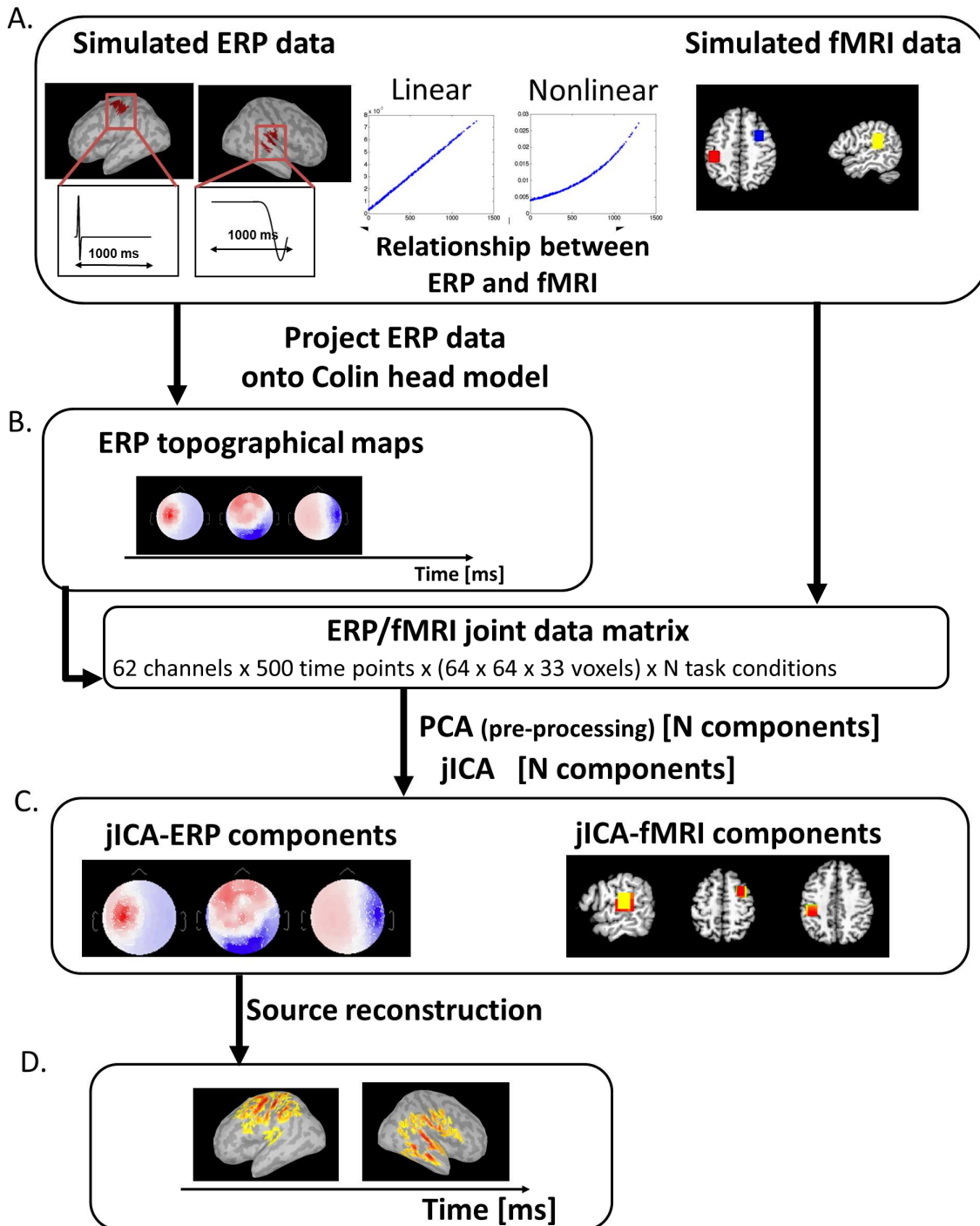
The detection and segregation of neural sources was examined along three dimensions, the number of independent ERP and fMRI data samples, the SNR of fMRI and ERP data, and the nature of the relationship between fMRI and ERP signals (linear, nonlinear, and uncoupled), to characterize the trade-offs between experimental design and source segregation in jICA. Multi-channel ERP waveforms and whole-brain fMRI maps were simulated for three neural "sources" located in brain regions implicated in auditory oddball detection (Liebenthal et al., 2003; Mangalathu-Arumana et al., 2012), in the right frontal cortex, right temporo-parietal cortex, and left motor cortex (Figure 3-2 - top right; blue, yellow, and red squares, respectively).

The neural sources were simulated as fMRI activation foci in a 3D whole brain MRI volume (64x64x33 voxels) in Talaraich space (Tournoux, 1988), using the Afni software (AFNI, Cox et al., 1996). Each source consisted of a cube (5x5x5 voxels, 4000µL) of active voxels characterized by a BOLD response that varied homogeneously in space as a function of an external "stimulus" vis-à-vis a parametric/nonparametric experimental design.

The ERP manifestation of each neural source was defined spatially on the cortical surface of the Colin brain (Holmes et al., 1998), as implemented in Brainstorm

(Brainstorm 3.1) (Tadel et al., 2011). The cortical surface consisted of a mesh of 15,000 vertices. Sample electric dipoles were positioned at each vertex with orientations constrained to be perpendicular to the cortical surface at that point. Cortical sources were created by projecting the fMRI sources to the cortical surface using Freesurfer (v 5.0) (Dale et al., 1999; Fischl et al., 1999). Voxels in the gray matter were projected along the direction normal to the surface using nearest neighbor interpolation. Each cortical source was assigned a current density profile over a 1000 ms epoch, and the amplitude was scaled as a function of the applied "stimulus" and the experimental design. The current source density profiles for the sources in right motor and right temporo-parietal cortex (Figure 3-2, top left) were simulated as gaussian-weighted sinusoids peaking at 100ms (with positive and negative phases) and 800ms (with a negative phase), respectively. The frontal fMRI source was simulated as uncoupled and had no ERP manifestation.

ERPs were formed through forward projection of the current source density profiles to the scalp surface of the Colin brain, using a 3-shell sphere head model in Brainstorm. Each simulated ERP consisted of the time-varying voltage waveforms obtained from sixty-two electrode locations on the scalp (positioned according to the 10-20 system), using a template electrode position file for the Colin brain.

Figure 3-2: Work flow of computational simulations.
Three sources were simulated, with fMRI activity in the right temporo-parietal cortex, right frontal cortex and left motor cortex (A. right panel). The volumetric fMRI data corresponding to the right temporo-parietal and left motor sources were projected onto a mesh of vertices on a cortical surface and simulated with gaussian-weighted sinusoidal temporal profiles (A. left panel). ERP topographical maps were generated by forward projecting the temporo-parietal and motor sources onto the scalp partition of the Colin head model (B.) fMRI and ERP signals co-varied linearly (temporo-parietal and motor source,

Simulation #1), nonlinearly (f(x)=1-exp(x), temporo-parietal and motor source, Simulation #2), or were uncoupled (f(x)=0, the frontal source). For jICA, the simulated fMRI and ERP data sets were concatenated into a single row to create a joint-matrix across all samples and imaging modalities (Mangalathu-Arumana et al., 2012), see also Figure 2-3. PCA was applied to the joint-matrix to whiten the signal and to limit the dimensionality of the dataset to twenty components. JICA was then performed on the PCA components. The resulting jICA components consisted of a spatial jICA-fMRI map and a spatiotemporal jICA-ERP map (C.). Source maps of the jICA-ERP channel data were computed and projected onto the Colin cortical surface model (D.) to facilitate comparison with the jICA-fMRI maps.

3.2.2 Parametric and non-parametric experimental design

In separate simulations, the amplitudes of the fMRI and ERP responses were varied across experimental samples, consistent with either a parametric or a non-parametric experimental design. In simulations of a parametric design, signal amplitudes of ERP and fMRI sources varied along a continuum defined by varying the values of a stimulus variable (e.g., change in frequency in a frequency discrimination task). ERP and fMRI amplitudes covaried across trials for each source. The relationships between fMRI and ERP signals associated with each neural source were simulated as a linear model (f(x)=x), an exponential model (f(x)=1-exp(x)) or an uncoupled model (f(x)=0). In simulations of a non-parametric design, ERP and fMRI signals covaried in a linear, nonlinear or uncoupled fashion, but there was no parametric relationship across the stimulus variable (i.e., experimental samples were independent). An illustration of the parametric and non-parametric designs and the relationship between ERP and fMRI is shown in Figure 3-1C and D.

3.2.3 Simulation parameters for computational model

For a given relationship between ERP and BOLD responses (linear or nonlinear), 484 simulations were run, examining the detection and segregation of neural sources as a function of the numbers of samples (4, 5, 6, 7, 8, 9, 10, 12, 15, 20, 30, 40, 50, 60, 80, 100, 140, 180, 220, 260, 300, 360), and paired SNRs for ERP (0.37, 0.41, 0.45, 0.49, 0.52, 0.55, 0.58, 0.64, 0.71, 0.83, 1.01, 1.17, 1.31, 1.43, 1.65, 1.85, 2.18, 2.48, 2.74, 2.98, 3.20, 3.5) and fMRI (0.79, 0.86, 0.93, 1.01, 1.11, 1.26, 1.50, 1.67, 1.93, 2.12, 2.37, 2.74, 3.35, 3.87, 4.32, 4.74, 4.99, 5.30, 5.66, 6.12, 6.70, 7.0). The uncoupled relationship (frontal source) was included in both sets of simulations. The range of SNRs in each imaging modality was chosen based on measures obtained from previous experimental data for a single trial (low SNR: ERP=0.35, fMRI = 0.8) and an experimental condition obtained from averaging 72 trials (high SNR: ERP=3.5, fMRI = 7) (Mangalathu-Arumana et al., 2012). For ERP signals, SNR was defined as the maximum ERP amplitude in the post-stimulus window divided by the standard deviation of the prestimulus baseline. For fMRI signals, SNR was defined as the score of a paired t-test between task and rest conditions. In the context of a typical experimental design, the extremes of the SNR ranges (ERP: 0.37 and 3.5; fMRI: 0.8 and 7) and numbers of samples (4 and 360) represent examples of a parametric design with a small number of samples and high SNR per sample (due to averaging), and a trial-by-trial design with a large number of samples and low SNR per sample. The performance of jICA as a function of these variables was evaluated based on the accuracy of source retrieval and the separation between sources as described in Section 3.2.7.

Analyses were performed using the 128 node high-performance computing cluster at Marquette University (8 cores and 24 GB RAM per node). Simulations were implemented on a distributed cluster, where each combination of paired ERP/fMRI SNR and number of samples was run as an independent simulation on a single node. Simulations were submitted through the CONDOR job scheduler (Condor, 7.7.6), using a condor script to automatically generate the fMRI and ERP datasets for each simulation on the fly at each compute node using a compiled (stand-alone) Matlab executable script together with AFNI. FMRI datasets were created using AFNI and loaded into Matlab. ERP datasets were created using the brainstorm toolbox run through Matlab. Following data generation, the Matlab script performed jICA on the datasets. Amplitude and cluster thresholding on jICA-fMRI datasets was subsequently performed in AFNI. Normalized source detection values were extracted (see Section 3.2.7 for details) using Matlab and the results returned via the job scheduler for analysis. ERP datasets were back-transformed onto the cortical surface using a distributed source reconstruction in Brainstorm and amplitude thresholded using Matlab. Normalized source detection values were extracted from the thresholded ERP source maps in Matlab and the results returned via the job scheduler for analysis.

3.2.4   Temporal and Spatial ICA

Temporal and spatial ICA were applied to the ERP and fMRI data, respectively, and served as a "benchmark" to evaluate the effectiveness of jICA in segregating neural sources as a function of SNR and number of samples based on the underlying statistics of

the data. The "general" ICA approach represented the "ideal" case for ICA source detection within a single imaging modality, meaning that the sources extracted within a single imaging modality should ideally match the original simulated source. This analysis defines the best possible performance of ICA within the limitation of the type of signal, SNR and number of samples used.

Temporal ICA was applied to the ERP temporal profiles across electrodes, and spatial ICA was applied to the fMRI flattened image volumes. Prior to analysis, principal component analysis (PCA) was applied to the data in each modality separately to whiten the signal and reduce the dimensionality of the data for datasets with more than twenty samples. To keep the analysis computationally tractable, temporal and spatial ICA were performed on the ERP and fMRI PCA-extracted components, respectively.

For spatial ICA, the components consisted of a spatial ICA-fMRI map and for temporal ICA, the components consisted of a spatiotemporal ICA-ERP map (specifically, a time series of scalp-topography maps). Distributed source reconstructions of temporal ICA-ERP components were used to facilitate comparisons between the spatial locations of the ERP and fMRI activity. Source localization of the ICA-ERP maps was performed using the weighted minimum norm estimate (wMNE) to solve the inverse problem for a distributed representation of electric dipoles located at each vertex on the cortical surface model and oriented perpendicular to the cortical surface. (Brainstorm 3.0, Matlab 2010b). The Colin head volume conductor and cortical surface models used to simulate the sources were also used to reconstruct the cortical source activity from each temporal ICA-ERP component.

3.2.5   JICA

The fusion of fMRI and ERP data was performed using a within-subject parametric form of jICA described by Mangalathu-Arumana et al. (Mangalathu-Arumana et al., 2012). In this approach, the variation in ERP and fMRI signals is described across different levels of a data set in a single subject (as opposed to across subjects, as in other forms of jICA) (see Section 2.2.7 for a detailed description). In each simulation, jICA was used to compute jointly varying spatially and temporally independent ERP and fMRI components. Prior to analysis, the fMRI and ERP data sets were concatenated into a single row to create a joint-matrix encompassing the full data set obtained across all samples and imaging modalities, see Figure 2-3. Similar to the temporal and spatial ICA, PCA was applied to the joint-matrix to whiten the signal and to reduce the dimensionality of the dataset to twenty components for simulations containing more than 20 samples. JICA was then performed on the PCA-extracted components. Each of the resulting jICA components consisted of a spatial jICA-fMRI map and a spatiotemporal jICA-ERP map containing linear projections of the joint fMRI/ERP data across experimental samples that maximized the statistical independence across jICA components. Distributed source reconstructions of the jICA-ERP components were used to facilitate comparisons between the spatial locations of the neural sources corresponding to the ERP and fMRI activity (Section 3.2.2).

3.2.6   Statistical analysis

JICA-fMRI and ICA-fMRI maps were thresholded at p<0.01 (voxelwise, relative to the distribution of jICA-fMRI and ICA-fMRI activity from all components respectively) to identify regions of significant activity within each component. A corrected map-wise cluster threshold of α<0.05 was applied to identify significant regions of activity relative to a chance distribution computed by randomizing the jICA-fMRI and ICA-fMRI voxel values, respectively, across all extracted components. JICA-ERP and temporal ICA-ERP source maps were thresholded at p<0.01 relative to the post-stimulus distribution across all vertices and components to identify regions on the cortical surface with statistically significant activity.

3.2.7   Characterization of Source Detection

The ability of jICA to detect and parse neural sources was evaluated by computing two metrics, the normalized source detection and source segregation values (described below), for each neural source and jICA component.

In the simulations, vertices corresponding to each source were predetermined and therefore analysis was based on these vertices only. For each jICA-fMRI component, the mean signal of all significantly active voxels (p<0.01, α<0.05) in each of the three source volumes ($\overline{s^{fMRI}}$) was computed, and the normalized contribution of the Nth jICA-fMRI component to the overall source activity, s_N^{fMRI}, was defined as

$$s_N^{fMRI} = \frac{\overline{s^{fMRI}}}{\sum\limits_{j=1}^{N_{comp}} \overline{s^{fMRI}}} \qquad [1]$$

to characterize the separation of each source across components. The maximum

normalized source detection value for jICA-fMRI and spatial ICA-fMRI, max(s_N^{fMRI}),was

computed to determine the component with the highest contribution to the original neural

source.

For each jICA-ERP component (in the form of current density source maps), the

time course of the signal in vertices that survived the significance threshold were

correlated against the time course of the current source density maps of the original

simulated sources to characterize the correspondence between the input ERP and output

jICA-ERP and temporal ICA-ERP signals. The normalized contribution of each jICA-

ERP component to the current density of each simulated source, s_N^{ERP}, was defined as

$$s_N^{EEG} = \frac{\sum\limits_{i=1}^{N_{vert}} r_{xy}}{\sum\limits_{j=1}^{N_{comp}} \sum\limits_{i=1}^{N_{vert}} r_{xy}} \qquad [2]$$

where r_{xy} denotes the vertex-wise correlation between the input and jICA-ERP current

sources density profiles summed across the total number, N_{vert}, of significantly active

vertices within a component ($p<0.01$) and across all jICA components (N_{comp}). The

maximum normalized source detection value for jICA-ERP and temporal ICA-ERP, max

(s_N^{ERP}), was computed to determine the component with the highest contribution to the

source.

3.3   Results
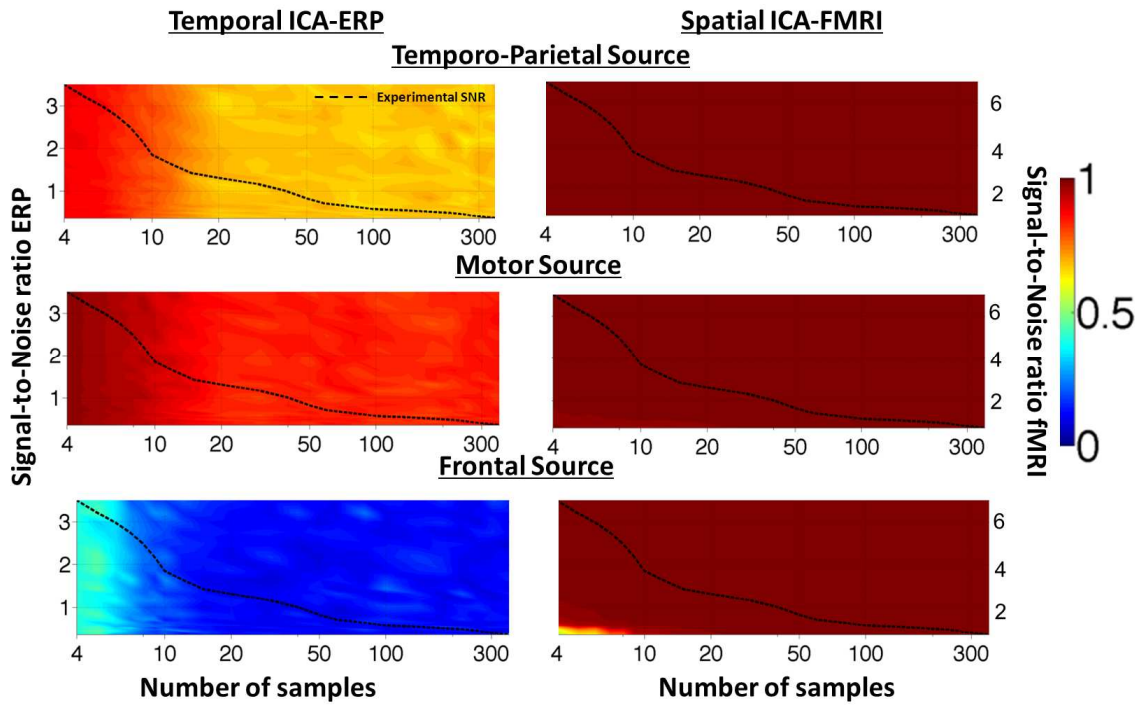
3.3.1   Temporal and spatial ICA: SNR vs. number of samples in a non-parametric design

The first set of simulations examined source segregation in the context of a non-parametric experimental design in which the experimental samples were independent. The relationship between ERP and fMRI signals was linear. This type of design applies to experiments with complex (non-systematic) variations in the physiological response between experimental samples (e.g., disparate experimental conditions or trials, for example, in a resting state experiment). Temporal and spatial ICA were applied to the ERP and fMRI data, respectively, as a reference for comparison with jICA results. The segregation of sources using temporal ICA for ERP and spatial ICA for fMRI is shown as a function of the SNR and number of samples in Figure 3-3. The degree of source separation across ICA components was evaluated using the normalized source detection values, max(s_N^{EEG}) and max(s_N^{fMRI}), for each source.

For source separation of ERPs using temporal ICA, 70-90% of the temporo-parietal (s_N^{EEG} = [0.7, 0.9]) and 80-100% of the motor source activity were captured by a single component (Figure 3-3 – left). Source segregation degraded systematically as the number of samples increased, but there was little effect of SNR. For the uncoupled right frontal source, simulated with no corresponding ERP source, the ICA-ERP time course

showed a small correlation with the (spatially closest) temporo-parietal source, resulting

in very low maximum normalized source detection values, s_N^{EEG}, ranging 0.1-0.3.

Source separation of fMRI using spatial ICA showed maximum normalized

source detection values ranging 0.8-1 for all sources, and all but the smallest SNRs

(ERP=~0.4-0.5 and fMRI=~0.9-1.2) and numbers of samples (4-6) (Figure 3-3, right

panel). In those cases, max(s_N^{fMRI}) ranged 0.4-0.5, indicating a split in the underlying

neural sources between components. Overall, spatial ICA showed little dependence on

SNR or number of samples, with source activity typically assigned to a single component.

Figure 3-3: Maximum normalized source detection of within-subject temporal and spatial ICA with a nonparametric experimental paradigm.

Maximum normalized source detection values for temporal ICA of ERP and spatial ICA of fMRI, max(s_N^{EEG}) and max(s_N^{fMRI}) respectively, using a non-parametric experimental paradigm. Source separation is shown for the three simulated sources as a function of the SNR and the number of experimental samples. The dashed line in each graph shows the √N decrease in SNR with number of trials averaged per sample, with the start and end points of the curve taken from experimental data (Mangalathu-Arumana et al., 2012). The maximum normalized source detection values range 0-1, with a value of 1 corresponding to extraction of the complete source into a single component. A value of 0.5 indicates that 50 % of the source activity was extracted into one component and the remaining activity attributed to at least one additional component. A value of 0 indicates a finding of no source activity.
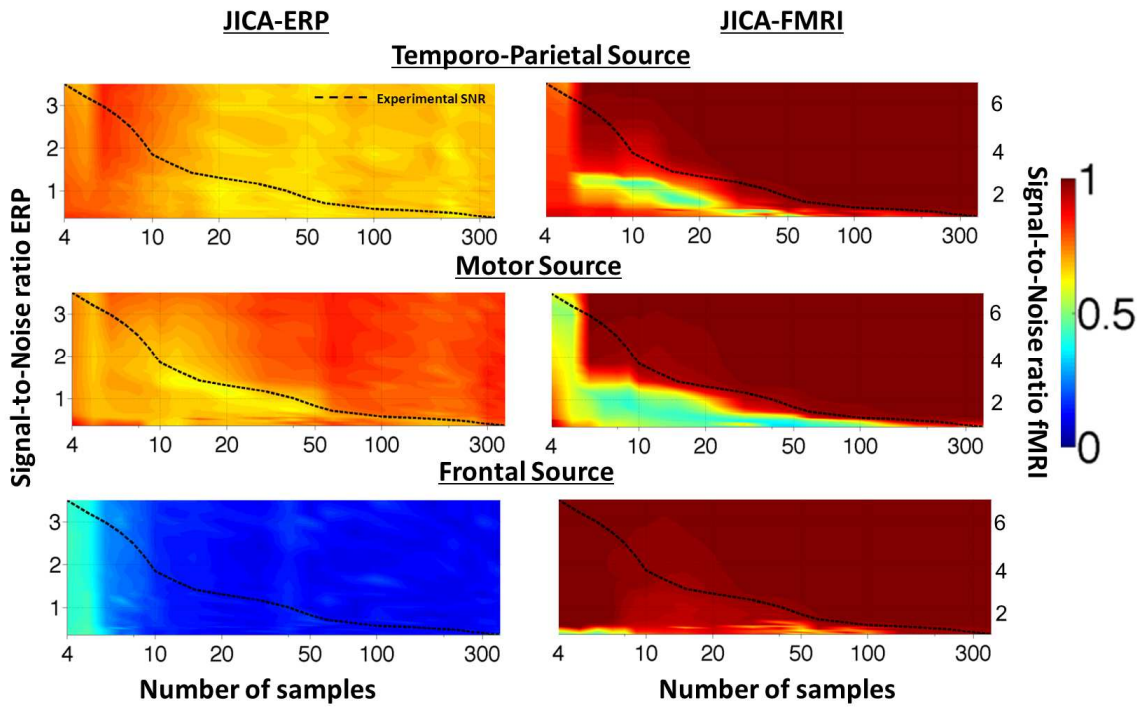
3.3.2   JICA: SNR vs. number of samples in a non-parametric design

The segregation of neural sources in fMRI/ERP data using jICA in a non-parametric design when there is a linear relationship between ERP and fMRI is shown in Figure 3-4. Simulation results for jICA-ERP showed normalized detection values ranging 0.7-0.9 for the temporo-parietal and motor sources, and 0.1-0.3 for the frontal source, similar to those for temporal ICA. For the temporo-parietal source, normalized detection values decreased with the increase in number of samples, consistent with the temporal ICA-results. However the motor source showed a reverse trend, suggesting that it was mainly extracted into a single component. At low SNR, increasing the number of samples improves the separation of the motor source into a single component, resulting in an overall opposite trend for this source. These findings emphasize that in order to determine how sources are split across components, it is necessary to examine not only the maximum normalized source detection value (as shown in Figure 3-4), but also the normalized values of each component. This type of analysis is shown and discussed in section 3.3.4 in more detail.

JICA-fMRI results for the right temporo-parietal and left motor source showed normalized source detection values, max(s_N^{fMRI}), ranging 0.4-1. Source separation into a single component was less likely at low SNRs and for small numbers of samples, (s_N^{fMRI} = [0.4, 0.6]), but increased quickly with SNR and the number of samples (s_N^{fMRI} = [0.8, 1]).   Results also showed that the boundary for separation into a single component
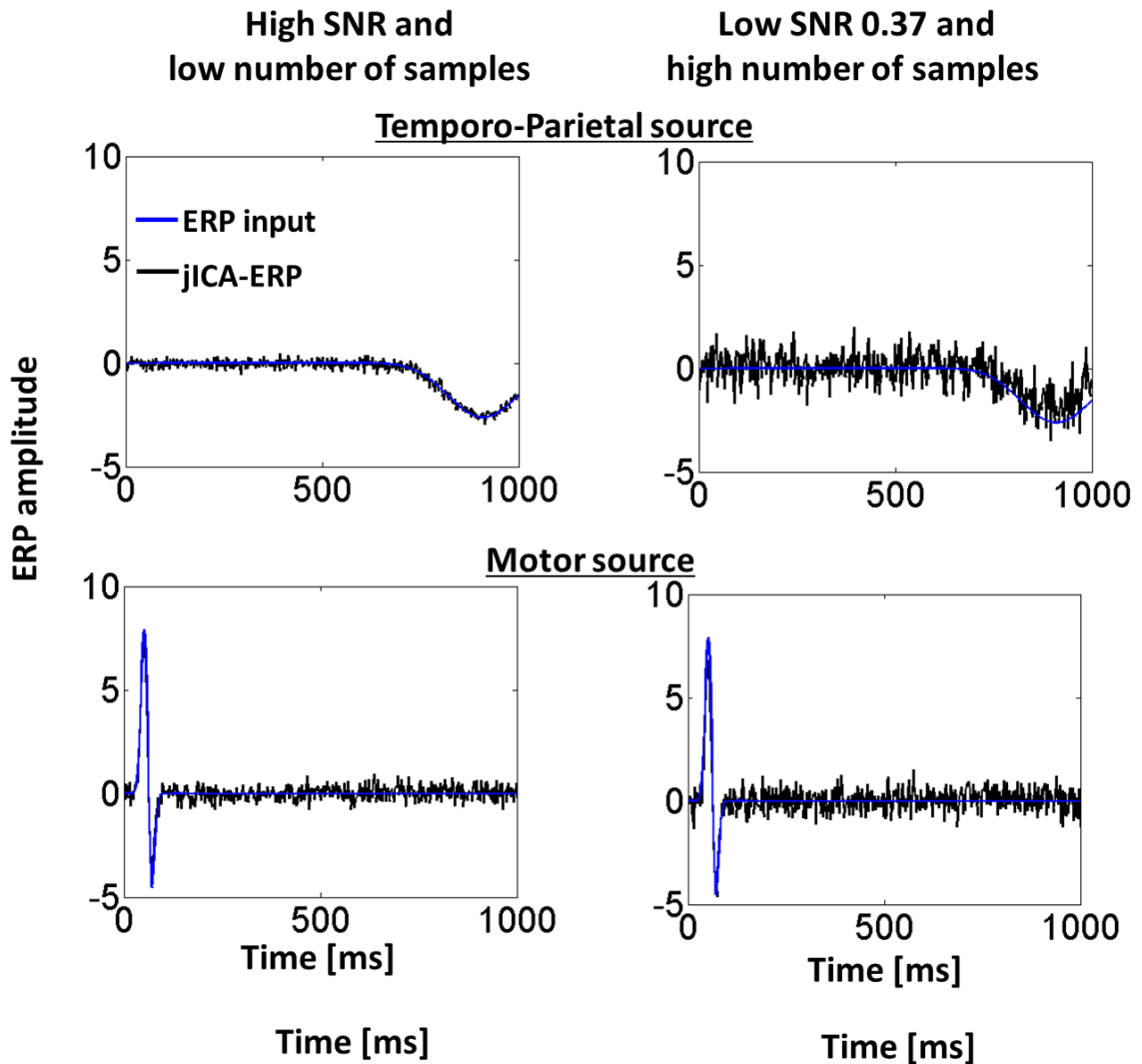
(roughly, values above 0.8) fell along SNR/samples combinations approximating those of a typical parametric experimental design (black dotted line in the graph). The maximum normalized source detection values for the uncoupled frontal source also ranged 0.4-1, but the degree of separation into multiple components was very limited compared to the two other sources, suggesting that sources with representation in a single modality may be extracted with jICA.

Figure 3-5 shows the temporal profile of the jICA-ERP source density output (black) and the simulated ERP input (blue) for representative vertices of the temporo-parietal and motor sources, at SNR=3.5 and 6 samples (left panel), and at SNR=0.37 and 360 samples (right panel). The temporal profiles of the original and re-constructed sources where highly correlated ($r^2 > 0.98$) at both SNR and sample combinations, suggesting that jICA-ERP was able to accurately extract the simulated sources in each case. Significant activation was not found in brain areas removed from those simulated in the temporo-parietal and motor cortex. However, activation was observed in areas immediately adjacent to the simulated cortical areas, possibly due to limitations in the spatial resolution of the ERP source reconstruction.

Figure 3-4: Maximum normalized source detection for within-subject jICA in a nonparametric experimental paradigm.

Maximum normalized source detection values for jICA-ERP and jICA-fMRI, max(s_N^{EEG}) and max(s_N^{fMRI}) respectively, using a non-parametric experimental paradigm. Source separation, measured via the source detection values, is shown for the three sources as a function of the SNR and number of experimental samples. The temporo-parietal and motor sources were simulated with linear coupling between the ERP and fMRI responses. The frontal source, consisting of an fMRI response only, was uncoupled. Other conventions are as in Figure 3-3.

Figure 3-5: Temporal profiles of ERP and jICA-ERP responses for representative vertices chosen from the temporo-parietal and motor sources.
JICA-ERP source density temporal profile (black line) and ERP source density input temporal profile (shown here without noise added for visual clarity, blue line) for the temporo-parietal (top) and motor (bottom) sources (left, SNR=3.5 and 6 samples; right, SNR=0.37 and 360 samples).
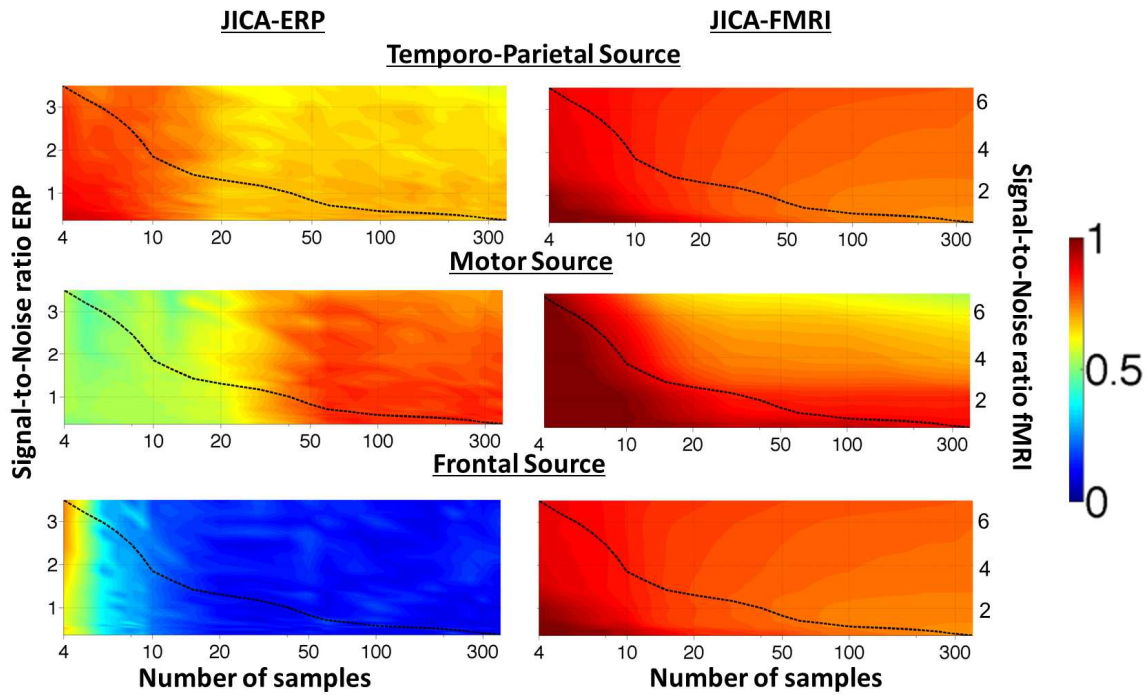
3.3.3   JICA: SNR vs. number of samples in a parametric design

In a separate set of simulations, the performance of jICA with a linear relationship between ERP and fMRI was evaluated in the context of a parametric design. In this type of experimental design, there is a systematic relationship between the input and physiological response across trials. As a result, there is a relatively strong correlation between sources. Thus, the sources simulated in this study were not independent (unlike those in the non-parametric experimental design), but rather were part of a neural network activated in a correlated manner across trials, as is often the case in experimental data (for example, in an auditory oddball paradigm).

The segregation of neural sources in fMRI/ERP data, using jICA in a parametric design, is shown in Figure 3-6. Simulation results for jICA-ERP showed normalized detection values ranging 0.7-0.9 for the temporo-parietal source, 0.5-0.9 for the motor source, and 0.1-0.6 for the frontal source. In the case of the frontal source, which had no ERP response associated with it, the increased correlation is due to the procedure of normalizing source detection values across components. Higher normalized values for the source were observed when the overall number of samples (and components) was low, and one component carried slightly higher correlation values. The raw (unnormalized) correlation values for the frontal source never exceeded $r^2=0.2$. Generally, normalized source detection was applied to extract the component that carried the majority of the activity of a source. These results show that the raw source detection values are also a useful source of information when examining the results. For the temporo-parietal source, normalized detection values decreased with the increase in number of samples, consistent

with the jICA-results in the non-parametric simulations. The motor source, as in the non-parametric design, showed a reverse trend, indicating that it was increasingly extracted into a single component as the number of samples increased.

JICA-fMRI results showed normalized source detection values, max(s_N^{fMRI}), ranging 0.8-1 for the temporo-parietal source, 0.5-1 for the motor source and 0.8-1 for the frontal source. Source separation into a single component was less likely at higher SNRs and numbers of samples, (s_N^{fMRI} = [0.5, 0.7]), but increased quickly as both the SNR and number of sample decreased (s_N^{fMRI} = [0.8, 1]). These results are reversed from those for the non-parametric design, in which sources were more likely to be separated when the number of samples and SNR was low. In the parametric design, the sources simulated were strongly correlated by design and were therefore not separated into different components. Further analysis of the source segregation pattern is given in section 3.3.5.

Figure 3-6: Maximum normalized source detection for within-subject jICA in a parametric experimental paradigm.

Maximum normalized source detection values for jICA-ERP and jICA-fMRI, max(s_N^{EEG}) and max(s_N^{fMRI}) respectively, using a parametric experimental paradigm. Source separation, measured via the source detection values, is shown for the three sources as a function of the SNR and number of experimental samples. The temporo-parietal and motor sources were simulated with linear coupling between the ERP and fMRI responses. The frontal source, consisting of an fMRI response only, was uncoupled. Other conventions are as in Figure 3-3.

3.3.4 JICA Source Segregation with Linear ERP-fMRI Relationship: Non-parametric design
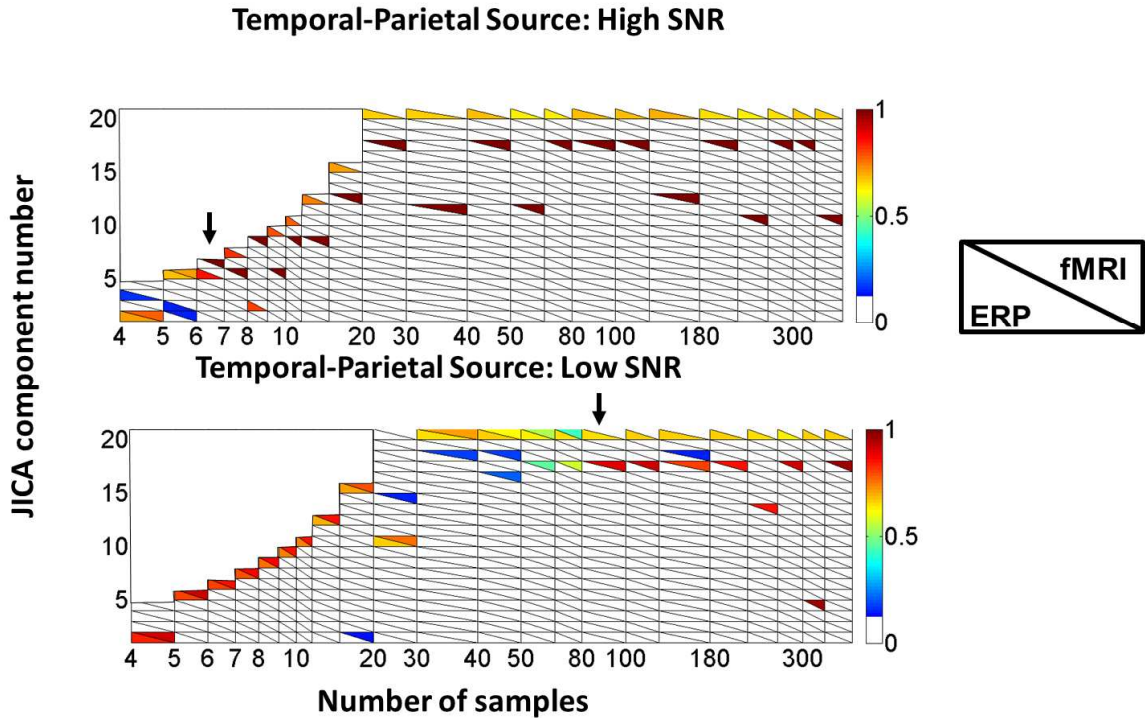
To better understand how sources are segregated with jICA, the representation of the sources across all components was examined. Figure 3-7 shows the correspondence between all twenty jICA-ERP and jICA-fMRI components obtained in a nonparametric experimental paradigm, as a function of the number of samples, for the temporo-parietal source, at two levels of SNR. The normalized source detection values, s_N^{EEG} and s_N^{fMRI}, are used to index the contribution of each jICA-ERP (lower triangles) and jICA-fMRI (upper triangles) component to the source. Only values exceeding a source detection threshold of 0.1 are shown. This type of analysis is important to differentiate cases where sources are not (or are only partially) retrieved with jICA from cases where the sources are split into more than component (within a neuroimaging modality or between modalities).

At high SNR (3.5, Figure 3-7, top panel), the ERP and fMRI responses for the same source are segregated into different components when the number of samples is higher than six. With six or fewer samples, one joint component carries both the ERP and fMRI activity for the temporo-parietal source. At low SNR (0.37, Figure 3-7, bottom panel), the ERP and fMRI responses of the temporo-parietal source are not segregated into separate components until the number of samples exceeds 80. These results show that jICA not only segregates different neural sources, but also segregates the same source in different imaging modalities. This result is likely due to the inherent differences in spatial and temporal statistics of the ERP and fMRI signals. However, an important

feature of jICA is that even when the ERP and fMRI responses associated with the same source are split into separate components, the component in each modality also carries a residual of the activity related to this source in the other modality. For example, a component carrying significant ERP activity will also contain a residual of the corresponding fMRI response. This presence of the residual provides a quantitative measure that can be used to link fMRI and ERP components associated with a common neural source. Specifically, an ERP dominant component would exhibit a high correlation with an fMRI dominant component associated with the same source, because of the residual activity of the other modality that each of them carries. Thus, jICA, unlike unimodal ICA, can be used to link ERP and fMRI signals of a common source.

Similar results were obtained for the motor source (shown in the appendix, Figure 5-1). Finally, it is worth noting that the jICA components containing source-relevant activity always tend to be the component with the highest numbers. This is not an inherent feature of jICA itself, but is tied to the application of PCA prior to jICA, which orders components according to the highest eigenvalue.

Linear Relationship: Non-parametric design

Temporal-Parietal Source: High SNR

Temporal-Parietal Source: Low SNR

Number of samples

JICA component number
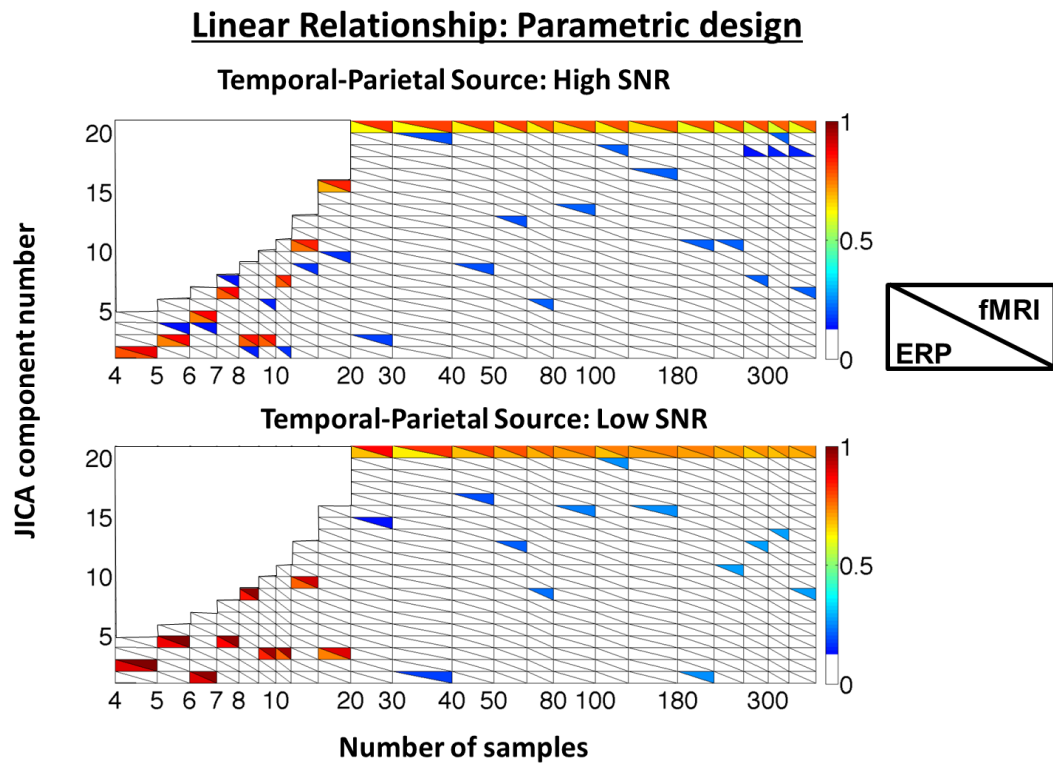
Figure 3-7: Normalized source detection for jICA in a non-parametric design
Normalized source detection values for jICA-ERP and jICA-fMRI in a nonparametric experimental design, for the temporo-parietal source as a function of the number of samples and number of extracted jICA components, for high SNR (ERP= 3.5; fMRI=7; top panel) and low SNR (ERP= 0.37; fMRI=0.8; bottom panel). The lower and upper triangle in each square represent max(s_N^{EEG}) and max(s_N^{fMRI}), respectively. In this simulation, the relationship between ERP and fMRI activity was linear. The black arrows indicate the point of separation of ERP and fMRI activity into separate components.

3.3.5 JICA Source Segregation with Linear ERP-fMRI Relationship: Parametric design
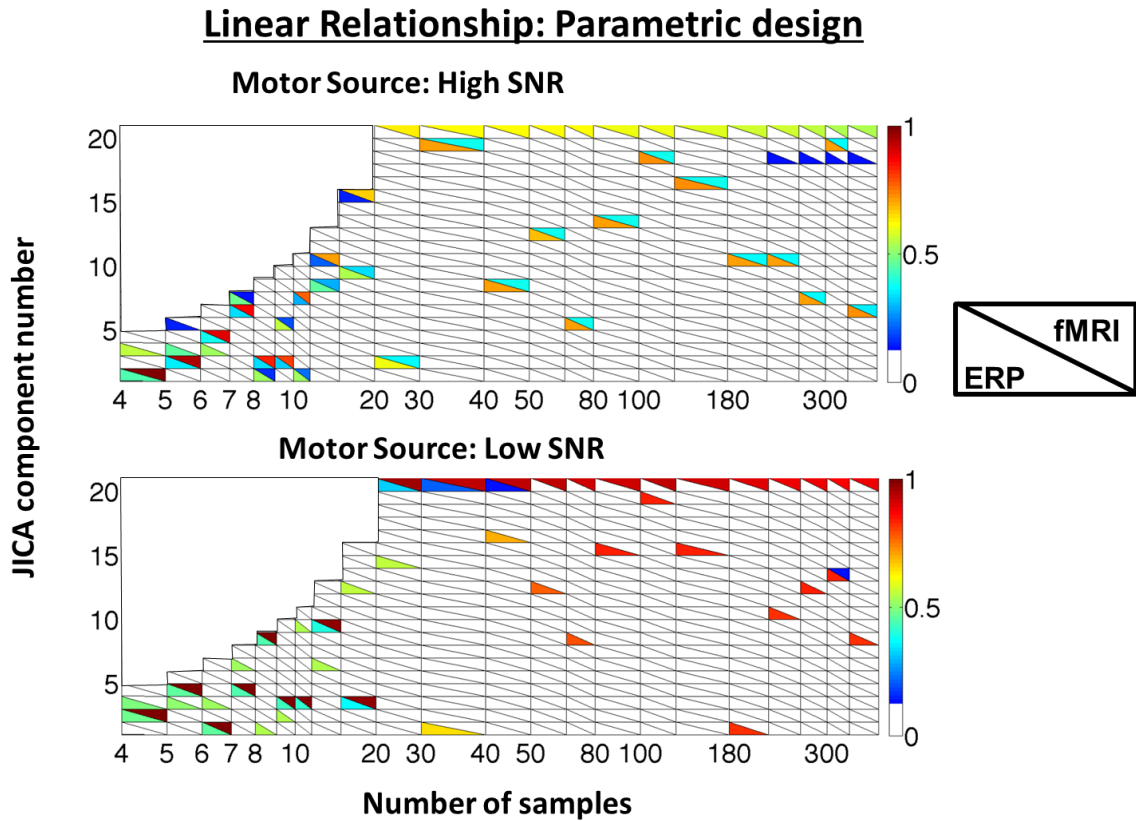
The correspondence between all twenty jICA-ERP and jICA-fMRI components in a parametric design is shown in Figure 3-9, as a function of the number of samples, for the temporo-parietal source at two levels of SNR. The results show that the ERP and fMRI responses associated with the temporo-parietal source were always represented in

the same component, with little dependence on the SNR. As mentioned previously, in the parametric design the sources are highly correlated and therefore less likely to be separated into different components. However, a different trend was observed for the motor source (Figure 3-9), where ERP and fMRI responses were separated into different components, similar to the pattern observed in the non-parametric design. The motor source was temporally more variable compared to the temporo-parietal source and therefore potentially more distinguishable. Similar results for each of these sources were also obtained with a nonlinear relationship between ERP and fMRI signals (Appendix: Figure 5-2 and Figure 5-3).

Figure 3-8: Normalized source detection for jICA in a parametric design
Normalized source detection values for jICA-ERP and jICA-fMRI in a parametric experimental design, for the temporo-parietal source as a function of the number of samples and number of extracted jICA components, for high SNR (ERP= 3.5; fMRI=7; top panel) and low SNR (ERP= 0.37; fMRI=0.8; bottom panel). The lower and upper triangle in each square represent max(s_N^{EEG}) and max(s_N^{fMRI}), respectively. In this simulation, the relationship between ERP and fMRI activity was linear.

Linear Relationship: Parametric design

Motor Source: High SNR

Motor Source: Low SNR

Figure 3-9: Normalized source detection for jICA in a parametric design
Normalized source detection values for jICA-ERP and jICA-fMRI in a parametric experimental design, for the motor source as a function of the number of samples and number of extracted jICA components, for high SNR (ERP= 3.5; fMRI=7; top panel) and low SNR (ERP= 0.37; fMRI=0.8; bottom panel). The lower and upper triangle in each square represent $\max(s_N^{EEG})$ and $\max(s_N^{fMRI})$, respectively. In this simulation, the relationship between ERP and fMRI activity was linear. The black arrows indicate the point of separation of ERP and fMRI activity into separate components.

3.3.6 JICA Source Segregation with an Uncoupled source

Disease states or methodological issues can lead to uncoupled relationships between ERP and fMRI. As part of the analysis of jICA performance in both the parametric and nonparametric experimental designs, the frontal source was simulated as an uncoupled (fMRI-only) source such that it had fMRI but no ERP activity associated

with it. Figure 3-10 shows the normalized source detection values for jICA-ERP and jICA-fMRI, for the frontal source as a function of the number of samples and extracted components, at high (ERP=3.5; fMRI=7.0) and low (ERP=0.37; fMRI=0.8) SNR. Here source activity detected via the ERP, s_N^{EEG}, was computed by correlating the temporal profile of the frontal source activity against the temporal profile of the temporal-parietal source input (as the next closest spatially to the frontal source). The s_N^{EEG} values ranged 0-0.3 at both SNR levels. These results show that ERP activity was minimal with jICA in the frontal source area. Normalized source detection rates for fMRI activity with jICA, s_N^{fMRI}, ranged 0.9-1 at SNR=3.5 and 0.6-0.9 at SNR=0.37. Joint components for ERP and fMRI activity were not seen at either SNR levels, as expected. Similar results were obtained with a parametric design (Appendix: Figure 5-4).

Figure 3-10: Normalized source detection for jICA in a non-parametric design

Normalized source detection values for jICA-ERP and jICA-fMRI in a nonparametric experimental design, for the uncoupled frontal source as a function of the number of samples and number of extracted jICA components, for high SNR (ERP= 3.5; fMRI=7; top panel) and low SNR (ERP= 0.37; fMRI=0.8; bottom panel). The lower and upper triangle in each square represent max(s_N^{EEG}) and max(s_N^{fMRI}), respectively. In this simulation, the relationship between ERP and fMRI activity was linear.

3.3.7 JICA Source Segregation with a Nonlinear ERP-fMRI relationship: Non-parametric design

Nonlinear relationships between neural activity and cerebral blood flow have been reported, for example by Zhang et al. (Zhang et al., 2008b), raising the question of whether jICA could be used to extract such sources and identify the underlying relationship. In a separate set of simulations, we tested jICA performance with a nonlinear relationship (1-exp(x)) between ERP and fMRI signals for sources located in the temporo-parietal and motor cortex, for both the non-parametric and parametric experimental designs. The frontal source remained uncoupled (visible to fMRI only).

Figure 3-11 shows the normalized source detection values for jICA-ERP and jICA-fMRI, when the temporo-parietal source is characterized by a nonlinear relationship between fMRI and ERP in the case of a nonparametric experimental design. The jICA-ERP and jICA-fMRI sources are segregated into different components at similar but slightly higher sample numbers than for the linear relationship shown in Figure 3-9.

For the exponential ERP/fMRI relationship simulated here, ERP and fMRI sources were nearly segregated when 9 or more samples were obtained at high SNR, and when more than 100 samples were obtained at low SNR. However the segregated components were still linked in the sense that both components carried signal residuals of the other modality. Results for the motor source are shown in the supplement (Figure 5-5 of the Appendix).

In order to establish that the nonlinearity between ERP and fMRI activity was indeed extracted with jICA (and not only the linear component of the activity), the

mixing coefficients were used to determine the relationship between the activity of the linked ERP and fMRI jICA components. The mixing coefficient matrix "A" (see 2.2.7), describes the mixing of the underlying sources across samples. That is, the coefficients describe how ERP and fMRI signals vary across samples, and thereby the relationship between ERP and fMRI. ICA extracts the unmixing coefficients "W", which can be used to retrieve the mixing coefficients "A" by computing the pseudo-inverse of the unmixing coefficients (A = W^{-1}). Since jICA was applied on whitened and normalized data, the data first need to be unwhitened "D", and unnormalized for ERP "N$_E$" and fMRI "N$_F$"

$$A_{rE}(360x20) = (D(360x20) \times A(20x20) \cdot N_E(360x20) \qquad [3]$$
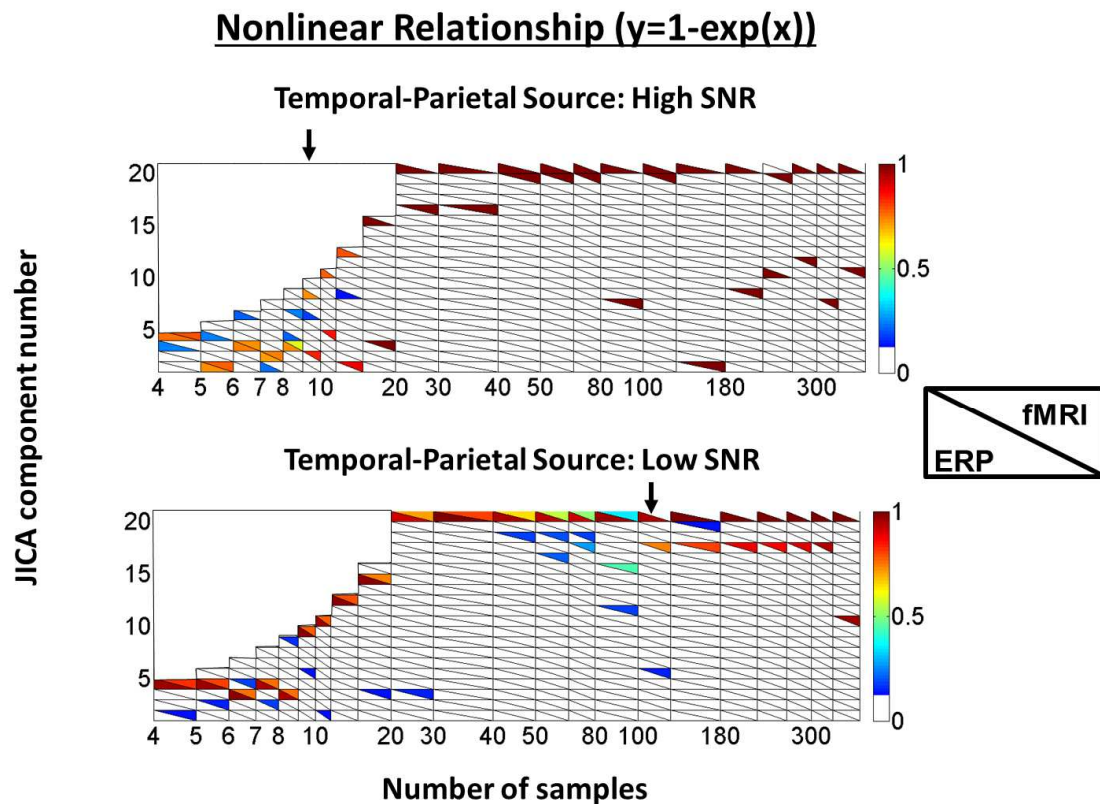
$$A_{rF}(360x20) = (D(360x20) \times A(20x20)) \cdot N_F(360x20) \qquad [4]$$

where D is the pseudo-inverse of the original whitening matrix, N$_E$ and N$_F$ are the pseudo-inverses of the normalization matrices applied to the ERP and fMRI data respectively, and describes the reconstructed coefficients for ERP "A$_{rE}$" and fMRI "A$_{rF}$". Figure 3-11 shows that for a larger number of samples, ERP and fMRI responses are separated into different jICA components. In Figure 3-12, the mixing coefficients of these split ERP and fMRI components are plotted against one another, for linear and nonlinear signal relationships (left and right panels, respectively). Results show that jICA can extract the underlying relationship between ERP and fMRI components, whether linear or non-linear. Sources are split between components in both modalities; a residual of the activity in each modality is still present in the component containing the primary activity associated with the other modality. This relationship between components provides a
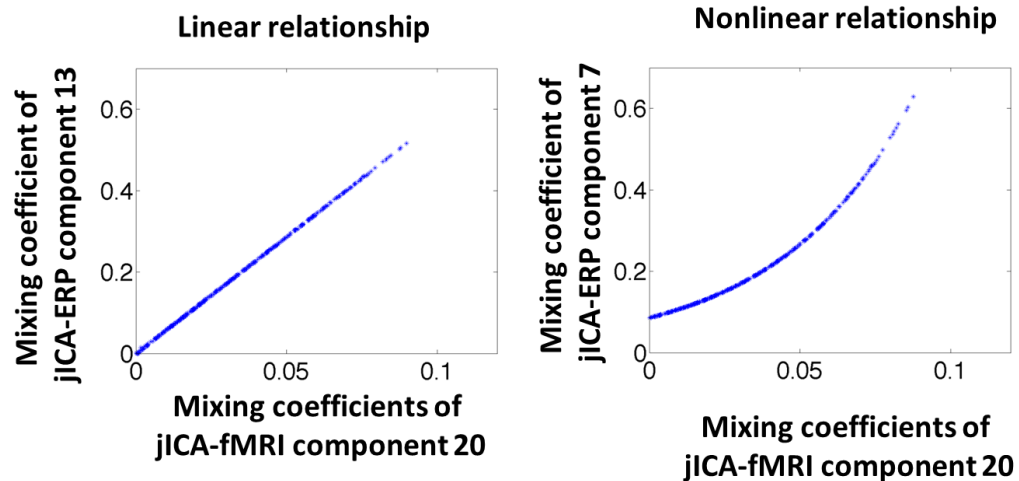
means for linking multi-modal activity correlated along overlapping dimensions, e.g., in space and time for ERP, and in space for fMRI. Components exhibiting high correlation with another component were assumed to be linked and the corresponding mixing coefficient of the component exhibiting high correlation in "A" was selected.


Figure 3-11: Normalized source detection for jICA in a non-parametric design
Normalized source detection values for jICA-ERP and jICA-fMRI in a non-parametric experimental design, for the temporo-parietal source as a function of the number of samples and number of extracted jICA components, for high SNR (ERP= 3.5; fMRI=7; top panel) and low SNR (ERP= 0.37; fMRI=0.8; bottom panel). The lower and upper triangle in each square represent max(s_N^{EEG}) and max(s_N^{fMRI}), respectively. In this simulation, the relationship between ERP and fMRI activity was nonlinear. The black arrows indicate the point of separation of ERP and fMRI activity into separate components.

Extraction of relationship between ERP and fMRI
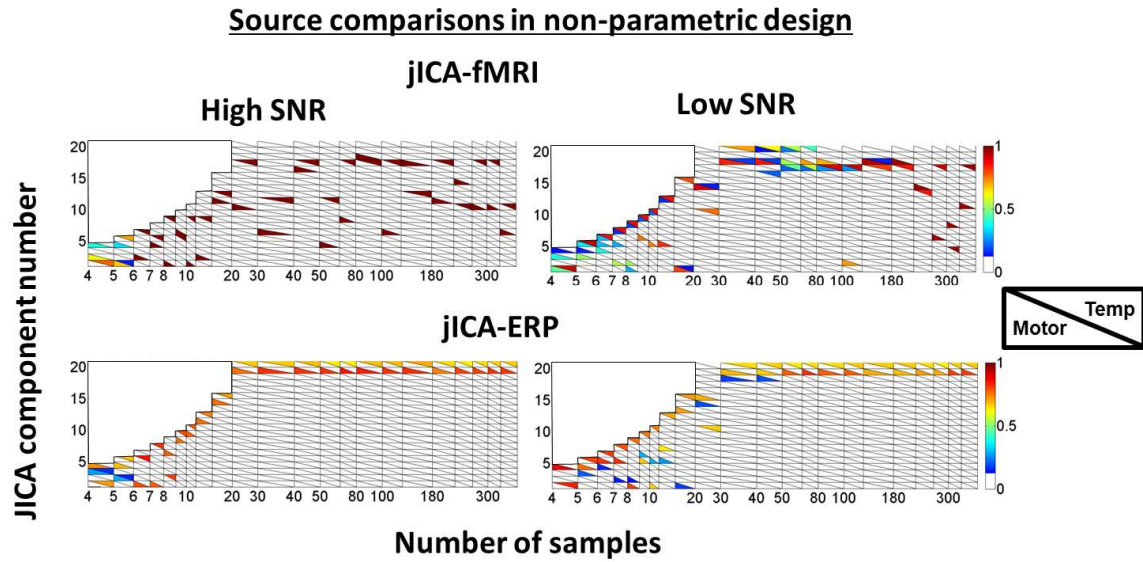
Figure 3-12: Relationship between ERP and fMRI joint components
The mixing coefficients of the jICA-ERP components are plotted against the mixing coefficients of the jICA-fMRI components, for linear (left) and nonlinear (right) relationships between fMRI and ERP signals in the temporo-parietal source, for a high number of samples (N=360) and low SNR (=0.37 for ERP and =0.8 for fMRI). Coefficients of components that showed the highest normalized source detection values for ERP and fMRI were selected for this analysis.

3.3.8 JICA source segregation: comparison of imaging modalities in a non-parametric design

The performance of jICA for segregating neural sources based on ERP and fMRI data was compared, using a linear relationship between ERP and fMRI signals in a non-parametric design. Results of the same analysis with a nonlinear relationship between ERP and fMRI were similar and are shown in the Appendix Figure 5-6. Figure 3-13 shows a comparison of jICA segregation of motor and temporo-parietal sources (lower and upper triangle in each square representing one data point, respectively), as a function of the number of samples and number of components in jICA-fMRI (top panels) and jICA-ERP (bottom panels), at high (=3.5, left panels) and low (=0.37, right panels) SNR. Results show that for a low SNR (0.37), the motor and temporo-parietal sources contributed to the same jICA-fMRI component when the number of samples was lower than seven. This is consistent with previous empirical jICA results (Mangalathu-Arumana et al., 2012). However, the sources were segregated into different jICA-ERP components even at a low SNR.

At a high SNR (3.5), the motor and temporo-parietal sources were segregated into different jICA-fMRI and jICA-ERP components with normalized detection values ranging 0.7-0.8 for s_N^{EEG} and 0.6-0.9 for s_N^{fMRI}. Results for other source comparisons were similar and are shown for the motor vs. frontal source in the supplement (Figure 5-7).
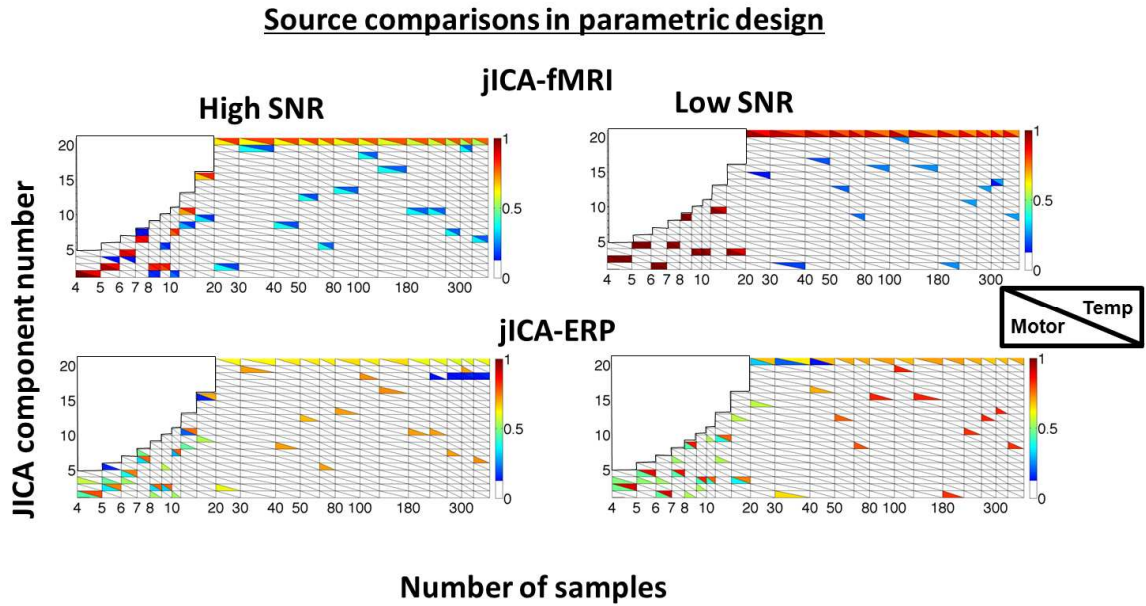
Figure 3-13: Source segregation with jICA-fMRI and jICA-ERP for two sources in non-parametric design
Comparison of normalized source detection values for jICA-fMRI (top panels) and jICA-ERP (lower panels) components of the motor and temporo-parietal sources (lower and upper triangle in each square representing one data point, respectively) is shown here for a linear fMRI/ERP relationship. The segregation of motor and temporo-parietal sources is shown as a function of the number of samples and number of components and for high SNR (ERP= 3.5; fMRI=7 (left) and low SNR (ERP= 0.37; fMRI=0.8 (right). The black arrow indicates separation of the temporal and motor sources into different components. At high SNR, motor and temporo-parietal were always segregated into separate components.

3.3.9   JICA source segregation: comparison of imaging modalities in parametric design

Figure 3-14 shows a comparison of jICA segregation of motor and temporo-parietal sources (lower and upper triangle in each square representing one data point, respectively) with fMRI and ERP responses that are related linearly in a parametric design. Results show that for both high and low SNRs, the motor and temporo-parietal sources contributed to the same jICA-fMRI component. However, the sources were always segregated into separate jICA-ERP components at high and low SNR.

Figure 3-14: Source segregation with jICA-fMRI and jICA-ERP for two sources in parametric design

Comparison of normalized source detection values for jICA-fMRI (top panels) and jICA-ERP (lower panels) components of the motor and temporo-parietal sources (lower and upper triangle in each square representing one data point, respectively) is shown here for a linear fMRI/ERP relationship. The segregation of motor and temporo-parietal sources is shown as a function of the number of samples and number of components and for high SNR (ERP= 3.5; fMRI=7 (left) and low SNR (ERP= 0.37; fMRI=0.8 (right). The black arrow indicates separation of the temporal and motor sources into different components. At high SNR, motor and temporo-parietal were always segregated into separate components.

3.4   Discussion

The integration of ERP and fMRI data can facilitate imaging of neural activity with high spatiotemporal resolution. JICA has successfully been applied to the integration of ERP and fMRI (Calhoun et al., 2006; Moosmann et al., 2008; Sui et al., 2011; Mangalathu-Arumana et al., 2012). Nevertheless, jICA (like other methods) is limited by the extent of variability in the data set, the SNR and the experimental design. Given that experiment duration is limited, there is a tradeoff between the number of independent samples or parametric levels that can practically be acquired and the SNR of each sample or level. Describing the dependence of jICA on these factors is useful for optimizing the design of future experiments wishing to use this method for ERP and fMRI data fusion.

A distinct feature of jICA is that it is not limited to linear relationships between ERP and fMRI, like linear regression models. Given that the relationship between ERP and fMRI signals may in some cases be nonlinear, or even uncoupled, it is important to understand the advantages and limitation of jICA with nonlinear signal variations.

Here we have used computer simulations to examine the performance of jICA as a function of SNR, number of samples, and the relationship between ERP and fMRI, in the case of parametric and non-parametric experimental designs. The jICA results revealed that simulated sources in the cortex can accurately be retrieved in time and space based on the ERP and fMRI signal covariations. However, the ability to retrieve a source in a single jICA component, measured here as the normalized source detection value, is dependent on multiple factors, including the SNR, the number of experimental samples and on the type of experimental design, whether parametric or non-parametric. JICA

successfully recovered linear, non-linear and uncoupled covariations between the ERP and fMRI signals in parametric and non-parametric designs.

For jICA-ERP, maximum normalized source detection values ranged 0.7-0.9 when ERP and fMRI sources co-varied linearly in a non-parametric experimental design, indicating that the majority of the source activity (70-90%) commonly varying from trial to trial was reflected in a single jICA-ERP component. This result was relatively robust to variations in SNR and number of samples for the ranges tested in this study. This finding is probably related to the large variability in space and time of the ERP data. Similar results were observed in the parametric design as well, suggesting that the type of experimental design did not have a significant effect on the extraction of ERP sources.

For jICA-fMRI, maximum normalized source detection values ranged 0.4-0.6 at low SNR and numbers of samples, and 0.8-1 at high SNR and number of samples, for ERP and fMRI sources that co-varied linearly in a non-parametric design. These results indicate that with low data variability, a high SNR is needed to recover the majority of the source into one component, whereas for high data variability jICA becomes relatively independent of the SNR. Since the goal is to extract linked sources, it might be advantageous to always correlate sources across components to identify linkages between ERP and fMRI dominant components, as was shown in Figure 3-12.

In the parametric design, the results obtained for jICA-fMRI were different from those obtained with the non-parametric design. JICA-fMRI maximum normalized source detection values ranged 0.8-1 at low SNR and numbers of samples, and 0.5-0.8 at high SNR and number of samples, for ERP and fMRI sources that co-varied linearly. In a parametric experimental design, there is a systematic relationship between the input and

physiological response across trials, resulting in a relatively strong correlation between sources. Thus, the sources simulated in this study were not independent (unlike those in the non-parametric experimental design), but rather were part of a neural network activated in a correlated manner across trials. In this case, jICA is not able to separate the sources.

For the uncoupled right frontal source, jICA-fMRI source detection values (s_N^{fMRI}) ranged 0.4-1 in the non-parametric design, but the values were largely biased toward the upper end of this range compared to those for the coupled sources. These findings can be understood in terms of the extent of functional correlation between sources. Sources varying in only one modality can be thought of as less functionally correlated with sources varying in both modalities. As a result, a lesser amount of signal variability or lower SNR is required for separation of an uncoupled source from coupled sources with jICA-fMRI (compared to separation of two coupled sources). Similar results were observed for the parametric design at both SNR levels (not shown).

When ERP and fMRI signals co-varied linearly in a non-parametric paradigm, sources were segregated into different jICA-ERP and jICA-fMRI components when the number of experimental samples increased (beyond 6 at high SNR and 80 at low SNR). This finding is probably due again to the difference between ERP and fMRI data, where ERP signals vary in time and in space, an fMRI signals solely in space. This understanding of the basis of jICA is critical for accurate interpretation of analysis results. Specifically, with high signal variability or high SNR, activity from the same neural source can be attributed to different jICA-fMRI and jICA-ERP components. In these cases, a secondary analysis, to identify linked ERP and fMRI components, is necessary to

determine the correspondence between fMRI and ERP activity. This could be accomplished through spatial correlation of significant voxel activity in the fMRI and temporal and spatial correlation of significant vertex activity in the ERP source maps across components to identify corresponding ERP and fMRI components. The strength of jICA is that it extracts the relevant information necessary for making conclusive observations. When ERP and fMRI signals co-varied nonlinearly in a non-parametric experimental design, ERP and fMRI activity was segregated into different components at similar sample numbers as those observed for a linear relationship (beyond 9 at high SNR and 100 at low SNR).

When ERP and fMRI signals co-varied linearly in a parametric paradigm, ERP and fMRI activity related to the temporo-parietal source was always attributed to one joint component. However, different results were observed with the motor source in both the parametric and non-parametric designs, where ERP and fMRI activity was separated into different jICA-ERP and jICA-fMRI components. The motor source was distinct in that it had a biphasic ERP temporal profile, whereas the temporo-parietal source had a single phase. It is possible that jICA separated the ERP and fMRI activity of the motor source into different components because this source was temporally more variable and therefore more distinguishable. However, more simulations are needed to test jICA on different types of ERP temporal variations and investigate the effect of this factor on source segregation.

In this work, the full array of spatial and temporal information from ERPs and the full spatial information from fMRI were incorporated into the jICA approach. The temporal ICA used the same ERP data and the spatial ICA used the same fMRI data.

Normalized source detection results for temporal ICA-ERP and spatial ICA-fMRI were similar to those observed with the jICA method, suggesting that source extraction with jICA was comparable to unimodal ICA approaches. However, the performance of jICA was poorer with low sample numbers and low SNRs. These results can be understood in the context of the increased complexity of the combined fMRI and ERP data used for jICA compared to the unimodal data used for temporal and spatial ICA. Since jICA extracts non-gaussian signals, it will not only separate different types of sources, but also imaging modalities. However, the primary advantage of jICA is precisely that it extracts joint components commonly varying across both imaging modalities and therefore presumably representing the same neural source. Importantly, the present work demonstrates that with optimal selection of paradigm parameters, jICA can provide comparable source separation results to temporal and spatial ICA, with the advantage of extracting joint activity between ERP and fMRI.

In summary, the jICA approach used here, incorporating spatiotemporal information from both fMRI and ERP data, revealed a dependence on SNR and the number of samples for resolving neural sources. The findings could help determine the optimal number of trials and conditions in parametric and non-parametric experiments that are necessary for segregation of neural sources into separate components using the jICA approach. Under optimal conditions, jICA was able to extract linear as well as nonlinear relationships, which could be advantageous when the relationship between ERP and fMRI signals is unknown, or when it is suspected to be nonlinear due to an underlying pathological condition. JICA was also found to extract uncoupled sources, which could be of clinical relevance in pathological conditions, such as stroke. Finally,

jICA reveals the underlying relationship between ERP and fMRI representations, which could be important for understanding the signals observed with fMRI and ERP in health, and in pathological conditions in which neurovascular coupling may be affected.

CHAPTER 4

Summary of Results

The focus of the work presented in this dissertation was the integration of ERP and fMRI with high temporal and spatial resolution, using jICA. In Chapter 2, the potential advantages of using jICA to fully integrate parametric fMRI and ERP P300 data within-subject was examined, relative to using the P300 ERP peak amplitude as a regressor in a general linear model. The jICA approach depicts linear and non-linear covariations between the ERP and fMRI signals, and therefore has the potential to be more sensitive and comprehensive than the general linear regression model. In addition, the full array of ERP electrodes and ERP data points was used here in the jICA approach, as opposed to the single electrode and point in time (peak activity) used (here and typically) in the linear regression analysis, thereby potentially allowing for more sensitive characterization of neural activity.

The empirical results showed that jICA successfully extracted neural sources with commonly varying ERP and fMRI activity. Using the entire spatio-temporal information of the ERP with the spatial information of the fMRI, enhanced the results observed with jICA. JICA results were superior to those of the P300 linear regression analysis, which used information from only one electrode at the time point of the P300 peak amplitude. Given that the nature of the relationship between ERP and fMRI signals in this study was unknown (whether nonlinearities were present), the superior sensitivity of the jICA relative to the general linear model (GLM) may largely be related to the inclusion of all spatio-temporal information from the ERPs. Another major finding was that jICA successfully recovered neural sources not only at the group level, but also at the individual data level. The single subject jICA-fMRI activity, and source reconstruction of the jICA-ERP activity within a component, were both consistent with the group jICA

maps. In contrast, the individual fMRI P300 regression maps and ERP source reconstructions were generally too noisy to evaluate, demonstrating an advantage of the jICA approach particularly for individual data analysis. This finding is particularly important because analysis of individual patient data is necessary for implementation of multimodal neuroimaging as a clinically relevant diagnostic tool.

In Chapter 3, computer simulations were used to characterize the ability of jICA to extract known neural sources within-subject as a function of data SNR, number of experimental samples and the relationship between the ERP and fMRI signals (linear vs. nonlinear, including uncoupled sources). The ability of jICA to detect and segregate neural sources measured with fMRI and ERPs was examined within-subject in the context of parametric and non-parametric experimental paradigms.

Simulation results showed that jICA performance varies as a function of SNR, number of experimental samples, experimental paradigm, and the relationship between fMRI and ERP sources. In a non-parametric design at low SNR and with low number of samples, the ERP and fMRI activity was extracted into a joint component with jICA. However, with increasing SNR and number of samples, ERP and fMRI activity was separated into different components. JICA extracted neural sources with linear as well as nonlinear relationships between ERP and fMRI signals. This feature of jICA is advantageous when the relationship between ERP and fMRI signals is unknown, or when it is suspected to be nonlinear due to an underlying pathological condition. JICA was also found to extract uncoupled sources, which could be of clinical relevance in pathological conditions, such as stroke. Another important finding was that jICA may in some cases (with high sample numbers) separate ERP and fMRI activity from the same source into

different components. However, split jICA-ERP and jICA-fMRI components can successfully be linked back together with a secondary correlation analysis. Nevertheless, future investigations need to be conducted to automate the linkage between ERP and fMRI sources. Another approach would be to take advantage of the temporal and spatial structure of the ERP and fMRI signal as part of an analysis such as complexity pursuit (Hyvarinen, 2001a). Most importantly, jICA could be used to extract the underlying relationship between ERP and fMRI signals. This type of information could be important for understanding physiological changes associated with pathological conditions affecting neurovascular coupling.

BIBLIOGRAPHY

Akgoren, N., Fabricius, M., Lauritzen, M., 1994. Importance of nitric oxide for local increases of blood flow in rat cerebellar cortex during electrical stimulation. Proc Natl Acad Sci U S A 91, 5903-5907.

Ances, B.M., Zarahn, E., Greenberg, J.H., Detre, J.A., 2000. Coupling of neural activation to blood flow in the somatosensory cortex of rats is time-intensity separable, but not linear. J Cereb Blood Flow Metab 20, 921-930.

Anderer, P., Pascual-Marqui, R.D., Semlitsch, H.V., Saletu, B., 1998. Differential effects of normal aging on sources of standard N1, target N1 and target P300 auditory event-related brain potentials revealed by low resolution electromagnetic tomography (LORETA). Electroencephalogr Clin Neurophysiol 108, 160-174.

Attwell, D., Iadecola, C., 2002. The neural basis of functional brain imaging signals. Trends Neurosci 25, 621-625.

Babiloni, F., Carducci, F., Cincotti, F., Del Gratta, C., Roberti, G.M., Romani, G.L., Rossini, P.M., Babiloni, C., 2000. Integration of high resolution EEG and functional magnetic resonance in the study of human movement-related potentials. Methods Inf Med 39, 179-182.

Babiloni, F., Cincotti, F., 2004. Multimodal imaging from neuroelectrictromagnetic and functional magnetic resonance recordings. In: He, B. (Ed.), Modeling and Imaging of Bioelectrical Activity
New York.

Basile, L.F., Rogers, R.L., Simos, P.G., Papanicolaou, A.C., 1997. Magnetoencephalographic evidence for common sources of long latency fields to rare target and rare novel visual stimuli. Int J Psychophysiol 25, 123-137.

Belin, P., Zatorre, R.J., Hoge, R., Evans, A.C., Pike, B., 1999. Event-related fMRI of the auditory cortex. Neuroimage 10, 417-429.

Bell, A.J., Sejnowski, T.J., 1995. An information-maximization approach to blind separation and blind deconvolution. Neural Comput 7, 1129-1159.

Belliveau, J.W., Rosen, B.R., Kantor, H.L., Rzedzian, R.R., Kennedy, D.N., McKinstry, R.C., Vevea, J.M., Cohen, M.S., Pykett, I.L., Brady, T.J., 1990. Functional cerebral imaging by susceptibility-contrast NMR. Magn Reson Med 14, 538-546.

Benar, C.G., Schon, D., Grimault, S., Nazarian, B., Burle, B., Roth, M., Badier, J.M., Marquis, P., Liegeois-Chauvel, C., Anton, J.L., 2007. Single-trial analysis of oddball event-related potentials in simultaneous EEG-fMRI. Hum Brain Mapp 28, 602-613.

Berger, H., 1929. Ueber das Elekroenkephalogram des Menschen. Arch f Psychiat 87, 527-570.

Birn, R.M., Bandettini, P.A., 2005. The effect of stimulus duty cycle and "off" duration on BOLD response linearity. Neuroimage 27, 70-82.

Bonmassar, G., Schwartz, D.P., Liu, A.K., Kwong, K.K., Dale, A.M., Belliveau, J.W., 2001. Spatiotemporal brain imaging of visual-evoked activity using interleaved EEG and fMRI recordings. Neuroimage 13, 1035-1043.

Boynton, G.M., Engel, S.A., Glover, G.H., Heeger, D.J., 1996. Linear systems analysis of functional magnetic resonance imaging in human V1. J Neurosci 16, 4207-4221.

Brookings, T., Ortigue, S., Grafton, S., Carlson, J., 2009. Using ICA and realistic BOLD models to obtain joint EEG/fMRI solutions to the problem of source localization. Neuroimage 44, 411-420.

Brown, K.S., Ortigue, S., Grafton, S.T., Carlson, J.M., 2010. Improving human brain mapping via joint inversion of brain electrodynamics and the BOLD signal. Neuroimage 49, 2401-2415.

Buerk, D.G., Ances, B.M., Greenberg, J.H., Detre, J.A., 2003. Temporal dynamics of brain tissue nitric oxide during functional forepaw stimulation in rats. Neuroimage 18, 1-9.

Calhoun, V., Wu, L., Kiehl, K., Eichele, T., Pearlson, G., 2010. Aberrant Processing of Deviant Stimuli in Schizophrenia Revealed by Fusion of FMRI and EEG Data. Acta Neuropsychiatr 22, 127-138.

Calhoun, V.D., Adali, T., Pearlson, G.D., Kiehl, K.A., 2006. Neuronal chronometry of target detection: fusion of hemodynamic and event-related potential data. Neuroimage 30, 544-553.

Calhoun, V.D., Liu, J., Adali, T., 2009. A review of group ICA for fMRI data and ICA for joint inference of imaging, genetic, and ERP data. Neuroimage 45, S163-172.

Coles, M.G., Gratton, G., Donchin, E., 1988. Detecting early communication: using measures of movement-related potentials to illuminate human information processing. Biol Psychol 26, 69-89.

Correa, N.M., Eichele, T., Adali, T., Li, Y.O., Calhoun, V.D., 2010. Multi-set canonical correlation analysis for the fusion of concurrent single trial ERP and functional MRI. Neuroimage 50, 1438-1445.

Correa, N.M., Li, Y.O., Adali, T., Calhoun, V.D., 2008. Canonical Correlation Analysis for Feature-Based Fusion of Biomedical Imaging Modalities and Its Application to Detection of Associative Networks in Schizophrenia. IEEE J Sel Top Signal Process 2, 998-1007.

Cox, R.W., 1996. AFNI: software for analysis and visualization of functional magnetic resonance neuroimages. Comput Biomed Res 29, 162-173.

Dale, A.M., Fischl, B., Sereno, M.I., 1999. Cortical surface-based analysis. I. Segmentation and surface reconstruction. Neuroimage 9, 179-194.

Dale, A.M., Halgren, E., 2001. Spatiotemporal mapping of brain activity by integration of multiple imaging modalities. Curr Opin Neurobiol 11, 202-208.

Daunizeau, J., Grova, C., Marrelec, G., Mattout, J., Jbabdi, S., Pelegrini-Issac, M., Lina, J.M., Benali, H., 2007. Symmetrical event-related EEG/fMRI information fusion in a variational Bayesian framework. Neuroimage 36, 69-87.

Debener, S., Ullsperger, M., Siegel, M., Fiehler, K., von Cramon, D.Y., Engel, A.K., 2005. Trial-by-trial coupling of concurrent electroencephalogram and functional magnetic resonance imaging identifies the dynamics of performance monitoring. J Neurosci 25, 11730-11737.

Desmond, J.E., Glover, G.H., 2002. Estimating sample size in functional MRI (fMRI) neuroimaging studies: statistical power analyses. J Neurosci Methods 118, 115-128.

Dubois, C., Otzenberger, H., Gounot, D., Sock, R., Metz-Lutz, M.N., 2012. Visemic processing in audiovisual discrimination of natural speech: A simultaneous fMRI-EEG study. Neuropsychologia.

Edmister, W.B., Talavage, T.M., Ledden, P.J., Weisskoff, R.M., 1999. Improved auditory cortex imaging using clustered volume acquisitions. Hum Brain Mapp 7, 89-97.

Edwards, B.G., Calhoun, V.D., Kiehl, K.A., 2011. Joint ICA of ERP and fMRI during error-monitoring. Neuroimage.

Eichele, T., Specht, K., Moosmann, M., Jongsma, M.L., Quiroga, R.Q., Nordby, H., Hugdahl, K., 2005. Assessing the spatiotemporal evolution of neuronal activation with single-trial event-related potentials and functional MRI. Proc Natl Acad Sci U S A 102, 17798-17803.

Esposito, F., Mulert, C., Goebel, R., 2009. Combined distributed source and single-trial EEG-fMRI modeling: application to effortful decision making processes. Neuroimage 47, 112-121.

Faro, S., 2006. Functional MRI: Basic Principles and Clinical Applications. Springer.

Feinberg, D.A., Moeller, S., Smith, S.M., Auerbach, E., Ramanna, S., Gunther, M., Glasser, M.F., Miller, K.L., Ugurbil, K., Yacoub, E., 2010. Multiplexed echo planar imaging for sub-second whole brain FMRI and fast diffusion imaging. PLoS One 5, e15710.

Fischl, B., Sereno, M.I., Dale, A.M., 1999. Cortical surface-based analysis. II: Inflation, flattening, and a surface-based coordinate system. Neuroimage 9, 195-207.

Friedman, D., Goldman, R., Stern, Y., Brown, T.R., 2009. The brain's orienting response: An event-related functional magnetic resonance imaging investigation. Hum Brain Mapp 30, 1144-1154.

Girouard, H., Iadecola, C., 2006. Neurovascular coupling in the normal brain and in hypertension, stroke, and Alzheimer disease. J Appl Physiol 100, 328-335.

Goldman, R.I., Wei, C.Y., Philiastides, M.G., Gerson, A.D., Friedman, D., Brown, T.R., Sajda, P., 2009. Single-trial discrimination for integrating simultaneous EEG and fMRI: identifying cortical areas contributing to trial-to-trial variability in the auditory oddball task. Neuroimage 47, 136-147.

Grafton, S.T., 2009. Embodied cognition and the simulation of action to understand others. Ann N Y Acad Sci 1156, 97-117.

Halgren, E., Marinkovic, K., Chauvel, P., 1998. Generators of the late cognitive potentials in auditory and visual oddball tasks. Electroencephalogr Clin Neurophysiol 106, 156-164.

Halgren, E., Squires, N.K., Wilson, C.L., Rohrbaugh, J.W., Babb, T.L., Crandall, P.H., 1980. Endogenous potentials generated in the human hippocampal formation and amygdala by infrequent events. Science 210, 803-805.

Hall, D.A., Haggard, M.P., Akeroyd, M.A., Palmer, A.R., Summerfield, A.Q., Elliott, M.R., Gurney, E.M., Bowtell, R.W., 1999. "Sparse" temporal sampling in auditory fMRI. Hum Brain Mapp 7, 213-223.

Heeger, D.J., Huk, A.C., Geisler, W.S., Albrecht, D.G., 2000. Spikes versus BOLD: what does neuroimaging tell us about neuronal activity? Nat Neurosci 3, 631-633.

Hewson-Stoate, N., Jones, M., Martindale, J., Berwick, J., Mayhew, J., 2005. Further nonlinearities in neurovascular coupling in rodent barrel cortex. Neuroimage 24, 565-574.

Holmes, C.J., Hoge, R., Collins, L., Woods, R., Toga, A.W., Evans, A.C., 1998. Enhancement of MR images using registration for signal averaging. J Comput Assist Tomogr 22, 324-333.

Horovitz, S.G., Skudlarski, P., Gore, J.C., 2002. Correlations and dissociations between BOLD signal and P300 amplitude in an auditory oddball task: a parametric approach to combining fMRI and ERP. Magn Reson Imaging 20, 319-325.

Huettel, S., Song, A., McCarthy, G., 2009. Functional Magnetic Resonance Imaging, Sunderland.

Huster, R.J., Debener, S., Eichele, T., Herrmann, C.S., 2012. Methods for Simultaneous EEG-fMRI: An Introductory Review. J Neurosci 32, 6053-6060.

Huster, R.J., Eichele, T., Enriquez-Geppert, S., Wollbrink, A., Kugel, H., Konrad, C., Pantev, C., 2011. Multimodal imaging of functional networks and event-related potentials in performance monitoring. Neuroimage 56, 1588-1597.

Hyvarinen, A., 2001a. Complexity pursuit: separating interesting components from time series. Neural Comput 13, 883-898.

Hyvarinen, J.K.E.O.A., 2001b. Independent Component Analysis. John Wiley & Sons.

Iadecola, C., Li, J., Ebner, T.J., Xu, X., 1995. Nitric oxide contributes to functional hyperemia in cerebellar cortex. Am J Physiol 268, R1153-1162.

Ibarretxe-Bilbao, N., Junque, C., Marti, M.J., Tolosa, E., 2011. Cerebral basis of visual hallucinations in Parkinson's disease: structural and functional MRI studies. J Neurol Sci 310, 79-81.

Jasper, H., 1958. Report of committee on methods of clinical exam in EEG. Clin Neurophysiol.

Kiehl, K.A., Liddle, P.F., 2003. Reproducibility of the hemodynamic response to auditory oddball stimuli: a six-week test-retest study. Hum Brain Mapp 18, 42-52.

Kiehl, K.A., Stevens, M.C., Laurens, K.R., Pearlson, G., Calhoun, V.D., Liddle, P.F., 2005. An adaptive reflexive processing model of neurocognitive function: supporting evidence from a large scale (n = 100) fMRI study of an auditory oddball task. Neuroimage 25, 899-915.

Knight, R.T., 1984. Decreased response to novel stimuli after prefrontal lesions in man. Electroencephalogr Clin Neurophysiol 59, 9-20.

Kraiuhin, C., Gordon, E., Stanfield, P., Meares, R., Howson, A., 1986. P300 and the effects of aging: relevance to the diagnosis of dementia. Exp Aging Res 12, 187-192.

Kruggel, F., Herrmann, C.S., Wiggins, C.J., von Cramon, D.Y., 2001. Hemodynamic and electroencephalographic responses to illusory figures: recording of the evoked potentials during functional MRI. Neuroimage 14, 1327-1336.

Kuschinsky, W., Wahl, M., Bosse, O., Thurau, K., 1972. Perivascular potassium and pH as determinants of local pial arterial diameter in cats. A microapplication study. Circ Res 31, 240-247.

Lantz, G., Grave de Peralta Menendez, R., Gonzalez Andino, S., Michel, C.M., 2001. Noninvasive localization of electromagnetic epileptic activity. II. Demonstration of sublobar accuracy in patients with simultaneous surface and depth recordings. Brain Topogr 14, 139-147.

Laufs, H., Daunizeau, J., Carmichael, D.W., Kleinschmidt, A., 2008. Recent advances in recording electrophysiological data simultaneously with magnetic resonance imaging. Neuroimage 40, 515-528.

Lauterbur, P.C., 1973. Image formation by induced local interactions. Examples employing nuclear magnetic resonance. 1973. Clin Orthop Relat Res, 3-6.

Lee, K., Tak, S., Ye, J.C., 2010. A data-driven sparse GLM for fMRI analysis using sparse dictionary learning with MDL criterion. IEEE Trans Med Imaging 30, 1076-1089.

Lei, X., Qiu, C., Xu, P., Yao, D., 2010. A parallel framework for simultaneous EEG/fMRI analysis: methodology and simulation. Neuroimage 52, 1123-1134.

Lemieux, L., Salek-Haddadi, A., Josephs, O., Allen, P., Toms, N., Scott, C., Krakow, K., Turner, R., Fish, D.R., 2001. Event-related fMRI with simultaneous and continuous EEG: description of the method and initial case report. Neuroimage 14, 780-787.

Liebenthal, E., Desai, R., Ellingson, M.M., Ramachandran, B., Desai, A., Binder, J.R., 2010. Specialization along the left superior temporal sulcus for auditory categorization. Cereb Cortex 20, 2958-2970.

Liebenthal, E., Ellingson, M.L., Spanaki, M.V., Prieto, T.E., Ropella, K.M., Binder, J.R., 2003. Simultaneous ERP and fMRI of the auditory cortex in a passive oddball paradigm. Neuroimage 19, 1395-1404.

Lindauer, U., Megow, D., Matsuda, H., Dirnagl, U., 1999. Nitric oxide: a modulator, but not a mediator, of neurovascular coupling in rat somatosensory cortex. Am J Physiol 277, H799-811.

Linden, D.E., 2005. The p300: where in the brain is it produced and what does it tell us? Neuroscientist 11, 563-576.

Linden, D.E., Prvulovic, D., Formisano, E., Vollinger, M., Zanella, F.E., Goebel, R., Dierks, T., 1999. The functional neuroanatomy of target detection: an fMRI study of visual and auditory oddball tasks. Cereb Cortex 9, 815-823.

Liu, Z., Rios, C., Zhang, N., Yang, L., Chen, W., He, B., 2010. Linear and nonlinear relationships between visual stimuli, EEG and BOLD fMRI signals. Neuroimage 50, 1054-1066.

Logothetis, N.K., Pauls, J., Augath, M., Trinath, T., Oeltermann, A., 2001. Neurophysiological investigation of the basis of the fMRI signal. Nature 412, 150-157.

Louza, M.R., Maurer, K., 1989. Differences between paranoid and nonparanoid schizophrenic patients on the somatosensory P300 event-related potential. Neuropsychobiology 21, 59-66.

Louza, M.R., Maurer, K., Neuhauser, B., 1992. Changes in P300 latency and amplitude in schizophrenic patients and healthy controls during the examination. Electromyogr Clin Neurophysiol 32, 603-610.

Luessi, M., Babacan, S.D., Molina, R., Booth, J.R., Katsaggelos, A.K., 2010. Bayesian symmetrical EEG/fMRI fusion with spatially adaptive priors. Neuroimage 55, 113-132.

Mackert, B.M., Leistner, S., Sander, T., Liebert, A., Wabnitz, H., Burghoff, M., Trahms, L., Macdonald, R., Curio, G., 2008. Dynamics of cortical neurovascular coupling analyzed by simultaneous DC-magnetoencephalography and time-resolved near-infrared spectroscopy. Neuroimage 39, 979-986.

Mangalathu-Arumana, J., Beardsley, S.A., Liebenthal, E., 2012. Within-subject joint independent component analysis of simultaneous fMRI/ERP in an auditory oddball paradigm. Neuroimage 60, 2247-2257.

Martinez-Montes, E., Valdes-Sosa, P.A., Miwakeichi, F., Goldman, R.I., Cohen, M.S., 2004. Concurrent EEG/fMRI analysis by multiway Partial Least Squares. Neuroimage 22, 1023-1034.

Mathiesen, C., Caesar, K., Akgoren, N., Lauritzen, M., 1998. Modification of activity-dependent increases of cerebral blood flow by excitatory synaptic activity and spikes in rat cerebellar cortex. J Physiol 512 (Pt 2), 555-566.

McCarthy, G., Wood, C.C., Williamson, P.D., Spencer, D.D., 1989. Task-dependent field potentials in human hippocampal formation. J Neurosci 9, 4253-4268.

Mechelli, A., Friston, K.J., Price, C.J., 2000. The effects of presentation rate during word and pseudoword reading: a comparison of PET and fMRI. J Cogn Neurosci 12 Suppl 2, 145-156.

Mecklinger, A., Maess, B., Opitz, B., Pfeifer, E., Cheyne, D., Weinberg, H., 1998. A MEG analysis of the P300 in visual discrimination tasks. Electroencephalogr Clin Neurophysiol 108, 45-56.

Menon, V., Ford, J.M., Lim, K.O., Glover, G.H., Pfefferbaum, A., 1997. Combined event-related fMRI and EEG evidence for temporal-parietal cortex activation during target detection. Neuroreport 8, 3029-3037.

Michel, C.M., Lantz, G., Spinelli, L., De Peralta, R.G., Landis, T., Seeck, M., 2004. 128-channel EEG source imaging in epilepsy: clinical yield and localization precision. J Clin Neurophysiol 21, 71-83.

Mijovic, B., Vanderperren, K., Novitskiy, N., Vanrumste, B., Stiers, P., Van den Bergh, B., Lagae, L., Sunaert, S., Wagemans, J., Van Huffel, S., De Vos, M., 2012. The "why" and "how" of JointICA: Results from a visual detection task. Neuroimage.

Moosmann, M., Eichele, T., Nordby, H., Hugdahl, K., Calhoun, V.D., 2008. Joint independent component analysis for simultaneous EEG-fMRI: principle and simulation. Int J Psychophysiol 67, 212-221.

Mulert, C., Jager, L., Schmitt, R., Bussfeld, P., Pogarell, O., Moller, H.J., Juckel, G., Hegerl, U., 2004. Integration of fMRI and simultaneous EEG: towards a comprehensive understanding of localization and time-course of brain activity in target detection. Neuroimage 22, 83-94.

Ngai, A.C., Jolley, M.A., D'Ambrosio, R., Meno, J.R., Winn, H.R., 1999. Frequency-dependent changes in cerebral blood flow and evoked potentials during somatosensory stimulation in the rat. Brain Res 837, 221-228.

Nguyen, T.S., Winn, H.R., Janigro, D., 2000. ATP-sensitive potassium channels may participate in the coupling of neuronal activity and cerebrovascular tone. Am J Physiol Heart Circ Physiol 278, H878-885.

Northington, F.J., Matherne, G.P., Berne, R.M., 1992. Competitive inhibition of nitric oxide synthase prevents the cortical hyperemia associated with peripheral nerve stimulation. Proc Natl Acad Sci U S A 89, 6649-6652.

Nunez, P., Srinivasan, R., 2005. Electric Fields of the Brain: The Neurophysics of EEG, 2nd Edition ed. Oxford University.

Nunez, P.L., Silberstein, R.B., 2000. On the relationship of synaptic activity to macroscopic measurements: does co-registration of EEG with fMRI make sense? Brain Topogr 13, 79-96.

O'Connell, R.G., Balsters, J.H., Kilcullen, S.M., Campbell, W., Bokde, A.W., Lai, R., Upton, N., Robertson, I.H., 2012. A simultaneous ERP/fMRI investigation of the P300 aging effect. Neurobiol Aging.

Ogawa, S., Lee, T.M., Kay, A.R., Tank, D.W., 1990. Brain magnetic resonance imaging with contrast dependent on blood oxygenation. Proc Natl Acad Sci U S A 87, 9868-9872.

Opitz, B., Mecklinger, A., Von Cramon, D.Y., Kruggel, F., 1999. Combining electrophysiological and hemodynamic measures of the auditory oddball. Psychophysiology 36, 142-147.

Ou, W., Nummenmaa, A., Golland, P., Hamalainen, M.S., 2009. Multimodal functional imaging using fMRI-informed regional EEG/MEG source estimation. Conf Proc IEEE Eng Med Biol Soc 2009, 1926-1929.

Philiastides, M.G., Sajda, P., 2007. EEG-informed fMRI reveals spatiotemporal characteristics of perceptual decision making. J Neurosci 27, 13082-13091.

Picton, T.W., 1992. The P300 wave of the human event-related potential. J Clin Neurophysiol 9, 456-479.

Plis, S.M., Calhoun, V.D., Weisend, M.P., Eichele, T., Lane, T., 2010. MEG and fMRI Fusion for Non-Linear Estimation of Neural and BOLD Signal Changes. Front Neuroinform 4, 114.

Plonsey, R., 1969. Bioelectric phenomena. McGraw-Hill, New York.

Polich, J., 2007. Updating P300: an integrative theory of P3a and P3b. Clin Neurophysiol 118, 2128-2148.

Polich, J., Corey-Bloom, J., 2005. Alzheimer's disease and P300: review and evaluation of task and modality. Curr Alzheimer Res 2, 515-525.

Polich, J., Pitzer, A., 1999. P300 and Alzheimer's disease: oddball task difficulty and modality effects. Electroencephalogr Clin Neurophysiol Suppl 50, 281-287.

Prvulovic, D., Bokde, A.L., Faltraco, F., Hampel, H., 2011. Functional magnetic resonance imaging as a dynamic candidate biomarker for Alzheimer's disease. Prog Neurobiol 95, 557-569.

Rees, G., Friston, K., Koch, C., 2000. A direct quantitative relationship between the functional properties of human and macaque V5. Nat Neurosci 3, 716-723.

Rees, G., Howseman, A., Josephs, O., Frith, C.D., Friston, K.J., Frackowiak, R.S., Turner, R., 1997. Characterizing the relationship between BOLD contrast and regional cerebral blood flow measurements by varying the stimulus presentation rate. Neuroimage 6, 270-278.

Ritter, W., Vaughan, H.G., Jr., 1969. Averaged evoked responses in vigilance and discrimination: a reassessment. Science 164, 326-328.

Rosa, M.J., Daunizeau, J., Friston, K.J., 2011. EEG-fMRI integration: a critical review of biophysical modeling and data analysis approaches. J Integr Neurosci 9, 453-476.

Sanei, S., Chambers, J., 2007. EEG signal processing. John Wiley & Sons.

Sara, G., Kraiuhin, C., Gordon, E., Landau, P., James, L., Howson, A., Meares, R., 1988. The P300 event related potential component in the diagnosis of dementia. Aust N Z J Med 18, 657-660.

Shaywitz, B.A., Lyon, G.R., Shaywitz, S.E., 2006. The role of functional magnetic resonance imaging in understanding reading and dyslexia. Dev Neuropsychol 30, 613-632.

Smith, M.E., Halgren, E., Sokolik, M., Baudena, P., Musolino, A., Liegeois-Chauvel, C., Chauvel, P., 1990. The intracranial topography of the P3 event-related potential elicited during auditory oddball. Electroencephalogr Clin Neurophysiol 76, 235-248.

Sperling, R., 2011. Potential of functional MRI as a biomarker in early Alzheimer's disease. Neurobiol Aging 32 Suppl 1, S37-43.

Strobel, A., Debener, S., Sorger, B., Peters, J.C., Kranczioch, C., Hoechstetter, K., Engel, A.K., Brocke, B., Goebel, R., 2008. Novelty and target processing during an auditory novelty oddball: a simultaneous event-related potential and functional magnetic resonance imaging study. Neuroimage 40, 869-883.

Sui, J., Pearlson, G., Caprihan, A., Adali, T., Kiehl, K.A., Liu, J., Yamamoto, J., Calhoun, V.D., 2011. Discriminating schizophrenia and bipolar disorder by fusing fMRI and DTI in a multimodal CCA+ joint ICA model. Neuroimage 57, 839-855.

Swanson, S.J., Sabsevitz, D.S., Hammeke, T.A., Binder, J.R., 2007. Functional magnetic resonance imaging of language in epilepsy. Neuropsychol Rev 17, 491-504.

Tadel, F., Baillet, S., Mosher, J.C., Pantazis, D., Leahy, R.M., 2011. Brainstorm: a user-friendly application for MEG/EEG analysis. Comput Intell Neurosci 2011, 879716.

Tournoux, J.T.a.P., 1988. Co-Planar Stereotaxic Atlas of the Human Brain. Thieme Medical Publishers, New York.

Ullsperger, M., Debener, S., 2010. Simultaneous EEG and fMRI: Recording, Analysis and Applications. Oxford Univeristy Press, New York.

Vanni, S., Warnking, J., Dojat, M., Delon-Martin, C., Bullier, J., Segebarth, C., 2004. Sequence of pattern onset responses in the human visual areas: an fMRI constrained VEP source analysis. Neuroimage 21, 801-817.

Verleger, R., Heide, W., Butt, C., Kompf, D., 1994. Reduction of P3b in patients with temporo-parietal lesions. Brain Res Cogn Brain Res 2, 103-116.

Volpe, U., Mucci, A., Bucci, P., Merlotti, E., Galderisi, S., Maj, M., 2007. The cortical generators of P3a and P3b: a LORETA study. Brain Res Bull 73, 220-230.

Weber, R., Ramos-Cabrer, P., Justicia, C., Wiedermann, D., Strecker, C., Sprenger, C., Hoehn, M., 2008. Early prediction of functional recovery after experimental stroke: functional magnetic resonance imaging, electrophysiology, and behavioral testing in rats. J Neurosci 28, 1022-1029.

Yang, Y., Engelien, A., Engelien, W., Xu, S., Stern, E., Silbersweig, D.A., 2000. A silent event-related functional MRI technique for brain activation studies without interference of scanner acoustic noise. Magn Reson Med 43, 185-190.

Zarahn, E., Aguirre, G.K., D'Esposito, M., 1997. Empirical analyses of BOLD fMRI statistics. I. Spatially unsmoothed data collected under null-hypothesis conditions. Neuroimage 5, 179-197.

Zhang, N., Liu, Z., He, B., Chen, W., 2008a. Noninvasive study of neurovascular coupling during graded neuronal suppression. J Cereb Blood Flow Metab 28, 280-290.

Zhang, N., Zhu, X.H., Liu, Z., He, B., Chen, W., 2008b. Quantitatively Interpreting fMRI signal. Conf Proc IEEE Eng Med Biol Soc 2008, 4415-4418.

APPENDIX

Volume	Mean	Max	x	y	z	Lobe	Structure
Positive activations							
1612	2.32	2.98	60	-27	10	Right Temporal	Superior Temporal Gyrus
13523	2.32	3.62	20	-81	36	Right Parietal	Superior Parietal Lobule
1788	2.46	4.27	39	38	-4	Right Frontal	Middle Frontal Gyrus
1173	2.29	3.00	29	17	-4	Right	Insula
3327	2.48	4.42	-48	-23	-18		Inferior Temporal Gyrus
1301	2.35	2.98	-25	-76	-14	Left Temporal	Fusiform Gyrus
1297	2.22	2.59	-48	-24	13		Superior Temporal Gyrus
1103	2.39	3.39	-41	-56	4		Middle Temporal Gyrus
22704	2.34	4.03	-29	-77	42	Left Parietal	Inferior Parietal Lobule
4045	2.26	2.98	-10	-8	51		Frontal Gyrus
2482	2.54	4.39	-26	53	8	Left Frontal	Middle Frontal Gyrus
1109	2.27	2.89	-50	-5	11		Inferior Frontal Gyrus
2330	2.39	3.61	-1	-55	-23	Left Cerebellum	Cerebellum

Table 5-1: Cluster volumes of group fMRI maps
The volume (in µl), mean and maximum t-values, center of mass Talairach coordinates (Talairach and Tournoux, 1988), and lobe location and structure labels of clusters of fMRI activation for the group of twenty subjects, using the P300 peak as a regressor in the general linear model. Coordinates are reported in LPI orientation.

Volume	Mean	Max	x	y	z	Lobe	Structure
Positive activations							
118	2.44	3.16	55	-34	29	Right Temporal	Supramarginal Gyrus
298	2.31	2.80	22	-58	69	Right Parietal	Superior Parietal Lobule
223	2.25	2.59	10	-68	32	Right Occipital	Cuneus
379	2.34	3.04	31	28	46		Middle Frontal Gyrus
335	2.40	2.79	13	46	39		Superior Frontal Gyrus
214	2.28	2.76	25	11	62	Right Frontal	Middle Frontal Gyrus
150	2.53	3.17	34	4	32		Superior Frontal Gyrus
146	2.50	2.90	52	34	25		Middle Frontal Gyrus
125	2.40	3.23	-41	-73	22	Left Temporal	Middle Temporal Gyrus
189	2.61	3.39	-46	-37	25	Left Parietal	Inferior Parietal Lobule
295	2.20	2.60	-14	-19	74		Precentral Gyrus
179	2.20	2.51	-13	-35	70		Precentral Gyrus
161	2.61	3.25	-20	11	46	Left Frontal	Medial Frontal Gyrus
148	2.39	2.95	-2	2	64		Superior Frontal Gyrus
144	2.40	3.22	-25	-4	66		Superior Frontal Gyrus
195	2.58	3.54	-1	-43	22	Left	Posterior Cingulate
Negative activations							
105	-2.39	-2.86	46	-5	43	Right Frontal	Precentral Gyrus

Table 5-2: Cluster volumes of single subject 4138 fMRI maps
The volume (in µl), mean and maximum t-values, center of mass Talairach coordinates (Talairach and Tournoux, 1988), and lobe location and structure labels of clusters of fMRI activation for subject 4138, using the P300 peak as a regressor in the general linear model. Clusters smaller than 105 µl are not reported in the table, but are shown in the corresponding fMRI maps in the paper. Coordinates are reported from Left-to-Parietal-to-Inferior (LPI) orientation.

Volume	Mean	Max	x	y	z	Lobe	Structure
				Positive activations			
563	3.2152	4.0965	63.5	-36.5	14.5	Right Temporal	Superior Temporal Gyrus
1451	3.4126	5.2656	47.5	-38.5	23.5	Right	Inferior Parietal Lobule
503	3.2311	4.454	2.5	-51.5	42.5	Parietal	Precuneus
448	3.5221	5.5071	27.5	-58.5	47.5		Superior Parietal Lobule
936	3.3239	4.9576	48.5	-13.5	40.5	Right	Precentral Gyrus
594	4.0415	5.771	37.5	-17.5	54.5	Frontal	Precentral Gyrus
505	3.8673	6.2543	8.5	-51.5	-5.5	Right Cerebellum	Culmen
562	3.3763	4.8332	35.5	-9.5	20.5	Right	Insula
25055	3.6623	11.019	-32.5	-27.5	40.5		Postcentral Gyrus
1021	3.4652	5.7677	-15.5	-75.5	41.5	Left Parietal	Precuneus
1250	3.2999	4.7714	25.5	-79.5	22.5	Left Occipital	Cuneus
3751	3.5304	7.4036	-2.5	-19.5	47.5		Paracentral Lobule
1381	3.5282	5.7255	-27.5	27.5	32.5		Middle Frontal Gyrus
1028	3.6194	6.2478	-12.5	53.5	19.5	Left Frontal	Superior Frontal Gyrus
565	3.4441	5.5172	-39.5	20.5	18.5		Middle Frontal Gyrus
1107	3.4282	5.8927	-0.5	-60.5	-2.5	Left Cerebellum	Cerebellum
412	3.423	6.0185	-10.5	-23.5	12.5	Left	Thalamus

Table 5-3: Cluster volumes of group jICA-fMRI
The volume (in μl), mean and maximum t-values, center of mass Talairach coordinates (Talairach and Tournoux, 1988), and lobe location and structure labels of clusters of jICA-fMRI activation for the group of twenty subjects (Volumes were voxel-thresholded at p<0.01 to separate two large clusters (larger than 83000 □l) into smaller ones). Coordinates are reported in LPI orientation.
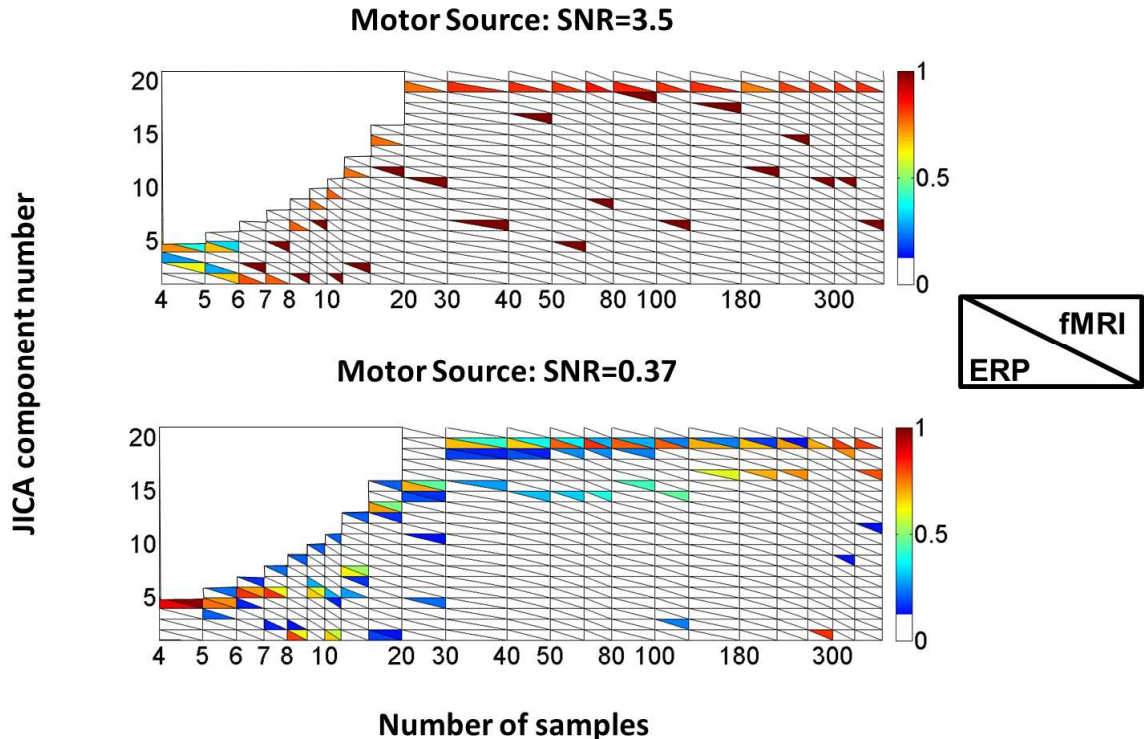
Volume	Mean	Max	x	y	z	Lobe	Structure
			Positive activations				
724	0.82	1.13	59	-41	-4		Middle Temporal Gyrus
724	0.85	1.33	59	-50	14	Right Temporal	Superior Temporal Gyrus
630	0.72	1.12	50	-38	10		Superior Temporal Gyrus
598	1.07	1.48	56	-26	14		Superior Temporal Gyrus
1166	0.87	2.21	56	-35	28		Inferior Parietal Lobule
788	1.02	1.45	59	-32	24	Right Parietal	Inferior Parietal Lobule
756	1.03	1.60	59	-41	17		Superior Temporal Gyrus
598	0.91	1.81	53	-26	17		Postcentral Gyrus
630	0.86	1.14	2	-77	28	Right	Cuneus
536	0.59	1.04	14	-74	-1	Occipital	Lingual Gyrus
567	0.95	1.49	11	53	10	Right Frontal	Superior Frontal Gyrus
724	0.77	1.50	8	8	31	Right	Cingulate Gyrus
662	0.91	1.52	-41	-32	45	Left Parietal	Inferior Parietal Lobule
693	0.64	1.20	-29	-26	52		Precentral Gyrus
630	0.26	-1.26	-35	35	24	Left Frontal	Middle Frontal Gyrus
976	0.77	1.01	-8	-38	-39	Left	Cerebellum
536	0.74	1.01	-11	-53	-4	Cerebellum	Cerebellum
			Negative activations				
2142	-0.67	-0.95	8	-41	63	Right Parietal	Postcentral Gyrus
1354	-0.69	-1.03	17	-50	59		Superior Parietal Lobule
1858	-0.65	-1.01	-26	-29	59	Left Parietal	Postcentral Gyrus
882	-0.64	-0.86	-17	-38	63		Postcentral Gyrus
756	-0.67	-0.90	-2	-2	63	Left Frontal	Superior frontal gyrus

Table 5-4: Cluster volumes of single subject jICA-fMRI maps
The volume (in µl), mean and maximum t-values, center of mass Talairach coordinates (Talairach and Tournoux, 1988), and lobe location and structure labels of clusters of jICA-fMRI activation for subject 4138. Coordinates are reported in LPI orientation.

Linear Relationship: Non-parametric design

Motor Source: SNR=3.5

Motor Source: SNR=0.37

JICA component number

Number of samples
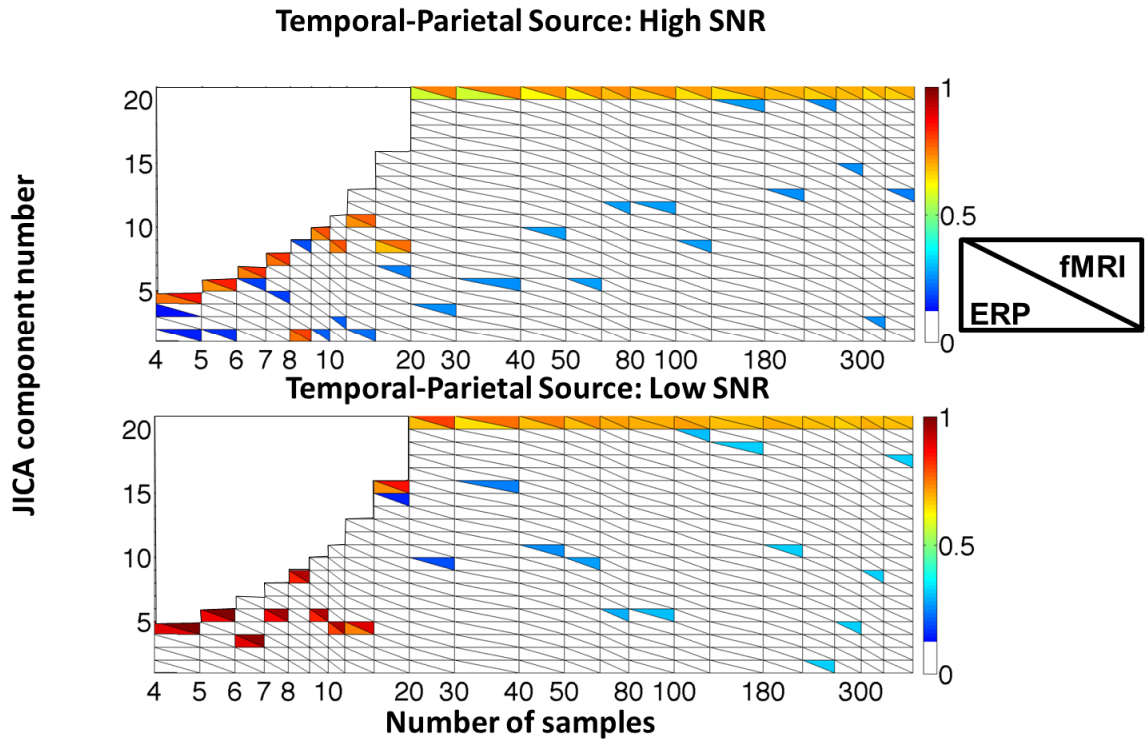
Figure 5-1: Normalized source detection for the motor source with linear relationship
Normalized source detection values for jICA-ERP and jICA-fMRI using a nonparametric experimental design, (lower and upper triangle in each square representing max(s_N^{EEG}) and max(s_N^{fMRI}), respectively), for the motor source as a function of the number of samples and number of extracted jICA components, for high SNR (ERP= 3.5; fMRI=7; top panel) and low SNR (ERP= 0.37; fMRI=0.9; bottom panel). In this simulation, the relationship between ERP source and fMRI activity was linear within a non-parametric design. The black arrows indicate the point of separation of ERP and fMRI activity into separate components.

Nonlinear Relationship (y=1-exp(x)): Parametric design

## Temporal-Parietal Source: High SNR
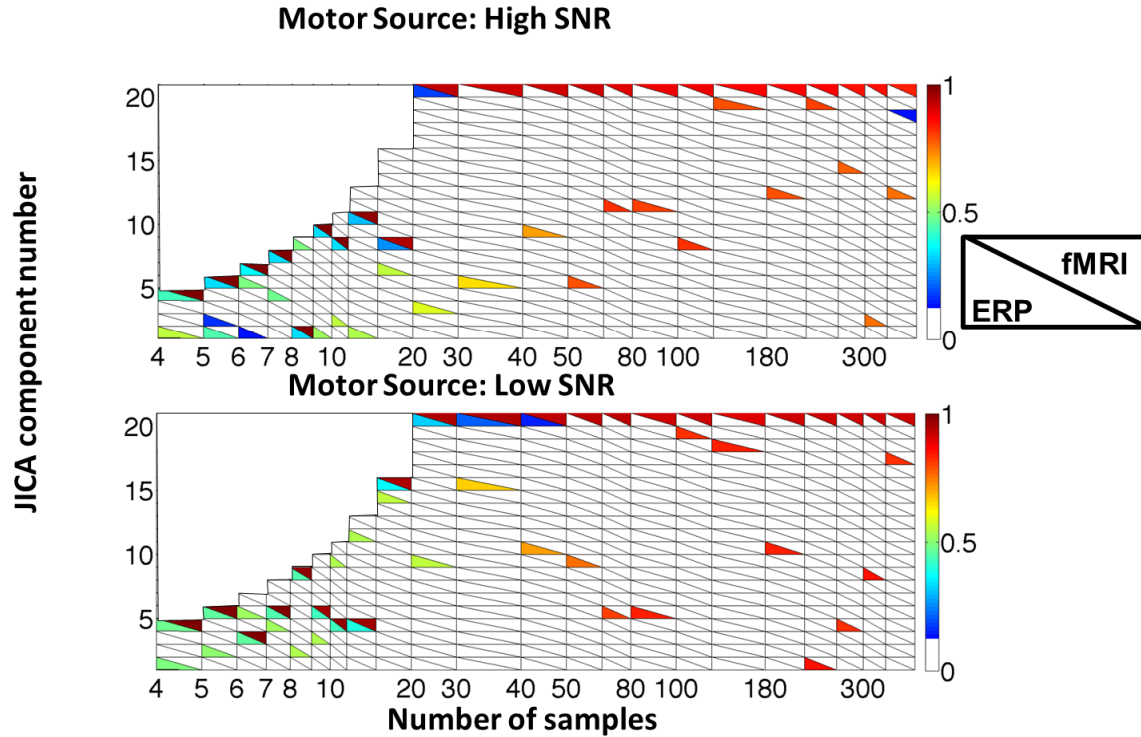
Figure 5-2: Normalized source detection for the temporo-parietal source with nonlinear relationship in a parametric design

Normalized source detection values for jICA-ERP and jICA-fMRI using a parametric experimental design, (lower and upper triangle in each square representing max(s_N^{EEG}) and max(s_N^{fMRI}), respectively), for the temporo-parietal source as a function of the number of samples and number of extracted jICA components, for high SNR (ERP= 3.5; fMRI=7; top panel) and low SNR (ERP= 0.37; fMRI=0.9; bottom panel). In this simulation, the relationship between ERP source and fMRI activity was nonlinear within a parametric design.

Nonlinear Relationship (y=1-exp(x)): Parametric design

Motor Source: High SNR
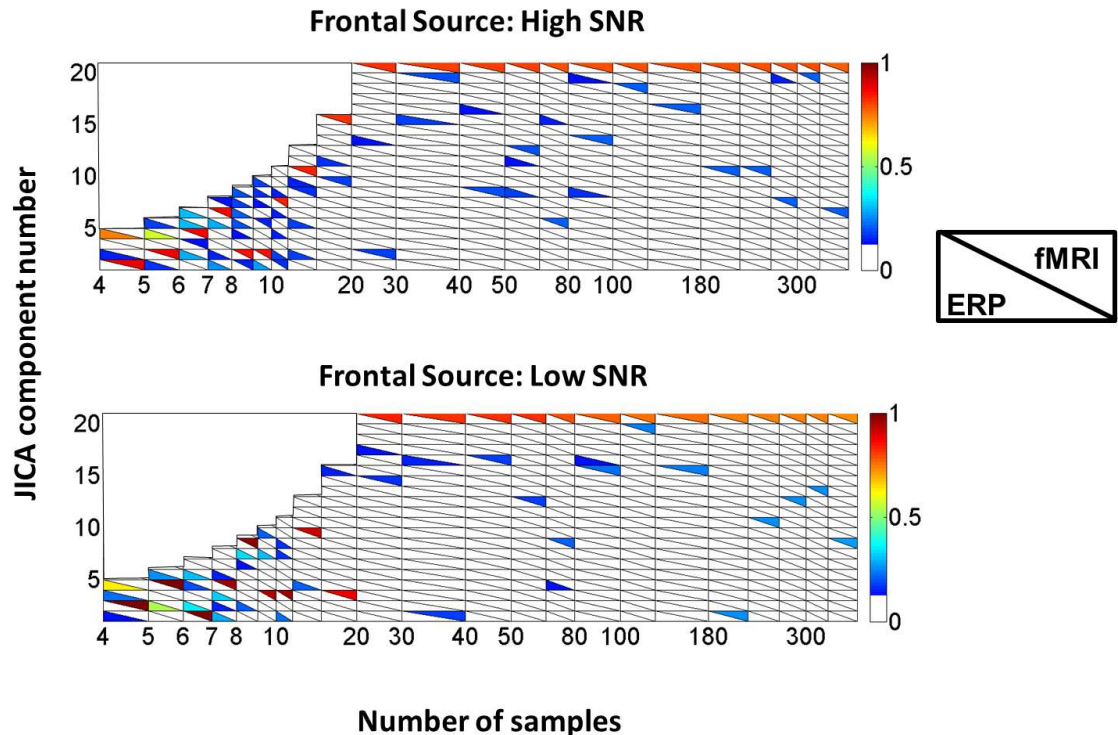
Figure 5-3: Normalized source detection for the motor source with nonlinear relationship in a parametric design

Normalized source detection values for jICA-ERP and jICA-fMRI using a parametric experimental design, (lower and upper triangle in each square representing max(s_N^{EEG}) and max(s_N^{fMRI}), respectively), for the motor source as a function of the number of samples and number of extracted jICA components, for high SNR (ERP= 3.5; fMRI=7; top panel) and low SNR (ERP= 0.37; fMRI=0.9; bottom panel). In this simulation, the relationship between ERP source and fMRI activity was nonlinear within a parametric design.

Linear Relationship: Parametric design

Frontal Source: High SNR

Frontal Source: Low SNR

Number of samples
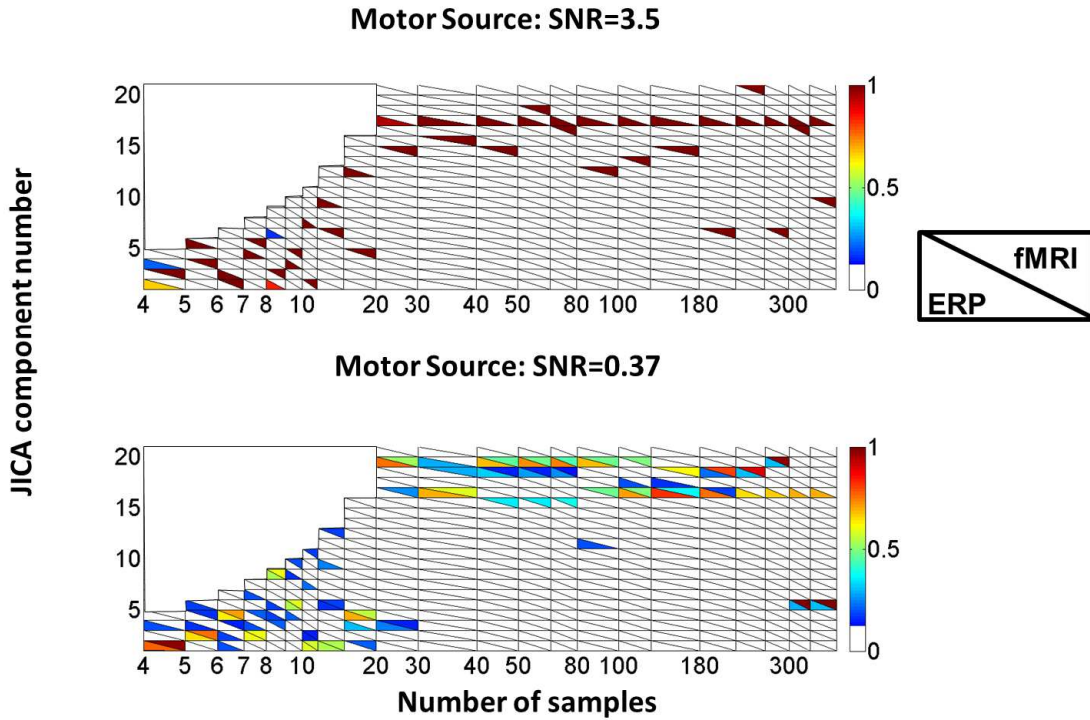
Figure 5-4: Normalized source detection for jICA in a parametric design
Normalized source detection values for jICA-ERP and jICA-fMRI in a parametric experimental design, for the uncoupled frontal source as a function of the number of samples and number of extracted jICA components, for high SNR (ERP= 3.5; fMRI=7; top panel) and low SNR (ERP= 0.37; fMRI=0.8; bottom panel). The lower and upper triangle in each square represent max(s_N^{EEG}) and max(s_J^{fMRI}), respectively. In this simulation, the relationship between ERP and fMRI activity was linear.

Nonlinear Relationship (f(x)=1-exp(x)): Non-parametric design

## Motor Source: SNR=3.5

Motor Source: SNR=0.37
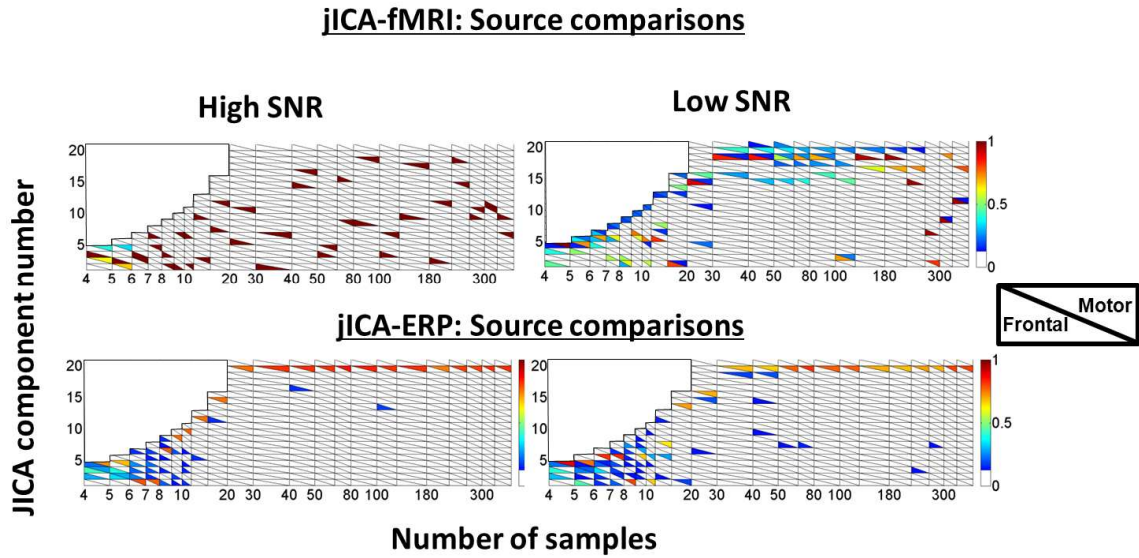
Figure 5-5: Normalized source detection for the motor source with non-linear relationship

Normalized source detection values for jICA-ERP and jICA-fMRI using a nonparametric experimental design, (lower and upper triangle in each square representing max(s_N^{EEG}) and max(s_N^{fMRI}), respectively), for the motor source as a function of the number of samples and number of extracted jICA components, for high SNR (ERP= 3.5; fMRI=7; top panel) and low SNR (ERP= 0.37; fMRI=0.8; bottom panel). In this simulation, the relationship between ERP source and fMRI activity was non-linear within a non-parametric design. The black arrows indicate the point of separation of ERP and fMRI activity into separate components.

Figure 5-6: Source segregation with jICA-fMRI and jICA-ERP for two sources in non-parametric design

Comparison of normalized source detection values for jICA-fMRI (top panels) and jICA-ERP (lower panels) components of the motor and temporo-parietal sources (lower and upper triangle in each square representing one data point, respectively) is shown here for a non-linear fMRI/ERP relationship. The segregation of motor and temporo-parietal sources is shown as a function of the number of samples and number of components and for high SNR (ERP= 3.5; fMRI=7 (left) and low SNR (ERP= 0.37; fMRI=0.8 (right). The black arrow indicates separation of the temporal and motor sources into different components. At high SNR, motor and temporo-parietal were always segregated into separate components.

Figure 5-7: Normalized source detection for jICA-fMRI and jICA-ERP for motor and frontal sources

Comparison of normalized source detection values for the jICA-fMRI (top panels) and jICA-ERP (lower panels) components of the motor and frontal sources (lower and upper triangle in each square representing one data point, respectively). The segregation of motor and frontal sources is shown as a function of the number of samples and number of components and for high SNR (ERP= 3.5; fMRI=7 (left) and low SNR (ERP= 0.37; fMRI=0.8 (right). The relationship between ERP and fMRI in this simulation was linear for the motor and uncoupled for the frontal sources.